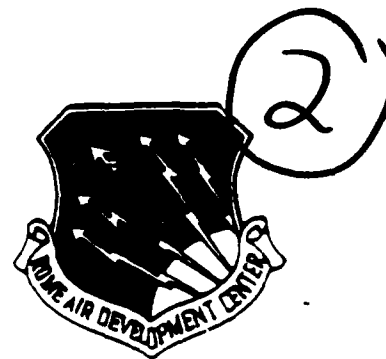


DTIC FILE COPY



RADC-TR-90-69
Final Technical Report
May 1990

AD-A223 309

A 94 GHz TRANSMISSOMETER

University of Dayton

Thomas J. Barnum



APPROVED FOR PUBLIC RELEASE; DISTRIBUTION UNLIMITED.

Rome Air Development Center
Air Force Systems Command
Griffiss Air Force Base, NY 13441-5700

90 06 25 007

This report has been reviewed by the RADC Public Affairs Division (PA) and is releasable to the National Technical Information Services (NTIS) At NTIS it will be releasable to the general public, including foreign nations.

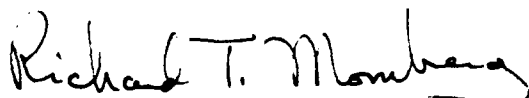
RADC-TR-90-69 has been reviewed and is approved for publication.

APPROVED:



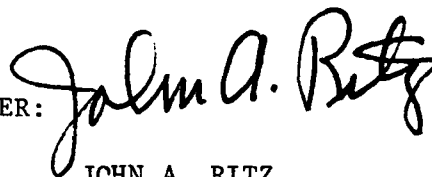
UVE H. W. LAMMERS
Project Engineer

APPROVED:



RICHARD T. MOMBERG, Lt Col, USAF
Deputy Director of Electromagnetics

FOR THE COMMANDER:



JOHN A. RITZ
Directorate of Plans & Programs

If your address has changed or if you wish to be removed from the RADC mailing list, or if the addressee is no longer employed by your organization, please notify RADC (EECP) Hanscom AFB MA 01731-5000. This will assist us in maintaining a current mailing list.

Do not return copies of this report unless contractual obligations or notices on a specific document require that it be returned.

REPORT DOCUMENTATION PAGE

Form Approved
OPM No. 0704-0188

Public reporting burden for this collection of information is estimated to average 1 hour per response, including the time for reviewing instructions, searching existing data sources, gathering and maintaining the data needed, and reviewing the collection of information. Send comments regarding this burden estimate or any other aspect of this collection of information, including suggestions for reducing this burden, to Washington Headquarters Services, Directorate for Information Operations and Reports, 1215 Jefferson Davis Highway, Suite 1204, Arlington, VA 22202-4302, and to the Office of Management and Budget, Paperwork Project, Washington, DC 20503.

1. AGENCY USE ONLY (Leave Blank)		2. REPORT DATE May 1990		3. REPORT TYPE AND DATES COVERED Final Jul 84 to Sep 85	
4. TITLE AND SUBTITLE A 94 GHz TRANSMISSOMETER				5. FUNDING NUMBERS C - F30602-81-C-0206 PE - 63707F PR - 2688 TA - 00 WU - P1	
6. AUTHOR(S) Thomas J. Barnum					
7. PERFORMING ORGANIZATION NAME(S) AND ADDRESS(ES) University of Dayton Research Institute Dayton OH 45469				8. PERFORMING ORGANIZATION REPORT NUMBER 716736-1	
9. SPONSORING/MONITORING AGENCY NAME(S) AND ADDRESS(ES) Avionics Laboratory (AFWAL) Wright-Patterson AFB OH 45433 Rome Air Development Center (EECP) Hanscom AFB MA 01731-5000				10. SPONSORING/MONITORING AGENCY REPORT NUMBER RADC-TR-90-69	
11. SUPPLEMENTARY NOTES RADC Project Engineer: Uve H. W. Lammers/EECP/(617) 377-3193					
12a. DISTRIBUTION/AVAILABILITY STATEMENT Approved for public release; distribution unlimited.				12b. DISTRIBUTION CODE	
13. ABSTRACT (Maximum 200 words) The physical implementation of a 94 GHz reflection transmissometer is documented. The instrument operates by reflecting a signal from a calibrated target but differs from a radar in that no range gate is used. The design is discussed and signals in the receiver are analyzed in order to document the operation and to ease troubleshooting. Test results are given both for calibration with an internal signal loop provided for that purpose and for outdoor tests with corner reflectors. The test results show that the transmissometer functions properly, although at a somewhat reduced range due to less return from the target than was predicted. The range is also limited by clutter which dominates the signal return at long ranges. The use of a modulated target is suggested to alleviate this problem, and a preliminary modulated target design is discussed.					
14. SUBJECT TERMS Atmospheric transmission, attenuation, millimeter waves, reflection transmissometer, atmospheric transmittance				15. NUMBER OF PAGES 148	
				16. PRICE CODE	
17. SECURITY CLASSIFICATION OF REPORT UNCLASSIFIED	18. SECURITY CLASSIFICATION OF THIS PAGE UNCLASSIFIED	19. SECURITY CLASSIFICATION OF ABSTRACT UNCLASSIFIED	20. LIMITATION OF ABSTRACT UL		

TABLE OF CONTENTS

CHAPTER	
I	INTRODUCTION 1
II	SYSTEM DESCRIPTION 4
A.	REQUIREMENTS 4
B.	PRINCIPLE OF OPERATION 5
C.	IMPLEMENTATION 7
1.	Overview 7
2.	The Transmitter 7
3.	The Receiver 11
4.	The Calibration Channel 19
D.	PHYSICAL DESCRIPTION AND SPECIFICATIONS 20
III	SIGNAL ANALYSIS 28
A.	INTRODUCTION 28
B.	ANALYSIS OF SIGNAL FREQUENCY AND PHASE THROUGHOUT THE RECEIVER 29
1.	Overview 29
2.	RF Section 29
3.	IF Section 32
4.	Audio Frequency Section 34

C.	ANALYSIS OF SIGNAL AMPLITUDE, NOISE POWER, AND SPECTRAL CHARACTERISTICS IN THE RECEIVER	43
1.	Signal Amplitude	43
2.	Noise Power	49
3.	Noise Spectral Characteristics	52
D.	SUMMARY	64
IV	TEST RESULTS	65
A.	INTRODUCTION	65
B.	CALIBRATION CHANNEL TEST RESULTS	66
1.	Overview	66
2.	Procedure	66
3.	Attenuation Equations	69
4.	Sensitivity and Dynamic Range	72
C.	OUTDOOR TEST RESULTS	72
D.	CLUTTER	81
E.	SUMMARY	83
V	OPERATING INSTRUCTIONS	85
A.	INTRODUCTION	85
B.	INITIAL SET-UP	85
C.	OPERATION	89
1.	Power on	89
2.	Checking Gunn Oscillator Operation	91
3.	Operation with Calibration Channel	91
4.	Operation with Calibrated Target	98
D.	DATA ACQUISITION	100
1.	V_{out}	100
2.	Gain Level	100
E.	TROUBLESHOOTING	101
1.	Locking Gunn Oscillator	101
2.	L.O. Gunn Oscillator	102
3.	Improper V_{sync}	103
VI	CONCLUSIONS AND RECOMMENDATIONS	104

APPENDICES	106
A MODULATED TARGET	106
A. ADVANTAGES	106
B. MODULATED TARGET IMPLEMENTATION	108
B INFREQUENTLY REQUIRED TUNING	115
A. PHASE-LOCKED GUNN OSCILLATORS	115
B. SQUARER ADJUSTMENT	117
C. GAIN SWITCHING POINTS	119
D. I, Q CHANNEL GAINS	119
C ATTENUATION EQUATION DERIVATION	121
D CIRCUIT DIAGRAMS	125
1. ESL 776 MHz, 33 dB Amplifier	125
2. Audio-Frequency Circuitry	125
REFERENCES	132



Accession File	
NTIS GRA&I	<input checked="" type="checkbox"/>
DTIC TAB	<input type="checkbox"/>
Unannounced	<input type="checkbox"/>
Justification	
By	
Distribution	
Availability Codes	
Dist	Availability Codes Special
A-1	

LIST OF PLATES

2.1	TRANSMISSOMETER FRONT VIEW (Absorber shrouds removed)	23
2.2	TRANSMISSOMETER SIDE VIEW (Absorber shrouds removed)	24
2.3	OVERVIEW OF TRANSMISSOMETER COMPONENTS	25
2.4	DETAIL OF BOTTOM HALF OF PLATE 2.3	26
2.5	DETAIL OF TOP HALF OF PLATE 2.3	27
5.1	TRANSMISSOMETER BOTTOM PANEL	86
5.2	TRANSMISSOMETER SIDE PANEL	90
5.3	POSITION OF WAVEGUIDE SWITCH	93
5.4	POSITION OF TELONIC ATTENUATOR KNOB	97
B.1	CIRCUIT BOARD A (OR B)	118

LIST OF TABLES

2.1	PHYSICAL SPECIFICATIONS	22
3.1	PROPORTIONALITY TERMS	39
3.2	SIGNAL POWER LEVELS IN THE RECEIVER IF SIGNAL CHANNEL	45
4.1	ATTENUATION EQUATION PARAMETERS	70
4.2	OUTDOOR TEST RESULTS	73
4.3	COMPARISON OF RADAR CROSS SECTION CALCULATIONS	80
5.1	CABLE CONNECTIONS	87

LIST OF FIGURES

1.1. Specific attenuation in clear air due to atmospheric gases (curve C) [3].	2
2.1. Transmissometer system. (Block diagram.)	6
2.2. Transmitter. (Block diagram.)	8
2.3. Receiver RF components. (Block diagram.)	12
2.4. Receiver IF components. (Block diagram.)	15
2.5. Audio frequency circuitry. (block diagram.)	18
2.6. Calibration Channel. (Block diagram.)	21
3.1. R_{min} versus theoretical radar cross section of target.	47
3.2. Signal-plus-noise spectrum at MCL ZAPD-1 power divider output, point {9}.	53
3.3. Close-up of modulated 776 MHz signal in Figure 3.3, showing carrier and sidebands.	53
3.4. Signal-plus-noise spectrum at ZEM-2 double balanced mixer outputs, points {10}, {20}.	54
3.5. Signal-plus-noise spectrum at squarer input, points {12}, {22}.	54
3.6. SxS spectrum at squarer output.	57
3.7. SxN spectrum at squarer output.	57
3.8. NxN spectrum at squarer output.	59
3.9. Signal-plus-noise spectrum at squarer output, points {13}, {23}.	59
3.10. Synchronous detector operation.	62
3.11. Signal-plus-noise spectrum at synchronous detector output, point {25}.	62

4.1.	V_{out} vs. received 94 GHz signal power, P_2 .	68
4.2.	V_{out} vs. received 94 GHz signal power, P_2 .	71
4.3.	Triangular trihedral corner reflector.	75
4.4.	Circular trihedral corner reflector.	75
5.1.	Proper synchronous detector output.	94
5.2.	Synchronous detector output, phase misadjusted.	94
5.3.	Synchronous detector output, symmetry misadjusted.	95
5.4.	V_{sync} clipped.	95
A.1.	Modulated target.	109
A.2.	Subreflector.	110
A.3.	Polarization-sensitive reflector.	111
A.4.	Angle "A".	112
B.1.	Gunn adjustment potentiometer positions.	116
B.2.	97 MHz phase-locked Gunn oscillator IF signal.	116
B.3.	Audio frequency circuit board #3.	120
D.1.	ESL 776 MHz, 33 dB gain amplifier circuit diagram.	126
D.2.	Audio frequency circuit board #1. Summer and synchronous detector and $\tau=1$ sec. low-pass filter circuit diagram.	127
D.3.	Audio frequency circuit board #2. 48 kHz clock generator circuit diagram.	128
D.4.	Audio frequency circuit board #3. Gain switching logic and $\tau=10$ sec. low-pass filter circuit diagram.	129
D.5.	Audio frequency circuit board #4. Audio frequency preamplifier (gain=1 or 10) circuit diagram.	130
D.6.	Audio frequency circuit board A,B. Anti-aliasing low-pass filter, digital bandpass filter, amplifier, and squarer circuit diagram.	131

CHAPTER I

INTRODUCTION

The objective of this project has been to produce an instrument to measure atmospheric attenuation at 94 GHz under various weather conditions, such as rain, snow, sleet and fog. Various systems were considered for this task under two previous studies [1,2], and the use of a 94 GHz reflection transmissometer with a quadrature receiver was recommended [2]. The implementation of this instrument is the subject of this report.

A great deal of research has been done in recent years in the area of millimeter wave propagation and a good deal of this work has dealt with propagation in the low molecular absorption "window" around 94 GHz. (See Figure 1.1.) Much of the work has been in theoretical modeling of millimeter wave propagation, as represented by References [4] to [8]. Experimental studies, such as those done at the U.S. Army Ballistic Research Laboratory, Aberdeen Proving Ground, Maryland and the U.S. Army Atmospheric Sciences Laboratory, White Sands Missile Range, NM, are cited in References [9] to [14].

In this report, Chapter II discusses the requirements which the transmissometer is asked to meet and, in broad outline, how this task is accomplished. It also gives a physical description of the device.

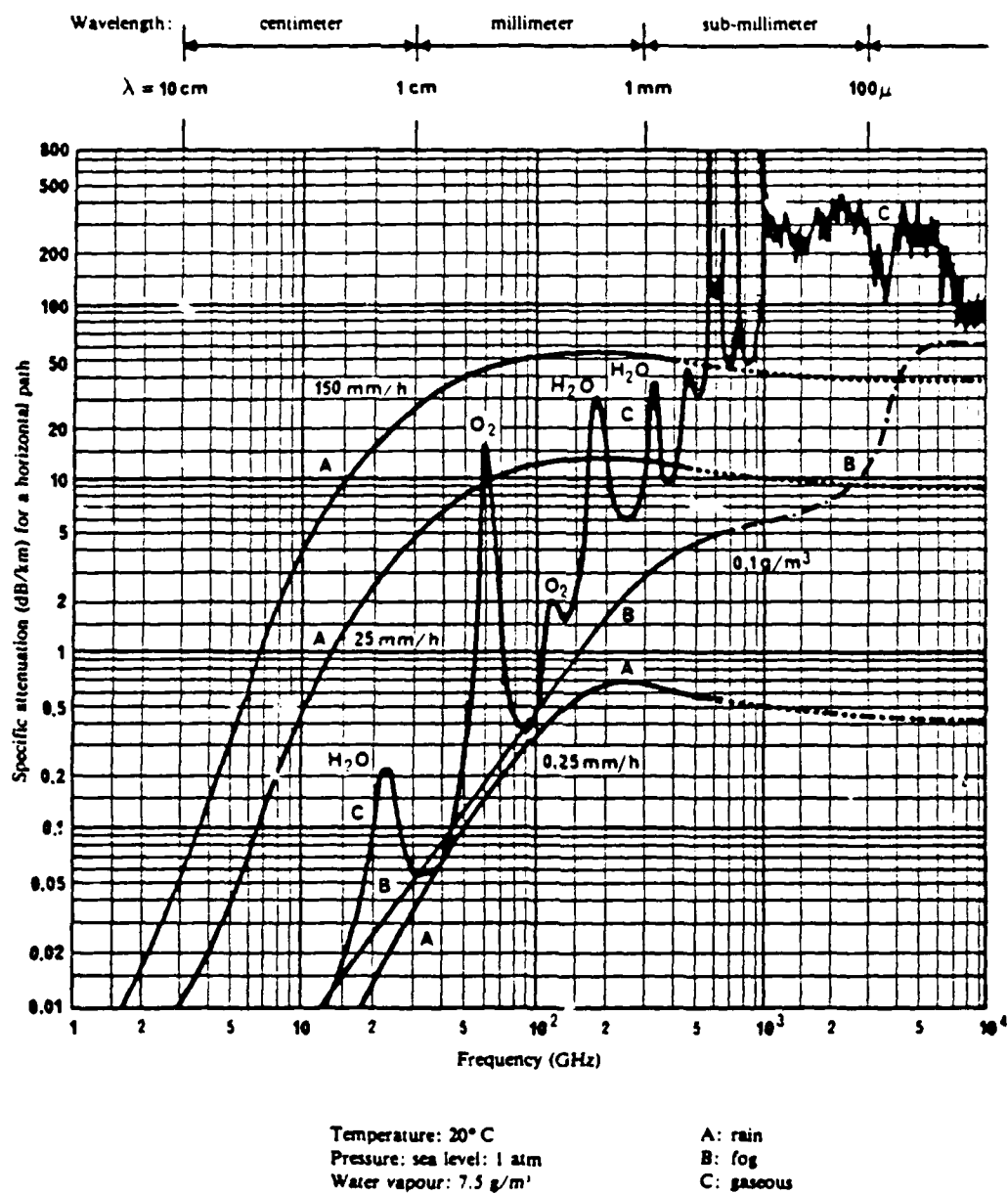


Figure 1.1. Specific attenuation in clear air due to atmospheric gases (curve C) [3].

Chapter III takes a detailed look at the signals and noise at various points in the system to explain why the device has been built as it is. Chapter IV shows test results from both bench calibration of the device and outdoor tests. Chapter V is intended as an operation manual for the transmissometer, giving both operating instructions and troubleshooting tips.

CHAPTER II

SYSTEM DESCRIPTION

A. REQUIREMENTS

By definition, a transmissometer is required to measure the electromagnetic propagation parameter known as transmittance, where transmittance is defined as the ratio of the plane-wave power density emerging from a transmission medium relative to the plane-wave power incident upon it. However, other often used parameters are the attenuation A , in dB, and the average specific attenuation α (alpha), in dB per kilometer, along a signal path. These parameters are related by

$$A = \alpha R, \quad (2.1)$$

$$t = 10^{-(A/10)} = 10^{-(\alpha R/10)}, \quad (2.2)$$

where t is the transmittance and R is the path length through the transmission medium. This transmissometer system is calibrated to measure received signal power, which can be numerically processed to determine t , A , and α .

A single-ended reflection transmissometer using a quadrature receiver was chosen for this task on the basis that a single-ended system may be operated and calibrated more easily (due to single-site operation) than a two-ended system, and that a quadrature receiver

yields greater sensitivity. Another factor in choosing a single-ended system is that the range can be changed by moving only the calibrated target, as opposed to the entire receiver [2].

B. PRINCIPLE OF OPERATION

The principle of operation of the transmissometer is the following. (Refer to Figure 2.1.) A 94 GHz signal is transmitted, reflected by a calibrated target at a distance R, and received with unknown attenuation and phase shift. The received 94 GHz signal is amplitude modulated. This modulation can be performed in the transmitter before transmission, or a continuous-wave signal can be transmitted and modulated by a modulated target. (For more on the modulated target, see Appendix A.) The requirement of the receiver is to produce at its output a DC voltage which is proportional to the power of that 94 GHz signal and independent of the phase of the returning 94 GHz signal. The returned power is determined from the DC voltage and compared to the returned power under conditions of negligible attenuation. If the two measurements are performed at different ranges and/or with different targets, a simple correction can be made for these changes as shown in Appendix C. The ratio of these two powers (corrected if required) is the square of the transmittance, and the attenuation in decibels caused by the meteorological condition occurring at the time the data was taken is given by

$$A = -10 \log_{10} t \quad (2.3)$$

which follows from Equation (2.2).

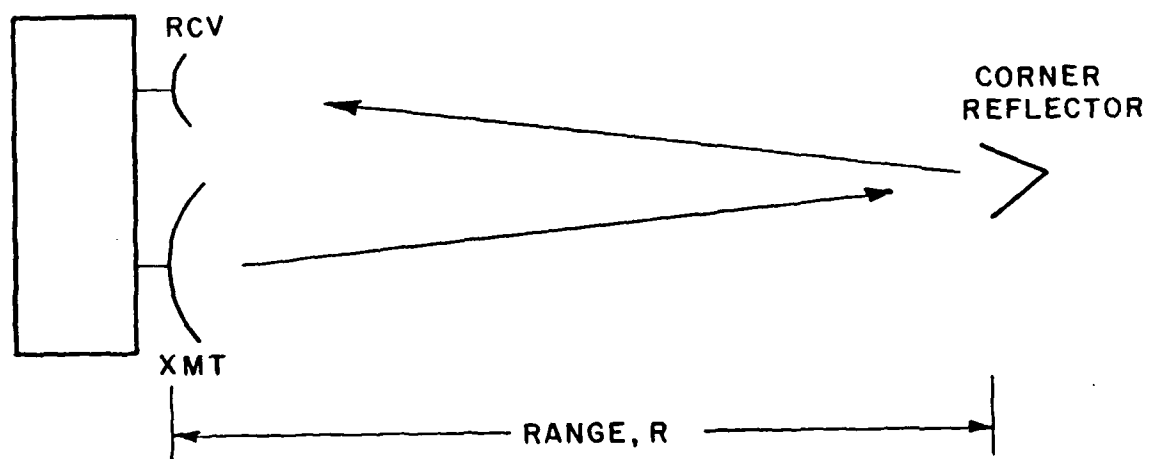


Figure 2.1. Transmissometer system. (Block diagram.)

C. IMPLEMENTATION

1. Overview

This section explains the structure and operation of the transmissometer. The reason for the choice of the particular configuration will be more apparent after the signal and noise at various ports of the system are considered in Chapter III.

2. The Transmitter

The transmissometer must transmit a modulated 94 GHz signal if the system is used with a corner reflector, or a continuous-wave signal if a modulated target is used. The 94 GHz signal is generated by a high power (200 mW) continuous-wave IMPATT source (Hughes 47196H-1120B) which is injection-locked [15], by a highly stable, but lower power (10 mW), 94.000000 GHz phase-locked Gunn oscillator (Hughes 47746H-1001) (see Figure 2.2). The stability of the Gunn oscillator is due to the fact that it is phase-locked to a signal derived from a highly stable 97.07224 MHz crystal.

The injection-locking of the IMPATT device is performed in the following way (refer again to Figure 2.2). The 94.000000 GHz signal from the Hughes 47746H-1001 Locking Gunn oscillator passes through a Faraday rotation isolator which protects the Locking Gunn oscillator from possible signal reflection and leakage from the high power IMPATT device, and which presents a well matched load to the Locking Gunn oscillator. The locking Gunn signal then passes through a circulator

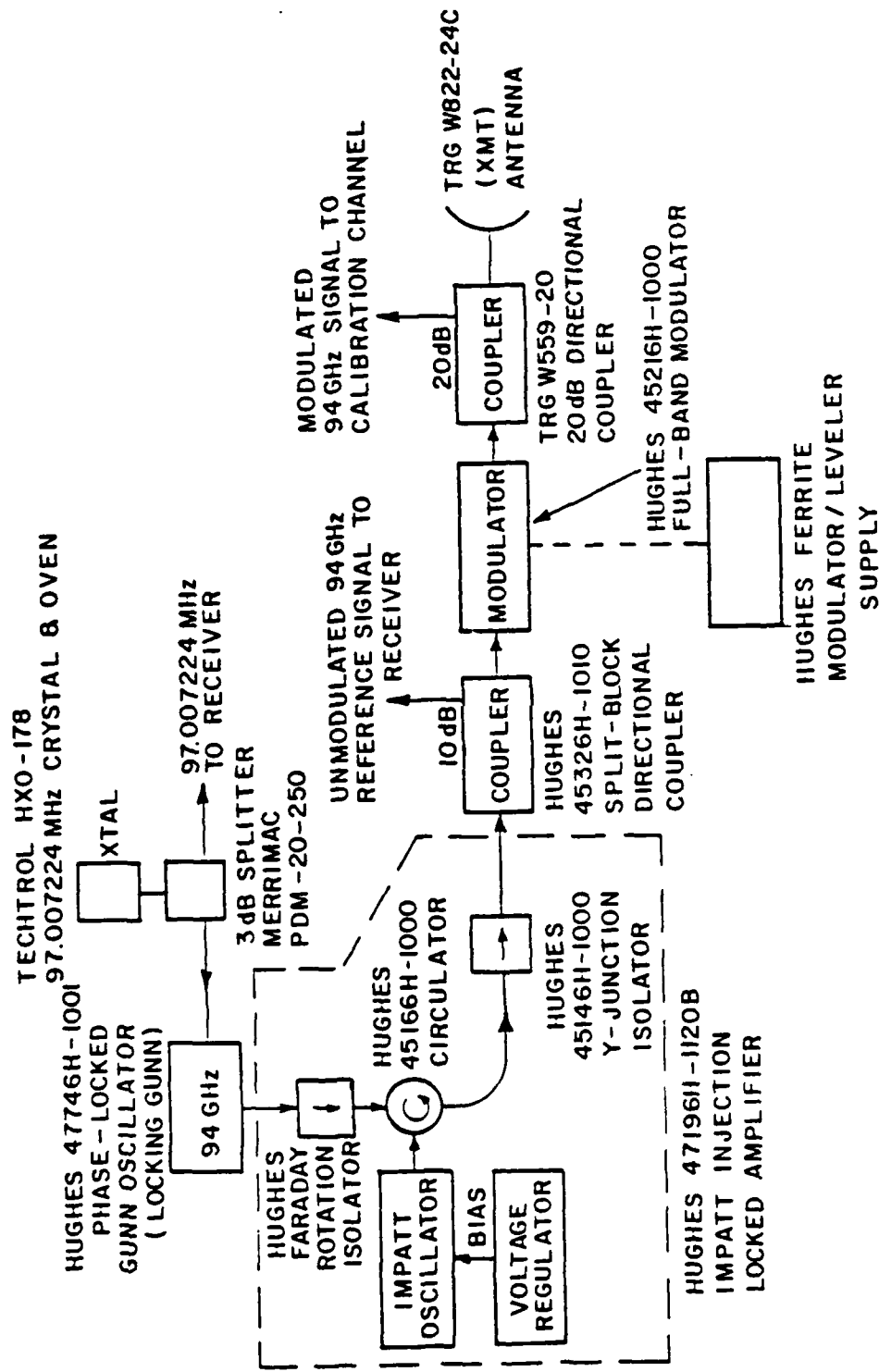


Figure 2.2. Transmitter. (Block diagram.)

and into the the IMPATT device to injection-lock it to 94.000000 GHz. These devices are engineered as a unit; the Hughes 47196-1120B Continuous Wave Injection-Locked Amplifier unit consists of the Faraday rotation Isolator (Hughes 45116H-1000), circulator (Hughes 45166H-1000), IMPATT oscillator in temperature stabilized waveguide cavity, and junction isolator (Hughes 45146H-1000).

By itself the IMPATT oscillator is not highly frequency stable, being subject to thermal drift and having a rather broad output spectrum (1 MHz at its 3 dB down points). However, when injection-locked, the IMPATT oscillator is as stable in center frequency as the Hughes 47746H-1001 Gunn oscillator used to injection-lock it, and the output spectrum is narrowed to that of the Hughes 47746H-1001 Gunn oscillator. This also produces an increase in power of 10 dB at the center frequency, since the IMPATT's energy is no longer spread over a wide band but concentrated at the Gunn frequency. The y-junction isolator (Hughes 45146H-1000) after the IMPATT oscillator protects both IMPATT and Gunn oscillators from possible damage by signal reflection and presents a matched load to the IMPATT oscillator.

The next item in the transmitter section signal path is a 10 dB directional coupler (Hughes 45326H-1010), used to tap off an unmodulated 94.000000 GHz reference signal needed in the receiver. This is followed by a modulator (Hughes 45216H-1000) which is used to amplitude modulate the 94.000000 GHz signal at 800 Hz when a corner reflector is used as a target, or allow a continuous-wave signal to pass when the system is used with a modulated target. Control of the modulator is provided by a

Hughes Ferrite Modulator/Leveler Supply (Hughes 47530H-5111) which can be used to adjust the modulating frequency from 600 to 1300 Hz or allow a continuous-wave signal to pass. If internal modulation is used, the frequency is normally set to 800 Hz, a frequency chosen for convenience, because it matches the modulating frequency produced by the modulated target discussed in Appendix A.

The 20 dB directional coupler (TRG W559-20) which follows in the transmitter signal path is used to tap off a calibration signal, which is a modulated 94.000000 GHz signal when the modulator is turned on, for use in testing and calibrating the receiver. The primary signal is then sent to the TRG W822-24C twenty-four inch diameter, 53 dB gain, linearly polarized, machined aluminum Cassegrain antenna (chosen on the basis of availability), where it is transmitted towards the target.

The power delivered to the transmitting antenna is approximately 30 mW due to the insertion loss of the components and waveguide between the IMPATT oscillator and the antenna. The insertion loss from each component is as follows: Hughes 45166H-1000 circulator, 0.8 dB; Hughes 45146-1000 y-junction isolator, 0.8 dB; Hughes 45325H-1010 10 dB directional coupler, 1.4 dB; Hughes 45216H-1000 full-band modulator, 2.5 dB; TRG W559-20 20 dB directional coupler, 1.4 dB; and 12 inches of W-band silver waveguide, 1.2 dB. The total insertion loss in the transmitter is

$$L_t = 8.1 \text{ dB} \quad . \quad (2.4)$$

This corresponds to a transmittance of

$$t_t = 0.15 \quad . \quad (2.5)$$

3. The Receiver

Because the phase of the incoming signal to the receiver is unknown, it is essential that the performance of the receiver be independent of phase. This is accomplished by the use of a quadrature receiver [16,17], whose name is a result of the fact that the signal is broken down into in-phase and quadrature components, one proportional to $A \sin(\phi)$ and one proportional to $A \cos(\phi)$, where ϕ is the unknown signal phase. Note that by squaring and adding and filtering these two terms, a signal proportional to A^2 is obtained, independently of ϕ . Now a detailed explanation of the operation of the quadrature receiver is given.

In Figure 2.3, it is seen that there are three RF inputs to the receiver: the modulated 94.000000 GHz return from the target which is incident upon the receiving antenna, the 94.000000 GHz reference signal derived from the transmitter (see Figure 2.2) and the calibration signal, which is also derived from the transmitter but which, unlike the reference signal, is modulated since the transmissometer modulator is normally turned on when the calibration channel is used. The receiving antenna is a 12-inch, aluminum Cassegrain type of unknown origin, chosen on the basis of availability. The calibration signal will be discussed in Section C.4 of this chapter.

Before examining the effect that the receiver has on the various signals, it would be advantageous for the reader to refer to Plates 2.3, 2.4, and 2.5 in Section D of this chapter, which are labeled photographs

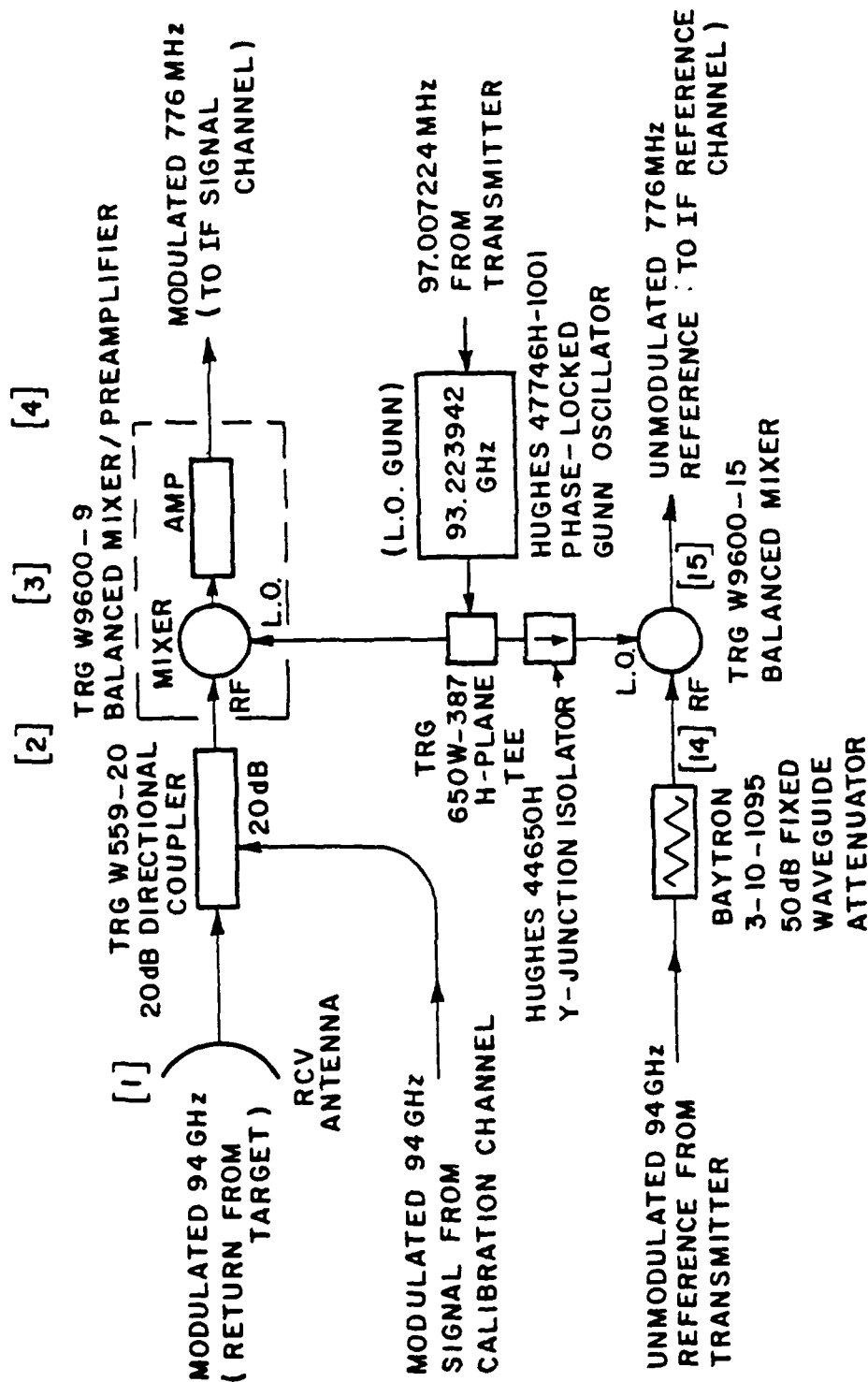


Figure 2.3. Receiver RF components. (Block diagram.)

showing the various components used in the transmissometer. Being familiar with the physical layout of the transmissometer may help the reader better visualize the operation of the system.

First consider the signal reflected from the target incident upon the receiving antenna. This signal is a modulated, phase-shifted, and attenuated version of the transmitted 94.000000 GHz signal. It is mixed, in a TRG W9600-9 balanced mixer, with a 93.223942 GHz local oscillator (L.O.) signal, known as the Gunn L.O. signal, which is derived from a second Hughes 47746H-1001 phase-locked Gunn oscillator, operating at 93.223942 GHz. The mixer output is a modulated intermediate frequency (IF) signal at 776.058 MHz, a frequency chosen on the basis of low potential interference from authorized transmissions near Dayton, Ohio.

This IF signal is at a very low level and deeply buried in broadband noise, therefore it must be filtered to reduce the noise bandwidth (by a Texscan 5BD776/15-3 coaxial bandpass filter, refer to Figure 2.4) and amplified by a 28 dB gain Avantek UTC10-115M integrated amplifier). Care must be exercised so that neither the noise nor signal saturate either the IF amplifiers or the following audio stages, as discussed further in Chapter III. For this reason, a Telonic 8120S 100 dB step attenuator, adjustable in 10 dB steps is used to adjust the signal levels, as discussed in Chapter III. The signal is then amplified by another 28 dB gain Avantek UTC10-115M integrated amplifier to its final IF level and split by a Mini-Circuits Lab ZAPD-1 3 dB zero degree power divider for use in the in-phase and quadrature channels.

Now consider the unmodulated 94.000000 GHz reference input (refer to Figure 2.3). This signal is mixed with the 93.223942 GHz Gunn L.O. signal in a TRG W9600-15 balanced mixer, producing an unmodulated 776.058 MHz IF reference signal at the mixer output. This IF reference signal and the modulated 776.058 MHz IF signal are coherent, because the two 94.000000 GHz signals used to produce the IF signals are both derived from the IMPATT signal and the two 93.223942 GHz signals used are both derived from the Gunn L.O. signal. Also, both the 94.000000 GHz and 93.223942 GHz signals are derived from the same 97.007224 MHz crystal. This common frequency reference ensures that if one Gunn signal drifts in frequency, that the other will drift with it, leaving the IF signal frequency unchanged.

Refer now to Figure 2.4. The IF reference signal from the mixer is attenuated by an Omni-Spectra 20510 fixed 10 dB attenuator, filtered by a Texscan 5BD776/15-3 Coaxial bandpass filter, amplified by an ESL* 776 MHz, 33 dB gain amplifier (see Appendix D for circuit diagram), attenuated by a Texscan RA-50 10 dB, one dB per step variable attenuator (used to control the signal level), and amplified by a 37 dB gain Avantek UTC10-109 integrated amplifier to the required level. It is then split by a Mini-Circuits Lab ZAPDQ-1 3 dB, 90 degree power divider to furnish the "L.O." signal to the Mini-Circuits Lab ZEM-2 double balanced mixers. To assure these two signals have exactly 90° of differential phase shift, two Midisco MDC-1089-1 adjustable coaxial

*ElectroScience Laboratory, The Ohio State University

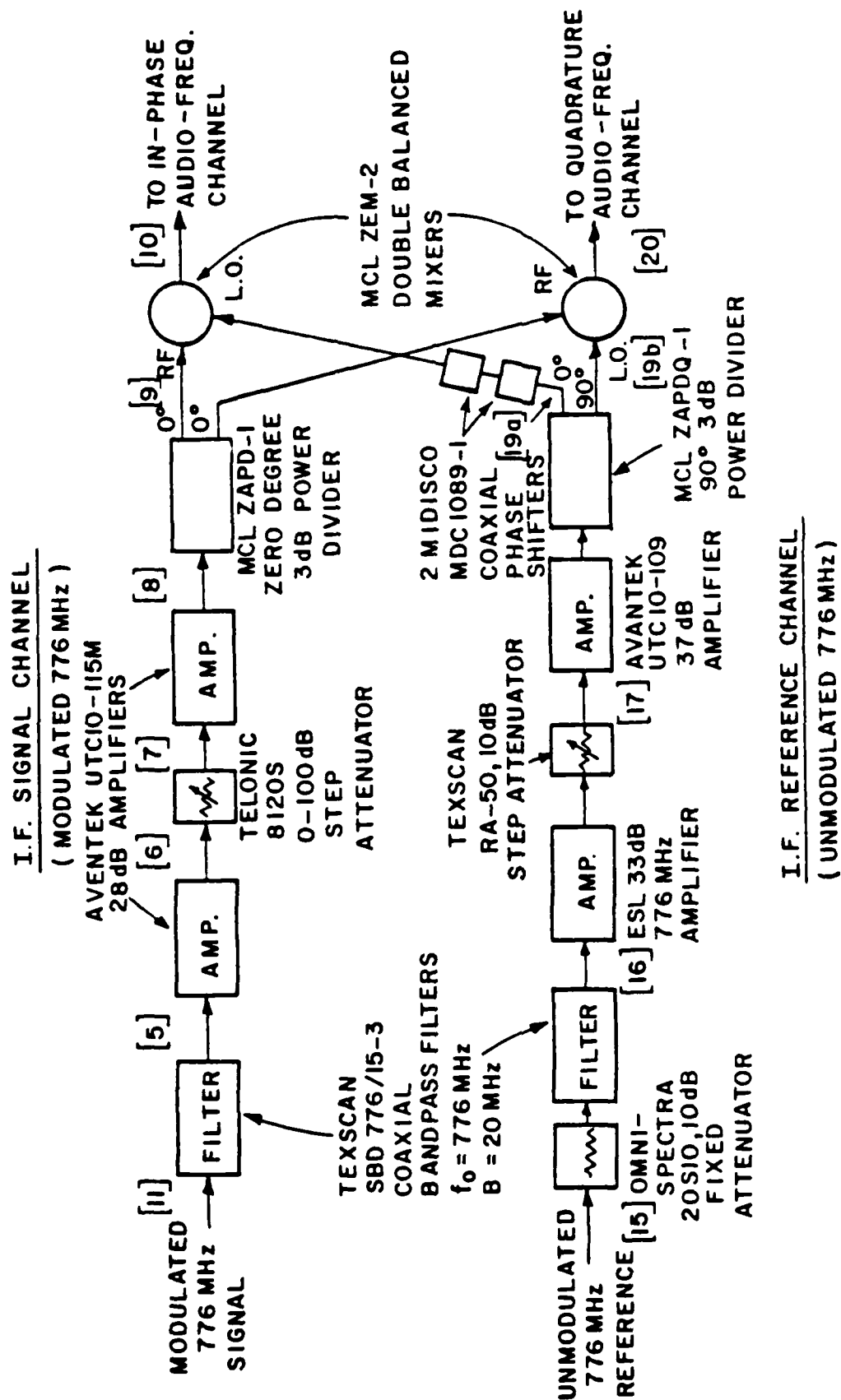


Figure 2.4. Receiver IF components. (Block diagram.)

phase shifters have been included in the zero degree leg of the ZAPDQ-1 output to allow for adjustment of the differential phase.

At the output of the ZAPD-1 zero degree power divider and ZAPDQ-1 90° power divider, there are four IF signals (refer to Figure 2.4). Two are identical modulated IF signals obtained at the outputs of the zero degree power divider, and the other two, obtained from the outputs of the 90° power divider are identical unmodulated IF reference signals, but with a 90° phase shift with respect to each other. Recall that both modulated and unmodulated 776 MHz IF signals are obtained by mixing 94 GHz and 93.223942 GHz signals. Thus the modulated and unmodulated IF signals are coherent, allowing them to be mixed to baseband to recover the modulation. Hereafter, signals derived from the 0° output port of the 90° power divider are referred to as "in-phase" or simply "I", while signals derived from the 90° output port of the power divider are referred to as "quadrature" or simply "Q".

The modulated 776.058 MHz signal contains the desired information about the returned signal power. Mixing this modulated IF signal with the unmodulated IF reference signal will yield a term at the 800 Hz modulating frequency whose amplitude is proportional to the received signal power. This is almost the desired result; however, it is shown in the signal analysis in Chapter III that the amplitude of the 800 Hz term in each channel is also dependent on the phase of the incoming modulated 94.000000 GHz signal and additional IF phase terms, which are unknown quantities. Thus it is necessary to establish a method by which

the amplitude of the 800 Hz term can be determined independently of the phase of the received 94.000000 GHz signal.

The amplitude of the 800 Hz term is determined by the following method. Both in-phase and quadrature reference signals are used to mix the modulated IF signal down to baseband, the 800 Hz modulation frequency (refer to Figure 2.4). The resulting signals are processed in the I (in-phase) and Q (quadrature) channels of the audio frequency signal processing section (refer to Figure 2.5). After filtering to remove noise, and amplification, the signals are squared and summed.

It is shown in Chapter III that the in-phase and quadrature relationship of the signals in the I and Q channels has the effect of making the amplitude A_i of the 800 Hz term in the I channel proportional to $\cos(\phi)$,

$$A_i = A \cos(\phi), \quad (2.6)$$

(where " ϕ " is the sum of the unknown RF and IF phase terms) and the amplitude A_q of the 800 Hz term in the Q channel proportional to $\sin(\phi)$,

$$A_q = A \sin(\phi) \quad . \quad (2.7)$$

By squaring the individual I and Q signals and then summing them, the signal at the output of the summer is

$$A^2 \cos^2(\phi) + A^2 \sin^2(\phi) = A^2 \quad , \quad (2.8)$$

which is the square of the amplitude of 800 Hz term, independent of the unknown RF phase. Thus the result of mixing quadrature signals, squaring and summing is that the square of the 800 Hz term is recovered, independently of the RF and IF phase terms.

IN - PHASE CHANNEL

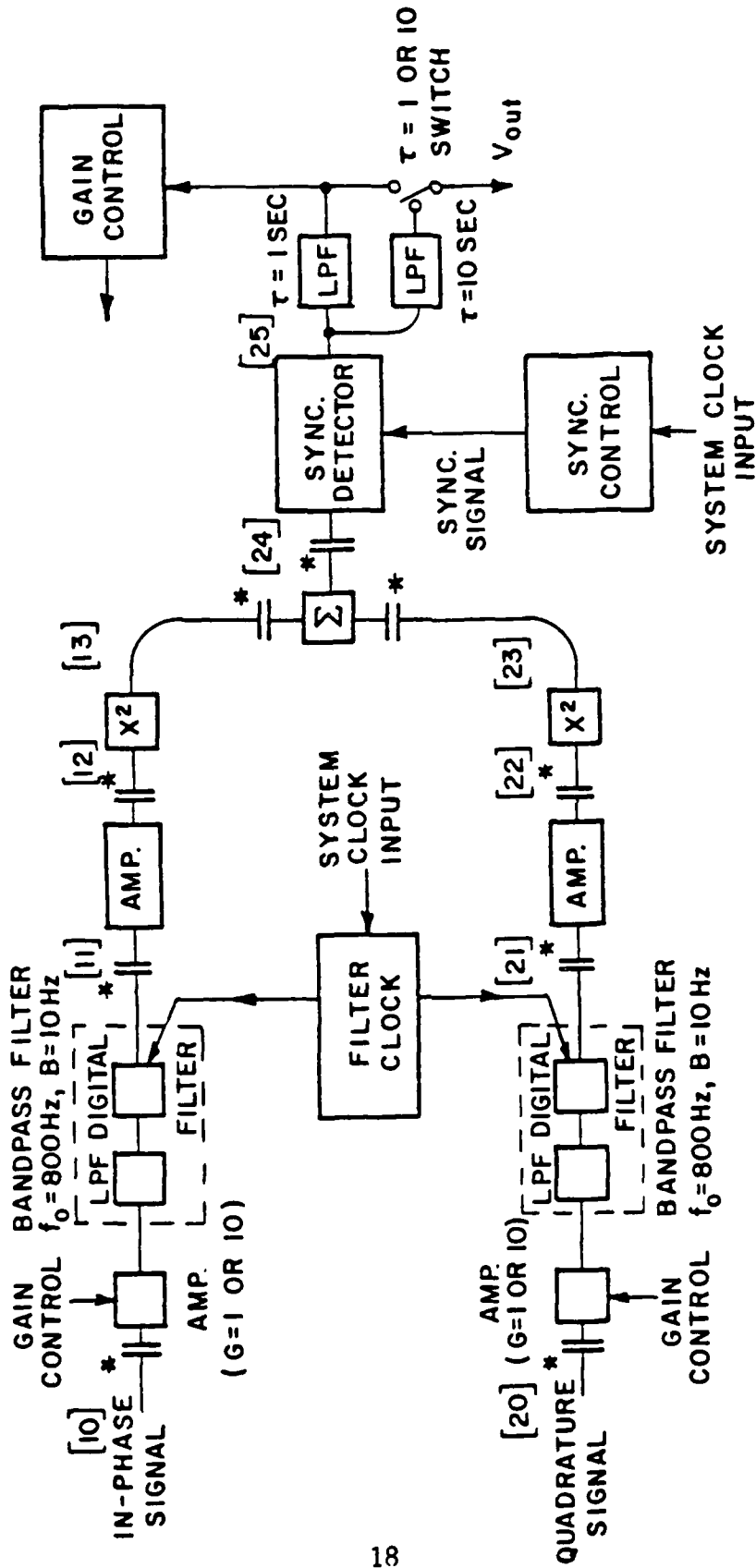


Figure 2.5. Audio frequency circuitry. (block diagram.)

Refer again to Figure 2.5. After the I and Q signals are summed, the signal contains a DC term and a 1600 Hz sinusoidal term as a result of squaring. Either of these terms could be used to determine the received RF power, and because the required output is a DC signal, the DC term would be simplest to use. However, Chapter III, Section C.3 shows that it is better to use the 1600 Hz term to improve the output signal-to-noise ratio.

To convert the 1600 Hz signal to DC, the signal is high-pass filtered to remove the DC component produced by squaring. It is then synchronously detected and low-pass filtered to remove unwanted harmonics and noise. The signal at the output, V_{out} is a DC voltage which is proportional to the square of the amplitude of the 1600 Hz term and therefore proportional to the received RF power. Further numerical processing may then be used to determine the attenuation over the path length.

4. The Calibration Channel

The calibration channel (refer to Figure 2.6, a block diagram of the calibration channel) is used only during calibration and trouble shooting. It begins with the signal tapped off by a TRG W559-20 20 dB directional coupler just before the TRG W822-24C transmitting antenna (see Figure 2.2) and ends where the signal is coupled by a TRG W559-20 20 dB directional coupler into the receiver just after the receiving antenna (see Figure 2.3). Included in the calibration channel are a Hughes 45766H-1200 phase shifter and TRG 510W/387 precision variable

waveguide attenuator used in calibration and a Hughes 45526H-1000 waveguide switch to turn this channel off during normal operation. Also, a signal is tapped by a TRG W559-6 6 dB directional coupler and run through a TRG W551 resonant cavity waveguide frequency meter to a Hughes 47326H-1011 flat-plate detector. The flat-plate detector is used to monitor the transmitter power level and is also used in conjunction with the frequency meter to monitor the transmitted frequency.

D. PHYSICAL DESCRIPTION AND SPECIFICATIONS

Front and side views of the transmissometer are shown in Plates 2.1 and 2.2. The components inside the transmissometer are shown in Plate 2.3, with Plates 2.4 and 2.5 giving close-up detail of the lower and upper halves of the components seen in Plate 2.3. Table 2.1 gives physical specifications of the transmissometer.

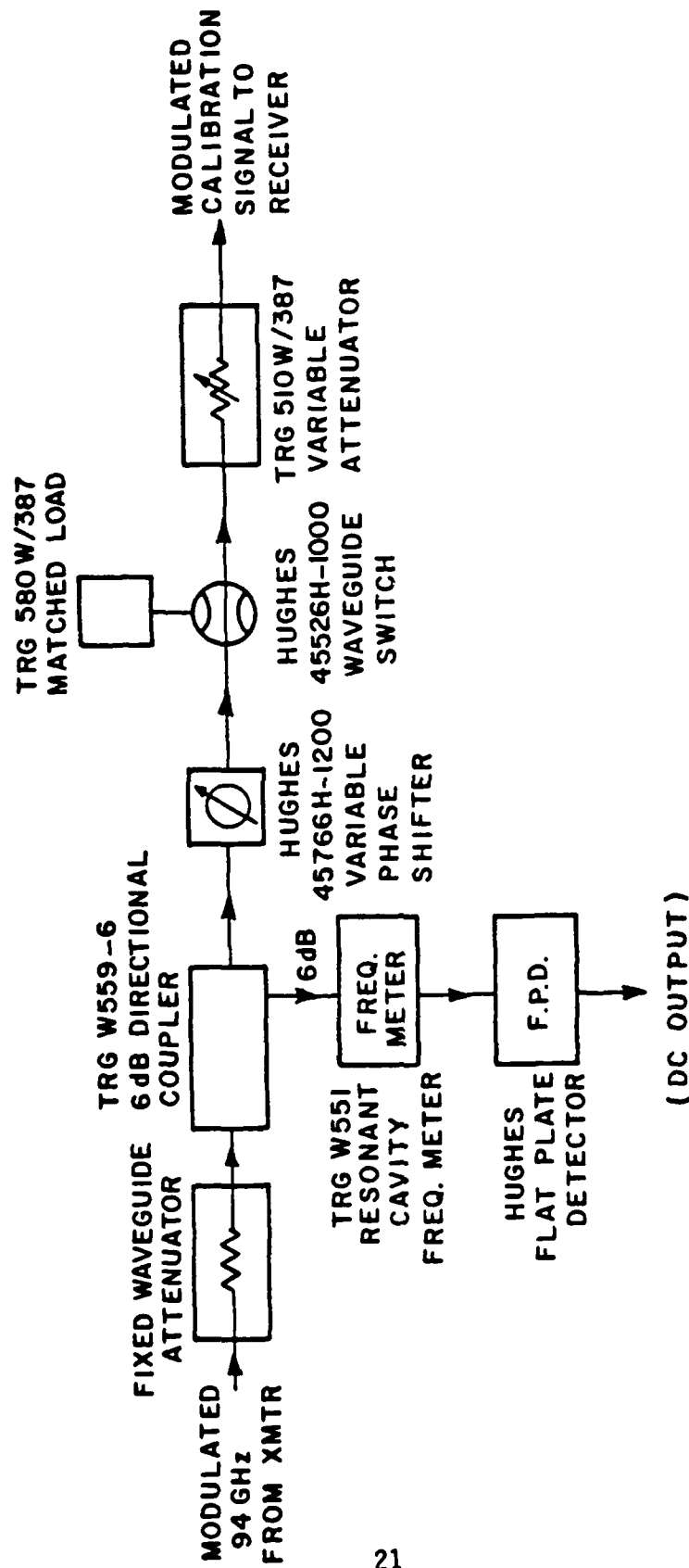


Figure 2.6. Calibration Channel. (Block diagram.)

TABLE 2.1
PHYSICAL SPECIFICATIONS

1. Height	56 inches (without wood base)
2. Width	20 inches (without wood base)
3. Depth	27 inches (without wood base)
4. Base height	5 inches
5. Base width	31 inches
6. Base depth	31 inches
7. Power supply requirements	+ 15 VDC, 5 A - 15 VDC, 1 A + 24 VDC, 100 mA 28 VDC, 3 A + 40 VDC, 500 mA 120 VAC, 60 Hz 120 VAC, 400 Hz, 0.5 A (with modulated target)
8. Operating temperature	15° to 22° c*
9. Mounting requirements (transmissometer)	Transmissometer must be firmly mounted in a position where both antennas will be kept free of moisture.
10. Mounting requirements (target)	Target must be firmly mounted to avoid swaying or vibration in the wind, and must be kept free of moisture.

*It is recommended that this range be extended by installation of a thermostatically controlled heater in the cabinet, see Chapter VI.

PLATE 2.1

TRANSMISSOMETER FRONT VIEW
(Absorber shrouds removed)

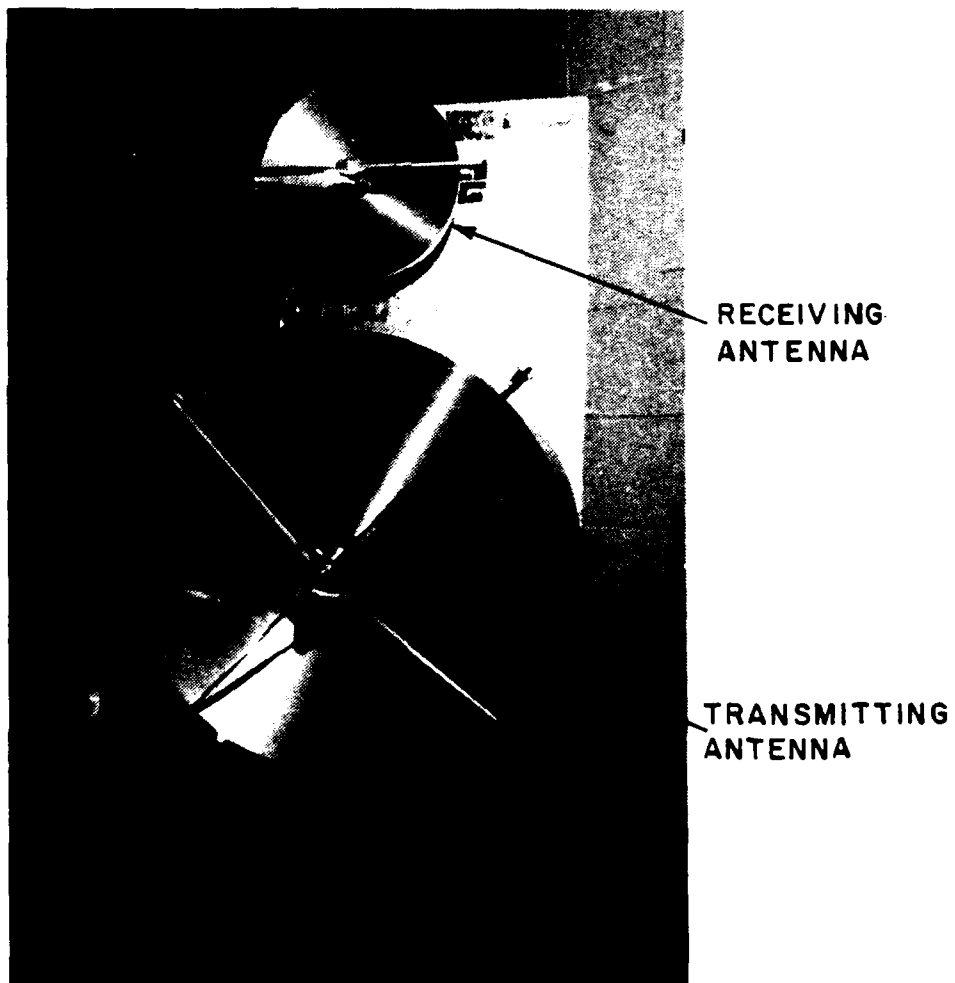


PLATE 2.2

TRANSMISSOMETER SIDE VIEW
(Absorber shrouds removed)

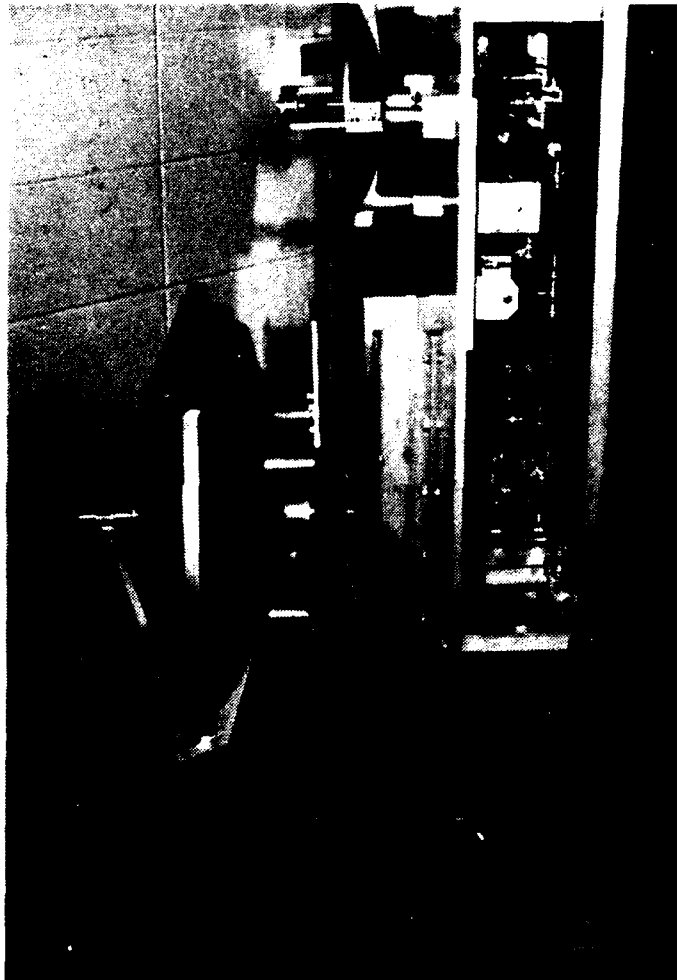


PLATE 2.3

OVERVIEW OF TRANSMISSOMETER COMPONENTS

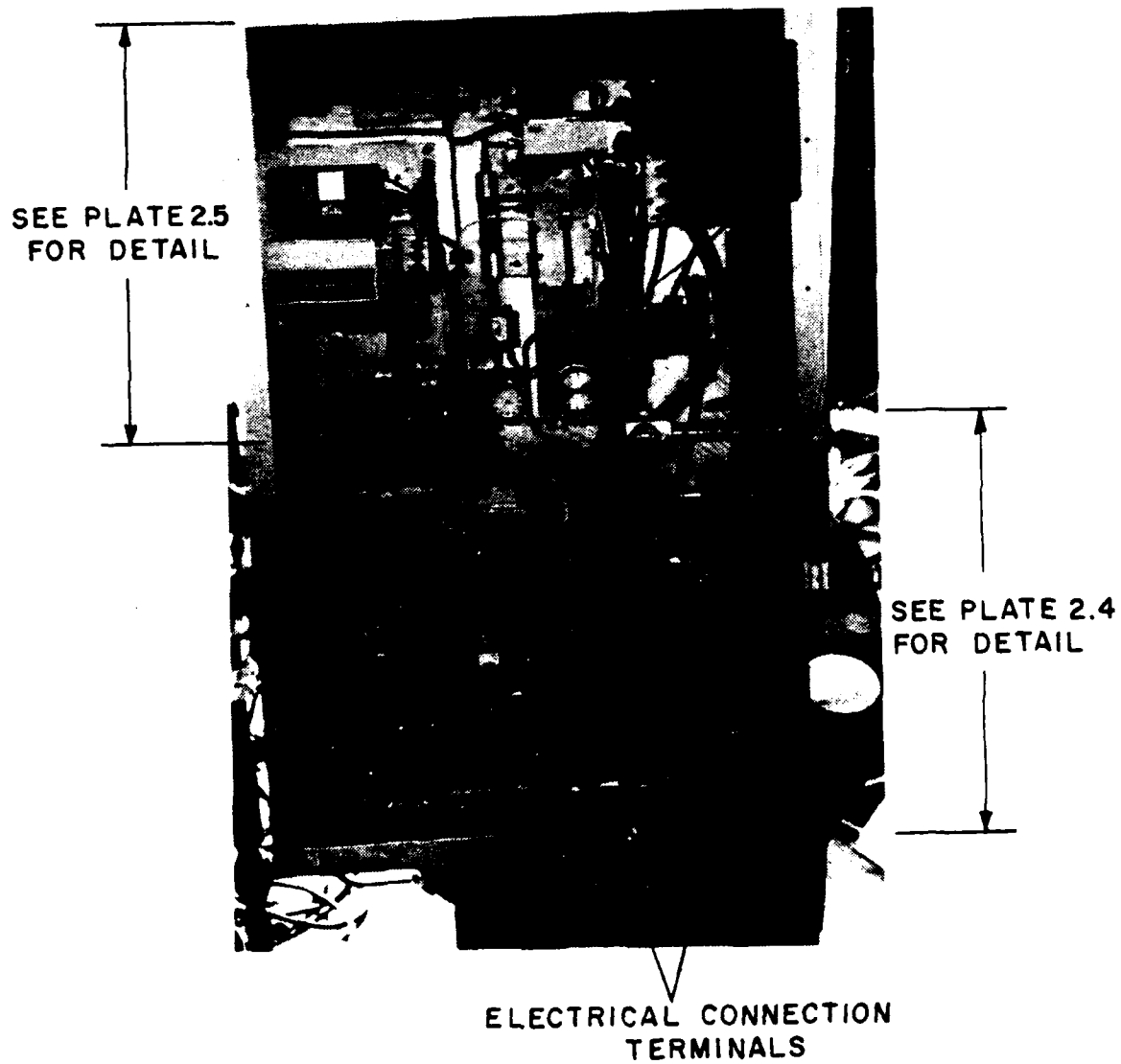
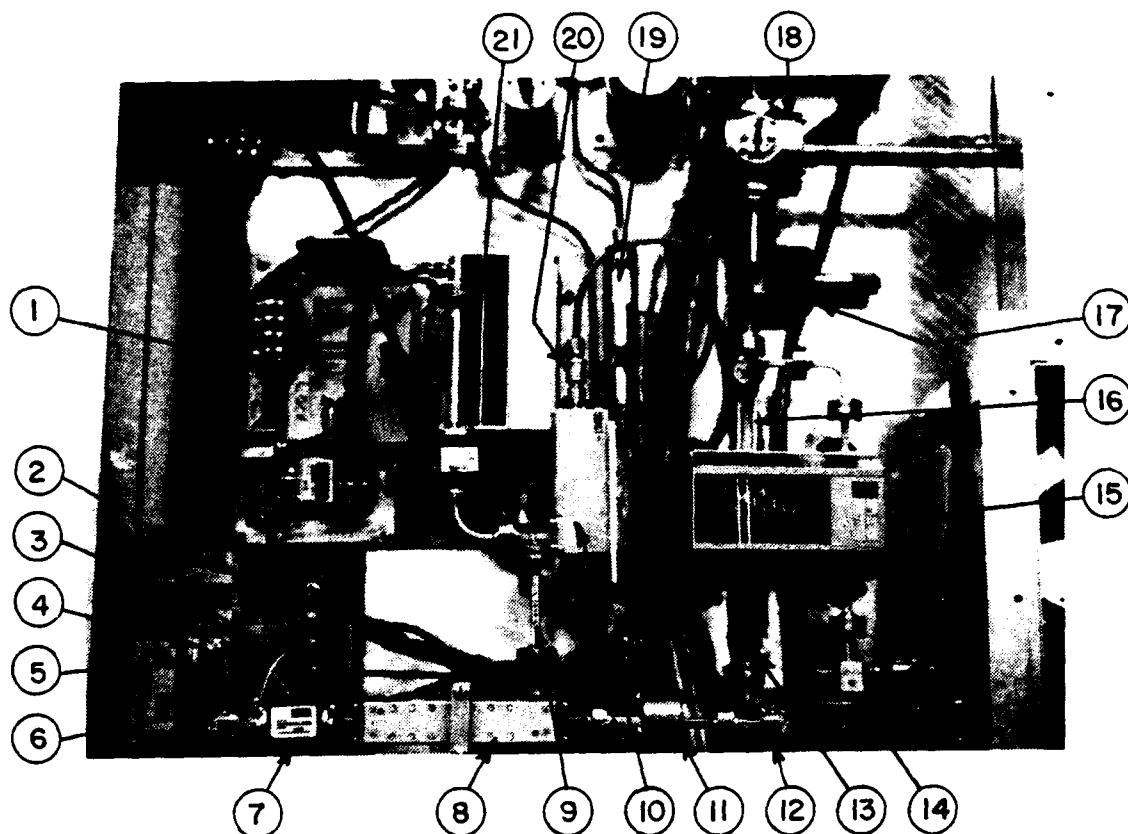


PLATE 2.4

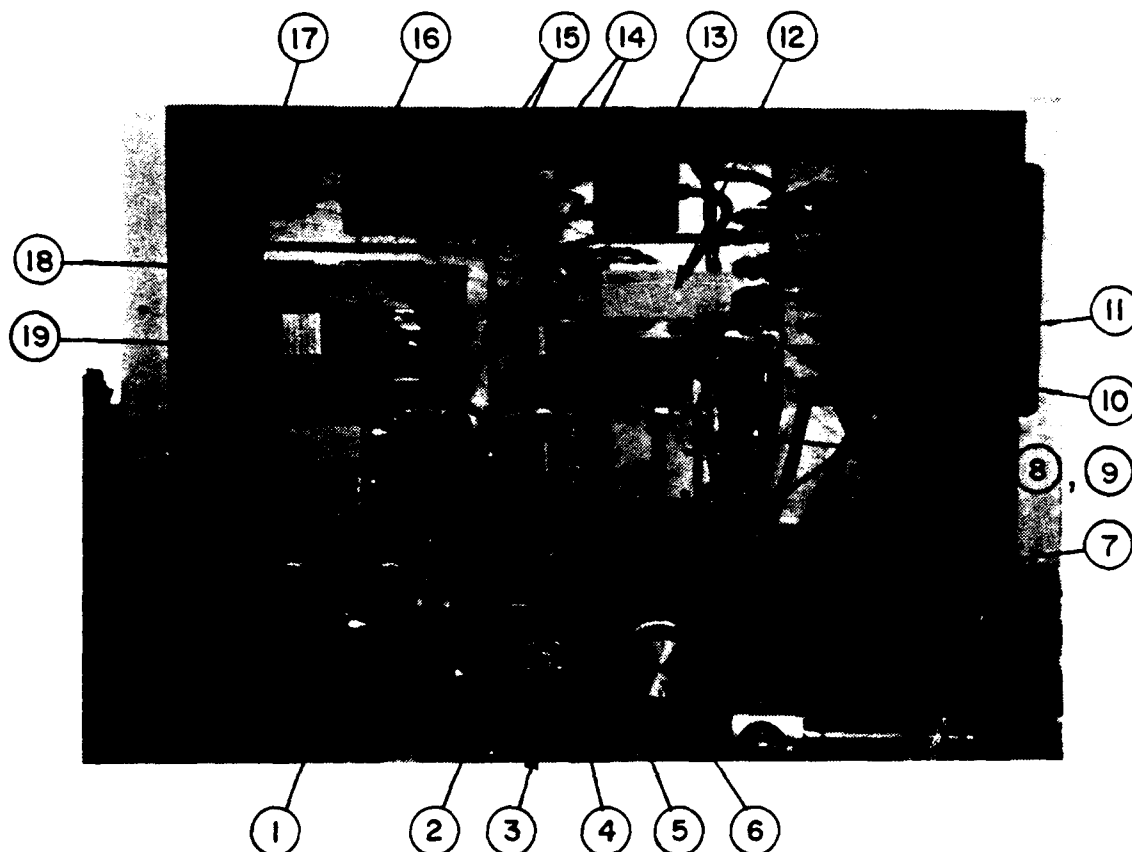
DETAIL OF BOTTOM HALF OF PLATE 2.3



1. Hughes 47764H-1001 Phase-Locked Gunn Oscillator (Locking Gunn)
2. Hughes Faraday-rotation isolator
3. Hughes 45166H-1000 circulator
4. Hughes IMPATT oscillator
5. IMPATT heater
6. IMPATT voltage regulator
7. Hughes 45146H-1000 y-junction isolator
(Items 2 through 7 are included in the Hughes 47196H-1120B CW injection-locked amplifier.)
8. Hughes 45326H-1010 directional coupler
9. Baytron 3-10-109S 50 dB fixed waveguide attenuator
10. TRG W9600-15 balanced mixer
11. Hughes 45216H-1000 full-band modulator
12. TRG W559-20 20 dB directional coupler
13. Baytron 3R-9/20 20 dB fixed waveguide attenuator
14. Hughes 47326H-1011 flat plate detector
15. TRG W551 Frequency Meter
16. TRG W559-6 6 dB directional coupler
17. Hughes 45766H-1200 variable phase shifter
18. Hughes 45526H-1000 waveguide switch
19. Texscan 5BD776/15-3 coaxial bandpass filter
20. Omni-Spectra 20510 10 dB fixed attenuator
21. Hughes 44650H y-junction isolator

PLATE 2.5

DETAIL OF TOP HALF OF PLATE 2.3



1. Hughes 47746H-1001 Phase-Locked Gun Oscillator (L.O. Gunn)
2. TRG 650W-387 H-Plane Tee
3. Telonic 8120S 100 dB step attenuator
4. Avantek UTC10-115M 28 dB amplifier
5. Texscan 5BD776/15-3 coaxial bandpass filter
6. Texscan RA-50 10 dB step attenuator
7. TRG 510W/387 variable attenuator
8. ESL 33 dB Gain 776 MHz amplifier
9. Avantek UTC10-109 37 dB gain amplifier (under 8)
10. TRG W559-20 20 dB directional coupler
11. Audio-frequency circuitry
12. TRG W9600-9 balanced mixer
13. MCL ZAPDQ-1 90 degree power divider
14. Midisco MDC 1089-1 adjustable phase shifters
15. MCL ZEM-2 Double Balanced Mixers
16. MCL ZAPD-1 Zero Degree Power Divider
17. Avantek UTC10-115M 28 dB amplifier
18. Merrimac PDM-20-250 3 dB power splitter
19. Techtrol HX0-178 97.007224 MHz Crystal with Oven.

CHAPTER III

SIGNAL ANALYSIS

A. INTRODUCTION

This chapter examines the frequency, phase, and amplitude characteristics of the signals processed by the receiver as well as the power and spectral characteristics of the noise. The frequency and phase characteristics are examined in part to show how the quadrature receiver functions independently of the phase of the received signal, but, more importantly, to develop an understanding of the waveforms and phase relationships which will be useful in understanding and trouble-shooting the receiver. The proportionality of the system output V_{out} and the amplitude of the received signal A_1 is discussed to determine how well the system will hold calibration. Signal amplitude characteristics are discussed to expose the points in the receiver where non-linearities would occur if signal levels were too high and how to guard against such non-linearities. Noise power is examined to assure that the noise level is sufficiently low so that the noise does not cause any non-linearity by saturating any component. The noise spectrum is examined in the audio frequency section to show how the synchronous detection process does indeed result in favorable signal-to-noise characteristics at the system output.

B. ANALYSIS OF SIGNAL FREQUENCY AND PHASE THROUGHOUT THE RECEIVER

1. Overview

In this section the operation of the receiver in terms of signal frequency and phase is examined by tracing a test signal through the receiver and observing changes in phase and frequency caused by various components in the RF, IF, and audio frequency sections. It is shown that the receiver functions properly independently of the received signal phase, as expected. The DC output signal V_{out} from the receiver is shown to be proportional to the amplitude A_1 of the received 94 GHz signal. Because Figures 2.3, 2.4 and 2.5 will be referred to extensively, it would be advantageous for the reader to have them readily accessibly to him while reading this chapter.

2. RF Section

At point {1} in Figure 2.3, the signal received by the receiving antenna is a modulated 94.000000 GHz signal of the form

$$v_1 = A_1 \cos(w_1 t + \phi_1) [1 + m \cos(w_3 t + \theta_1)] \quad (3.1)$$

where A_1 is the unknown amplitude, ϕ_1 is the phase of the 94 GHz signal, m is the modulation index, θ_1 is the phase of modulating signal,

$$w_1 = 2\pi \times 94 \text{ GHz} \quad , \quad (3.2)$$

and

$$w_3 = 2\pi \times 800 \text{ Hz} \quad , \quad (3.3)$$

where 800 Hz is the modulating frequency. In Equation (3.1) it is assumed that the modulation is sinusoidal for the sake of simplifying the analysis. The actual modulating signal is a square wave if the internal modulator is used, and roughly triangular in the case of the modulated target described in Appendix A. The notation of sinusoidal modulation can be used because all the additional sidebands are passed by the receiver RF and IF sections just like the w_3 term and the harmonics are then removed by filtering in the audio frequency section. At the TRG W9600-9 balanced mixer input, point {2}, there has been attenuation and phase shift resulting in a signal of the same form as Equation (3.1), but with new amplitude A_2 replacing A_1 and new RF phase ϕ_2 replacing ϕ_1 , so that

$$v_2 = A_2 \cos(w_1 t + \phi_2) [1 + m \cos(w_3 t + \theta_1)] \quad , \quad (3.4)$$

where

$$A_2 = t_1 A_1 \quad (3.5)$$

and t_1 is the transmittance of the waveguide and directional coupler between {1} and {2}. This signal is then mixed with the L.O. signal from the Hughes 47746H-1001 93.223942 GHz phase-locked Gunn oscillator which is of the form

$$v_{LO-1} = C_1 \cos(w_2 t + \phi_3) \quad (3.6)$$

where C_1 is the L.O. signal amplitude, ϕ_3 is the unknown L.O. phase, and

$$w_2 = 2\pi \times 93.223942 \text{ GHz} \quad . \quad (3.7)$$

Mixing these two signals yields a product term

$$v_3 = C_1 \cos(w_2 t + \phi_3) A_2 \cos(w_1 t + \phi_2) [1 + m \cos(w_3 t + \theta_1)] \quad (3.8)$$

or

$$v_3 = A_2 A_3 \{ \cos[(w_1 - w_2)t + \phi_2 - \phi_3] + \cos[(w_1 + w_2)t + \phi_2 + \phi_3] \} [1 + m \cos(w_3 t + \theta_1)] / 2 \quad (3.9)$$

The $\cos[(w_1 + w_2)t + \phi_2 + \phi_3]$ term from Equation (3.9) can be dropped because, at a frequency of 187 GHz, it is not passed through the preamplifier.

Thus, the modulated IF signal at point {4} is given by

$$v_4 = A_4 \{ \cos[w_4 t + \phi_2 - \phi_3] \} [1 + m \cos(w_3 t + \theta_1)] / 2, \quad (3.10)$$

where

$$w_4 = w_1 - w_2 = 2\pi \times 776.058 \text{ MHz} \quad , \quad (3.11)$$

and

$$A_4 = A_2 G_1 \quad , \quad (3.12)$$

where G_1 is the RF-to-IF gain of the TRG W9600-9 mixer/preamplifier.

The voltage v_4 is the modulated 776.058 MHz signal input to the IF signal channel (see Figure 2.4).

Performing a similar calculation when the reference input,

$$v_{14} = B_1 \cos w_1 t \quad , \quad (3.13)$$

is mixed with the L.O. signal V_{L0-2} present at the TRG W9600-15 balanced mixer, where

$$V_{L0-2} = C_2 \cos(w_2 t + \phi_5) \quad , \quad (3.14)$$

gives a product at the TRG W9600-15 balanced mixer output {15} after again dropping the $(w_1 + w_2)$ term,

$$v_{15} = [B_1 C_2 / 2L_c] [\cos(w_4 t - \phi_5)] \quad , \quad (3.15)$$

where L_c is the mixer conversion loss. Equation (3.15) represents the unmodulated 776.058 MHz IF reference signal at point {15}.

3. IF Section

Returning to the modulated 776.058 MHz signal, after preamplification in the TRG W9600-9 balanced mixer/preamplifier, filtering with the Texscan 5BD776/15-3 20 MHz tubular bandpass filter, amplification via a 28 dB gain Avantek UTC10-115M amplifier, attenuation with a Telonic 81205 attenuator, further amplification with another Avantek UTC10-115M, and splitting by a Mini-Circuits Lab ZAPD-1 zero degree power divider from points {3} to {9} in Figures 2.3 and 2.4, the signal is

$$v_9 = A_5 \cos(w_4 t + \phi_6) [1 + \cos(w_3 t + \theta_1)] \quad , \quad (3.16)$$

where

$$A_5 = t_2 G_2 t_3 G_3 t_4 A_4 \quad , \quad (3.17)$$

t_2 is the transmittance of the Texscan 5BD 776/15-3 bandpass filter, G_2 is the gain of the first Avantek UTC10-115M amplifier, t_3 is the transmittance of the Telonic 81205 attenuator, G_3 is the gain of the second Avantek UTC10-115M amplifier, t_4 is the transmittance of the

MCL ZAPD-1 power divider, and ϕ_6 is ϕ_4 plus additional IF phase shift introduced by the components from {3} to {9}.

Similarly, in the IF reference channel, after attenuation via an Omni-Spectra 20510 fixed 10 dB attenuator, filtering with a Texscan 5BD776/15-3 tubular bandpass filter, amplification with a 33 dB gain ESL-produced amplifier, attenuation via a Texscan RA-50 10 dB step attenuator, amplification by an Avantek UTC10-109 37 dB gain amplifier, and splitting with a Mini-Circuits Lab ZAPDQ-1 90° power divider, the signal from the zero degree port is

$$v_{19a} = B_2 \cos(\omega_4 t - \phi_7) \quad , \quad (3.18)$$

and that from the 90° port is

$$v_{19b} = B_2 \cos(\omega_4 t - \phi_7 - \pi/2) \quad , \quad (3.19)$$

where

$$B_2 = t_5 t_6 G_4 t_7 G_5 t_8 B_1 C_2 / (2L_c) \quad , \quad (3.20)$$

and t_5 is the transmittance of the Omni-Spectra 10 dB fixed attenuator, t_6 is the transmittance of the Texscan bandpass filter, G_4 is the gain of the ESL amplifier, t_7 is the transmittance of the Texscan step attenuator, G_5 is the gain of the Avantek UTC10-109 amplifier, t_8 is the transmittance of the MCL ZAPDQ-1 90° power divider, and ϕ_7 is ϕ_5 plus further IF phase shift introduced by components from {15} to {19}.

Thus Equation (3.16) represents the modulated IF signal at {9} and Equations (3.18) and (3.19) represent the in-phase and quadrature unmodulated IF reference signals, respectively, at {19}. These signals

are then mixed in Mini-Circuits Lab ZEM-2 mixers to yield the modulation in the audio frequency range. The result of mixing v_9 with v_{19a} is the in-phase (I) audio frequency signal and contains a term

$$v_{10} = [A_5/L_{c2}] \cos(w_4t+\phi_7) \cos(w_4t+\phi_6) \\ \times [1+m\cos(w_3t+\theta_1)] \quad (3.21)$$

$$= [A_5/2L_{c2}] [\cos\phi_6-\phi_7) \\ + \cos(2w_4t+\phi_6+\phi_7)] [1+m\cos(w_3t+\theta_1)] \quad (3.22)$$

at point {10}, where L_{c2} is the conversion loss in the MCL ZEM-2 double balanced mixer. Similarly, the result of mixing v_9 with v_{19b} is the quadrature (Q) audio frequency signal and contains a term

$$v_{20} = [A_5/L_{c2}] \cos(w_4t+\phi_7-\pi/2) \\ \times \cos(w_4t+\phi_6) [1+m\cos(w_3t+\theta_1)] \quad (3.23)$$

$$= [A_5/2L_{c2}] [\cos(\phi_6-\phi_7+\pi/2) \\ + \cos(2w_4t+\phi_6+\phi_7-\pi/2)] [1+m\cos(w_3t+\theta_1)] \quad (3.24)$$

at point {20}, where L_{c2} can be considered to be the same as in Equation (3.22), due to the use of mixers whose insertion loss varies by less than 0.2 dB between mixers.

4. Audio Frequency Section

Refer now to Figure 2.5. In the I channel, v_{10} is amplified and then processed by a low-pass filter which acts as an anti-aliasing

filter for the digital bandpass filter, centered at 800 Hz, which follows in the signal path. The signal at point {11} is

$$v_{11} = A_6 \cos(\phi_8) \cos(\omega_3 t + \theta_1 + \theta_2) \quad (3.25)$$

where θ_2 is an audio frequency phase shift introduced by the bandpass filter, G_6 is the gain of the amplifier and bandpass filter from {10} to {11}, and A_6 and ϕ_8 are defined by

$$A_6 = A_5 m G_6 / 2 L_{c2} \quad , \quad (3.26)$$

and

$$\phi_8 = \phi_6 - \phi_7 \quad . \quad (3.27)$$

At this point it becomes clear that the amplitude of this signal is dependent upon the $\cos(\phi_8)$ term in Equation (3.25) which is a function of the phase terms associated with the RF and IF signals. These phase terms are unknown and can be time-varying. Thus, the amplitude of the 800 Hz term must be determined without these unknown phase terms, a function which a quadrature receiver is designed to perform.

Amplification of the signal at {11} yields

$$v_{12} = A_7 \cos(\phi_8) \cos(\omega_3 t + \theta_1 + \theta_2 + \theta_3) \quad , \quad (3.28)$$

where

$$A_7 = G_7 A_6 \quad , \quad (3.29)$$

G_7 is the amplifier gain from {11} to {12} and θ_3 is an additional phase shift introduced by the coupling capacitors. Squaring the signal yields at {13}

$$v_{13} = [(A_7)^2/10] \cos^2(\phi_8) \cos^2(w_3t+\theta_1+\theta_3) \quad , \quad (3.30)$$

where the factor of 10 in the denominator is introduced by the squarer. This signal will be summed with the Q (quadrature) channel signal.

Refer now to the Q channel. In the same fashion as the I channel, the signal, v_{20} , is amplified and processed by a low-pass, anti-aliasing filter and then bandpass filtered to yield at {21}

$$v_{21} = A_6 \cos(\phi_8+\pi/2)\cos(w_3t+\theta_1+\theta_2) \quad , \quad (3.31)$$

where θ_2 is an audio frequency phase shift introduced by the bandpass filter. Amplification of the signal yields at {22}

$$v_{22} = A_7 \cos(\phi_8+\pi/2) \cos(w_3t+\theta_1+\theta_2+\theta_3) \quad (3.32)$$

where

$$A_7 = A_6 G_7 \quad , \quad (3.33)$$

G_7 is gain of the amplifier from {21} to {22} and θ_3 is the additional phase shift introduced by the coupling capacitors. The I and Q channels of the audio frequency circuitry have been tested to ensure the A_7 , θ_2 and θ_3 in Equation (3.22) are the same as A_7 , θ_2 and θ_3 , respectively, in Equation (3.28). Squaring the signal yields at {23}

$$v_{23} = [(A_7)^2/10] \cos^2(\phi_8+\pi/2)\cos^2(w_3t+\theta_1+\theta_2+\theta_3) \quad , \quad (3.34)$$

but since

$$\cos(x+\pi/2) = -\sin(x) \quad , \quad (3.35)$$

Equation (3.34) can be rewritten as

$$v_{23} = [(A_7)^2/10] \sin^2(\phi_8) \cos^2(w_3t+\theta_1+\theta_2+\theta_3) \quad . \quad (3.36)$$

Then the outputs of the I and Q channels, v_{13} and v_{23} , are summed to produce at {24}

$$v_{24} = [(A_7)^2/10] \cos^2(\omega_3 t + \theta_1 + \theta_2 + \theta_3) \times [\sin^2(\phi_8) + \cos^2(\phi_8)] \quad , \quad (3.37)$$

or since

$$\sin^2(\phi_8) + \cos^2(\phi_8) = 1 \quad , \quad (3.38)$$

Equation (3.37) can be rewritten as

$$v_{24} = [(A_7)^2/10] \cos^2(\omega_3 t + \theta_1 + \theta_2 + \theta_3) \quad . \quad (3.39)$$

Thus by using the quadrature signal, squaring, and summing, the signal is rid of dependence on the RF and IF phase terms represented by ϕ_8 , and the amplitude of the 800 Hz term can be determined independently of the unknown RF and IF phase terms.

Expanding the \cos^2 term in Equation (3.39), the equation can be rewritten as

$$v_{24} = [(A_7)^2/20] [1 + \cos(2\omega_3 t + 2\theta_1 + 2\theta_2 + 2\theta_3)] \quad , \quad (3.40)$$

which shows that the signal contains terms at two frequencies, at DC and twice the modulating frequency. It is possible to determine the magnitude of the modulation from either of these terms, but the $2\omega_3$ term will be used, since using this term reduces the noise, as will be shown in the discussion of the squarer in Section C.3 of this chapter. To remove the DC term, the signal is high-pass filtered. The signal is then processed by a synchronous detector, which is further discussed in Section C.3 of this chapter. This detection, which is performed using a synchronizing signal derived from the modulation source (modulated

target or Hughes modulator), results in the signal having a DC value, while the noise, though inverted each half cycle, remains zero-mean so that it can be reduced by a low-pass filter. The output of the low-pass filter at {25} is the system output V_{out} and is proportional to the $[(A_7)^2/10]$ term in Equation (3.40), which is proportional to $(A_1)^2$, the square of the amplitude of the received 94 GHz signal, in the following way:

$$V_{out} = \frac{k (t_1 t_2 t_3 t_4 G_1 G_2 G_3 G_6 G_7)^2}{10 (2L_{c2})^2} (A_1)^2, \quad (3.41)$$

where k is the proportionality term introduced by synchronous detection and low-pass filtering. The atmospheric attenuation, A , along the path can be determined from the ratio of A_{1-test} , the value of A_1 under test conditions, to $A_{1-clear}$, the value of A_1 under clear-air conditions. Using Equation (3.41), this can be calculated using the ratio of $V_{out-test}$, the value of V_{out} under test conditions, and $V_{out-clear}$, the value of V_{out} for negligible attenuation as in Equation (3.42*):

$$\frac{V_{out-test}}{V_{out-clear}} = \frac{(A_{1-test})^2}{(A_{1-clear})^2} \quad (3.42)$$

The accuracy of Equation (3.42) depends on whether or not the proportionality terms in Equation (3.41) remain constant from the time that $V_{out-clear}$ is recorded until $V_{out-test}$ is recorded. Table 3.1 lists each proportionality term in Equation (3.41) and its expected stability.

*It is assumed here for simplicity that all system parameters remain the same. Corrections for the case when this is not true are discussed in Appendix C; they do not affect the stability considerations discussed here.

TABLE 3.1
PROPORTIONALITY TERMS

TERM	SOURCE	STABILITY
<u>Transmittance Terms:</u>		
t_1	Waveguide and directional coupler from {1} to {2}	constant
t_2	Texscan bandpass filter	constant
t_3	Telonic attenuator	constant
t_4	MCL ZAP-1 power divider	constant
<u>Gain Terms:</u>		
G_1	TRG W9600 Mixer/Preamp.	depends on L.O. value, C_1^a
G_2	Avantek UTC10-115M	± 0.2 dB, -25 to 30°
G_3	Avantek UTC10-115M	± 0.2 dB, -25 to 30°
G_6	Audio-freq. amp and bandpass filter {10}-{11}	see note b.
G_7	Audio-freq. amp. {10}-{11}	see note b.
<u>Misc. Terms:</u>		
k	synchronous detector	see note b.
L_{c2}	MCL ZEM-2 mixers	Depends on IF ref. value, B_2^c
10	Audio-freq. squarer	see note b.
a.	See text below for discussion of C_1 .	
b.	See text below for discussion of audio-frequency circuitry temperature dependence.	
c.	See text below for discussion of B_2 .	

The value of C_1 , the amplitude of the L.O. Gunn Oscillator, is constant below 30° C and changes by -0.05 dB/°C from 30 to 50° C. The value of G_1 can therefore be considered constant.

The individual components of the audio-frequency circuitry have not been tested to determine their stability. However, it has been noted that temperature increase produced by briefly heating the circuit boards, which were initially at room temperature, with a heat gun caused a 3 dB decrease in V_{out} . Correction of this problem is one of the recommendations of Chapter VI.

The value of B_2 , the unmodulated 776.058 MHz reference signal used at the L.O. signal for the MCL ZEM-2 double balanced mixers, is dependent on the values of the reference channel proportionality terms as shown in Equation (3.43),

$$B_2 = t_5 t_6 t_7 t_8 G_4 G_5 B_1 C_2 / 2L_c, \quad (3.43)$$

where t_5, t_6, t_7 and t_8 are the transmittance of the Omni-Spectra 10 dB fixed attenuator, Texscan filter, Texscan attenuator, and MCL ZAPDQ-1 power divider, respectively, and can be considered constant. The symbols G_4 and G_5 denote the gains of the ESL-produced amplifier, an Avantek design using Avantek GPD-402 integrated circuits (see Appendix D), and the Avantek UTC10-109 amplifier. Both are subject to ± 0.2 dB gain variations over -25 to +30° C, which can be considered negligible. The 94 GHz reference signal amplitude B_1 can be considered constant, as it is derived from the IMPATT amplifier, which remains at a constant temperature because of the IMPATT heater. The drift of C_2 can be

considered negligible, as it is subject to the same specifications as C_1 . The conversion loss L_c in the TRG W9600-15 balanced mixer depends on the value of C_2 and thus can be considered stable. Since all the terms in Equation (3.43) are stable, the voltage B_2 can be considered a stable quantity.

Thus, the proportionality terms in Equation (3.41) remain constant with the exception of the terms from the audio-frequency circuitry. Future design changes might include a thermostatically controlled heater to keep the audio-frequency circuitry at a constant temperature, or redesign of the circuitry to eliminate the problem.

One further point must be noted with regard to the performance of the receiver with varying phase. In the preceding analysis, the RF and IF phase terms ϕ_1, ϕ_2 , etc., were considered to be arbitrary, but constant. However, this is not always a good assumption because the phase is subject to slow variations with temperature and possibly rapid variations due to changes in the target range (as the result, for example, of the target vibrating or moving slightly from a strong wind).

Such a time-varying phase term will not affect the RF or IF performance, but will be noticed in the audio frequency section. Consider Equation (3.22), which gives v_{10} , the input to the I channel. If one of the RF or IF phase terms is time-harmonic with an angular frequency w , the equation for v_{10} is

$$v_{10} = [A_5/L_c] \cos(w_4 t + \phi_7) \cos(w_4 t + \phi_6 + \beta \sin wt) \\ \times [1 + m \cos(w_3 t + \theta_1)] \quad (3.44)$$

or

$$v_{10} = [A_5/2L_c] [\cos(\phi_6 - \phi_7 + \beta \sin \omega t) + \cos(2\omega_4 t + \phi_6 + \phi_7 + \beta \sin \omega t)] [1 + m \cos(\omega_3 t + \theta_1)]. \quad (3.45)$$

The $\omega_4 t$ term in Equation (3.45) can be dropped because, at a frequency of 1552 MHz, it is not passed through the bandpass filter. Expanding the $\cos(\phi_6 - \phi_7 + \beta \sin \omega t)$ term in Equation (3.45) yields

$$v_{10} = [A_5/2L_c] \cos(\phi_6 - \phi_7 + \beta \sin \omega t) [1 + m \cos(\omega_3 t + \phi_1)], \quad (3.46)$$

which can also be written as

$$v_{10} = [A_5/2L_c] [\cos(\phi_6 - \phi_7) \cos(\beta \sin \omega t) + \sin(\phi_6 - \phi_7) \sin(\beta \sin \omega t)] [1 + m \cos(\omega_3 t + \phi_1)]. \quad (3.47)$$

Expanding the $\cos(\beta \sin \omega t)$ and $\sin(\beta \sin \omega t)$ terms in Equation (3.47) yields

$$v_{10} = [A_5/2L_c] \{ \cos(\phi_6 - \phi_7) [J_0(\beta) + 2J_2(\beta) \cos 2\omega t + 2J_4(\beta) \cos 4\omega t + \dots] + \sin(\phi_6 - \phi_7) [2J_1(\beta) \sin \omega t + 2J_3(\beta) \sin 3\omega t + \dots] \} [1 + m \cos(\omega_3 t + \theta_1)], \quad (3.48)$$

where $J_n(\beta)$ is the Bessel function of the first kind of order n .

Equation (3.48) has terms at DC, ω_3 , ω , $\omega_3 - \omega$, $\omega_3 + \omega$, 2ω , $\omega_3 - 2\omega$, $\omega_3 + 2\omega$, 3ω , $\omega_3 - 3\omega$, $\omega_3 + 3\omega$, etc. The desired ω_3 term is now weighted by $J_0(\beta)$.

For small β , $J_0(\beta)$ is near unity, but β is unknown and therefore the

value of the w_3 term is unpredictable. In addition to this, depending upon the value of w , unwanted terms may pass through the bandpass filter, add to the w_3 term and produce inaccurate results.

Under normal conditions, no problem of this nature was observed while using the system with a corner reflector. However, such a problem has been observed using a hand-held corner reflector as a target, and also with a corner reflector anchored to a ladder in a very strong wind. It is therefore recommended that the target be well fastened to a very firm support. The problems encountered with the modulated target may also be related to this effect (see Appendix A).

C. ANALYSIS OF SIGNAL AMPLITUDE, NOISE POWER, AND SPECTRAL CHARACTERISTICS IN THE RECEIVER

1. Signal Amplitude

As previously stated, the amplitude characteristic of the signals in the receiver must be known so that no component is driven into non-linear behavior. Table 3.2 lists the various components in the receiver I.F. signal channel, along with the maximum input power in dBm for which the device retains its linear behavior, the signal power in dBm at the input (assuming a power P_2 dBm at the TRG W9600-9 mixer/preamplifier input), and the device gain (positive) or insertion loss (negative) in dB.

Using Table 3.2, it is seen that only the TRG W9600-9 mixer/preamplifier, the two Avantek UTC10-115M amplifiers and the MCL ZEM-2 double balanced mixer play a role in determining the maximum

allowable signal levels in the receiver, since all other components have much higher power handling capabilities.

As an example, assume $P_2 = -80$ dBm and follow the signal level through Table 3.2. The first critical component in the signal path is the TRG mixer/preamplifier. With $P_2 = -80$ dBm, the mixer/preamplifier input is 56 dB below its maximum allowable value, and therefore the device remains linear. The second component to consider is the first Avantek UTC10-115M amplifier. With $P_2 = -80$ dBm, the input at the Avantek is

$$P_5 = P_2 + 20 \text{ dB} = -60 \text{ dBm}, \quad (3.49)$$

which is about 40 dB below its maximum allowable input of -21 dBm, so this amplifier is also operating in its linear range. The next critical component in line is the second Avantek amplifier, whose input power, with A_{if} set to zero, is

$$P_7 + P_2 + 47.75 \text{ dB} - A_{if} = -32.25 \text{ dBm} \quad , \quad (3.50)$$

which is about 12 dB below the maximum allowable input of -21 dBm, also in its linear range. The next component to consider is the MCL ZEM-2 double balanced mixer, whose input power is

$$P_9 = P_2 + 72.5 \text{ dB} - A_{if} = -7.5 \text{ dBm}, \quad (3.51)$$

which is just below the maximum allowable input for linear operation.

Therefore each IF component operates in its linear range for

$P_2 < -80$ dBm, when $A_{if} = 0$.

TABLE 3.2

SIGNAL POWER LEVELS IN THE RECEIVER IF SIGNAL CHANNEL

<u>Device</u>	<u>Maximum Input for Linear Operation</u>	<u>Signal Power at Input (dBm)</u>	<u>Device Gain or Insertion Loss</u>
TRG W9600-15 Mixer/Preamp	-24 dBm	P_2^a	+ 24 dB
Texscan Tubular Filter	+30 dBm	$P_4 = P_2 + 24 \text{ dB}$	- 4.0 dB
Avantek UTC10-115M Integrated Amplifier	-21 dBm	$P_5 = P_2 + 20 \text{ dB}$	+ 28 dB
Telonic 8120S Step Attenuator A_{if}^b	+27 dBm	$P_6 = P_2 + 48 \text{ dB}$	-0.25 dB
Avantek UTC10-115M Integrated Amplifier	-21 dBm	$P_7 = P_2 + 47.75 \text{ dB}$ $-A_{if}$	+ 28 dB
MCL ^c ZAPD-1 0° Power Divider	+40 dBm	$P_8 = P_2 + 72.75 \text{ dB}$ $-A_{if}$	-3.25 dB
MCL ZEM-2 Double Balanced Mixer	- 7 dBm	$P_9 = P_2 + 72.5 \text{ dB}$ $-A_{if}$	

a. P_2 , P_4 , etc., refer to the power level at points 2, 4, etc., in Figures 2.3 and 2.4.

b. A_{if} is the attenuation setting in dB of the 0 to 100 dB Telonic 8120S 10 dB step attenuator.

c. MCL denotes Mini-Circuits Lab.

Should P_2 ever be larger than -80 dBm, the Telonic step attenuator may be used to adjust A_{if} such that the input power levels to the components which follow in the signal path is acceptable. One must be cautious though, since adjusting A_{if} will only reduce the signal level after the Telonic attenuator. Thus, the power input level to the TRG mixer/preamplifier and the first Avantek UTC10-115M amplifier may be too high. Using Table 3.2, it can be seen that a power level of $P_2 = -41$ dBm, with $A_{if} = 40$ dB, results in a -21 dBm input at the first Avantek UTC10-115M amplifier, the maximum allowed. Thus $P_2 = -41$ dBm is the maximum for linear operation. Therefore, if a setting of greater than 40 dB is required for the Telonic attenuator, the first Avantek amplifier is saturated. A test for linear operation is given in Chapter V, Section C.4. The value of P_2 depends on the range and the reflectivity of the target. Figure 3.1 shows R_{min} , the minimum range, versus the radar cross section, σ , of the target. This was calculated using the radar equation (Equation 4.2), with the following parameters: $P_t = 0.2$ watts, $G_t = 10^{5.3}$, $G_r = 10^{4.7}$, $\lambda = 3.19 \times 10^{-3}$ meters, $t_t = 0.15$, and $t_r = 0.6$. The Telonic attenuator setting was assumed to be 40 dB and the theoretical triangular trihedral corner reflector sizes are calculated from the equation given in Figure 4.3.

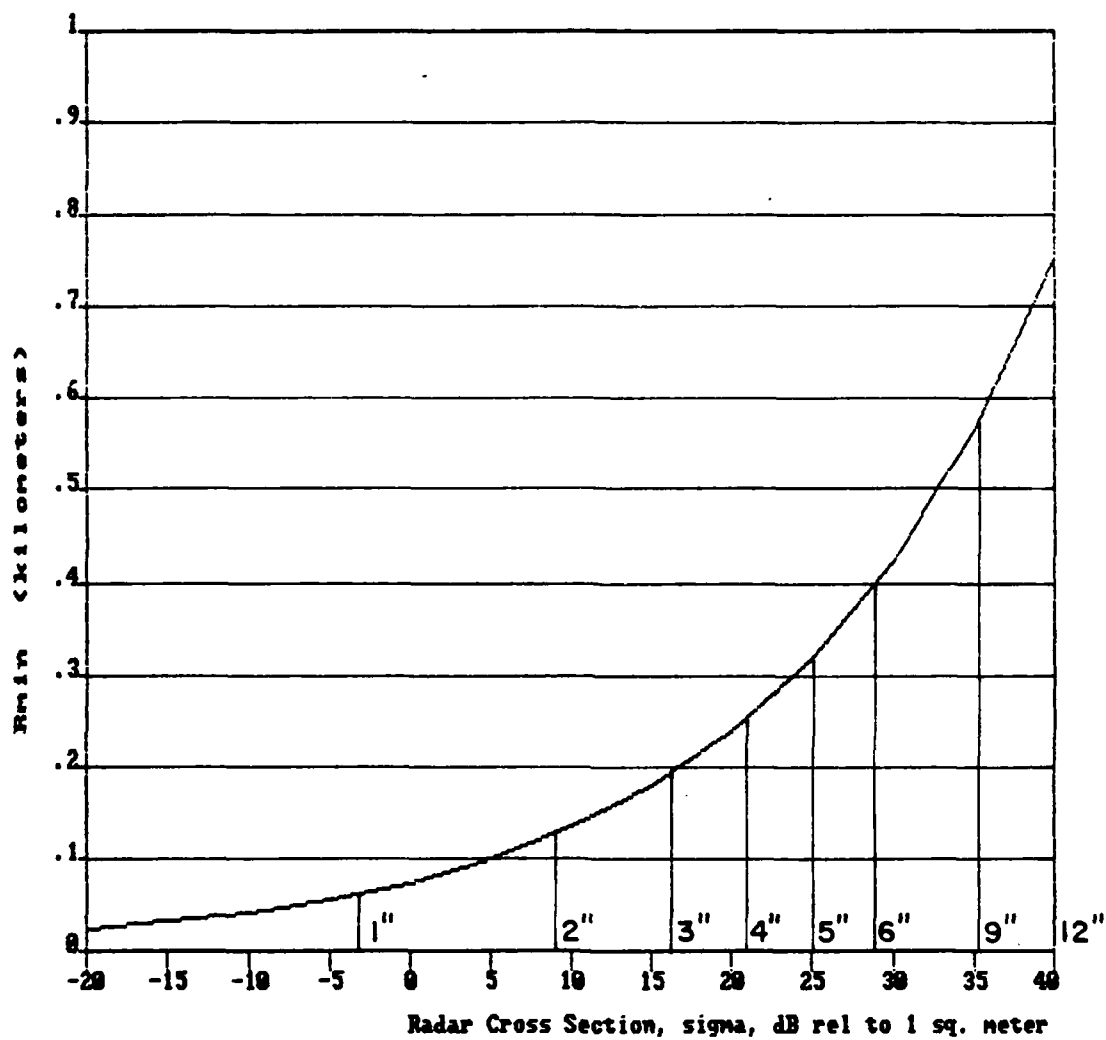


Figure 3.1. R_{min} versus theoretical radar cross section of target.

The audio frequency circuitry has been designed so that it will remain in its linear range as long as the input to the ZEM-2 double balanced mixer is below -7 dBm. Thus, for an input to the TRG W9600-9 mixer/preamplifier of $P_2 = -80$ dBm and with A_{if} set to zero, the audio frequency circuitry output is its maximum linear output value of 10.0 VDC.

Therefore there is no danger of overdriving any part of the system provided the minimum range of Figure 3.1 is not exceeded and the Telonic IF attenuation is set so that the output voltage V_{out} does not exceed 10 volts. Note that a measurement should always be begun with the Telonic attenuator set at maximum attenuation, and the attenuation should then be reduced gradually to bring V_{out} into its proper range.

Refer now to the IF reference channel (see Figures 2.3 and 2.4). The required signal level at the input to the MCL ZAPDQ-1 90° power divider is +10 dBm, or 10 mW, so that the MCL ZEM-2 double balanced mixers will be properly biased. Therefore the Texscan RA-50 zero-to-ten dB, one-dB-per-step rotary attenuator must be adjusted so that the +10 dBm level is present at the MCL ZAPDQ-1 90° power divider input after the signal is filtered by the Texscan 5BD776/15-3 tubular bandpass filter and amplified by the 33 dB ESL-produced amplifier and 37 dB Avantek UTC10-109 amplifier. The proper setting of the Texscan RA-50 attenuator has been determined experimentally to be 3 dB.

A question that may occur as the IF reference channel is studied is the purpose of the Baytron 3-10-109S 50 dB fixed waveguide attenuator (refer to Figure 2.3). It appears to do nothing more than attenuate the

unmodulated reference signal at 94 GHz, thus requiring the signal to be amplified more in the IF reference channel. It is, in fact, true that more IF amplification is needed because of the reduction of the 94 GHz reference by the Baytron fixed attenuator; however, the attenuator is required to control leakage of the unmodulated 94 GHz reference signal into the signal channel. It may not be obvious, but some of the reference signal entering the RF port of the TRG W9600-15 balanced mixer passes out of the LO port, through the Hughes 44650H y-junction isolator, through the TRG 650W-387 H-plane tee and into the LO port of the TRG W9600-9 balanced mixer/preamplifier, where it is converted to an unmodulated 776.058 MHz signal. The fact that this signal is unmodulated means that it will be ignored by the signal processing circuitry, which only responds to 800 Hz modulation, as long as the unmodulated 776.058 MHz leak is at a low enough level so that it does not saturate any components in the IF signal channel. Thus the Baytron 3-10-109S 50 dB fixed waveguide attenuator is used to insure that the leaking unmodulated 776.058 MHz signal remains at a harmlessly low level. The Hughes 44650H y-junction isolator serves the same purpose. Together, they reduce the leaking signal to a level of -130 dBm at the TRG W9600-9 mixer/preamplifier input, 50 dB below where it would cause any component to saturate.

2. Noise Power

In theory, noise contributions in the IF signal channel may come from several sources, such as antenna noise, noise from lossy waveguide,

mixers, amplifiers, and attenuators. However, more careful consideration and experimental results show that the only significant source of noise in the signal channel is the contribution from the TRG W9600-9 mixer/preamplifier. Theoretically, the contributions to noise of all components after the mixer/preamplifier are insignificant. To show that the antenna noise is negligible, the IF noise spectrum was observed with the receiving antenna first pointed into free space and then short circuited at the feed horn; no difference in IF noise level was observed. The TRG W9600-9 mixer/preamplifier contribution to the noise is calculated to be

$$N = kT_0 F, \quad (\text{W/Hz}) \quad (3.52)$$

where

$$k = 1.38 \times 10^{-23} \quad (\text{Boltzmann's constant}), \quad (3.53)$$

$$T_0 = 290 \text{ K}, \quad (3.54)$$

and

$$F_{\text{dB}} = 4.6 \text{ dB}, \quad (3.55)$$

or

$$F = 2.88 \text{ (numeric)} \quad (3.56)$$

is the TRG W9600-9 mixer/preamplifier standard noise figure. The total noise spectral density is then

$$N = 11.5 \times 10^{-21} \quad (\text{W/Hz}). \quad (3.57)$$

After the preamplifier, with a gain of 24 dB, the noise spectral density is

$$N = 2.90 \times 10^{-18} \quad (\text{W/Hz}). \quad (3.58)$$

and the noise power is

$$\begin{aligned} P_{n4} &= 2.9 \times 10^{-18} \quad (\text{W/Hz}) \times 900 \times 10^6 \quad (\text{Hz}) \\ &= 2.6 \times 10^{-9} \quad (\text{W}) \end{aligned} \quad (3.59)$$

at point {4} in Figure 2.3 and is spread over the entire 100 to 1000 MHz bandwidth of the preamplifier. If there were no filter to remove this noise, with A_{if} set to zero, the noise power at the ZEM-2 double balanced mixer would be

$$P_{n9} = 10 \log(2.6 \times 10^{-9}/10^{-3}) + 48.5 \text{ dB} = -7.3 \text{ dBm}, \quad (3.60)$$

which is approximately the allowable signal level! Thus the Texscan 5BD776/15-3 tubular filter is essential in reducing the total noise power. With the filter in the signal path, the noise power is reduced by 16.5 dB, so that the noise level at the ZEM-2 should be an acceptable -24 dBm (measurements show a -20 dBm noise level at this point). Note that signals on the order of -40 dBm are likely to be present also at the ZEM-2 input, so that the reduction of noise by the Texscan filter cannot be the final noise reduction if a satisfactory signal-to-noise ratio is to be achieved. It only assured that no components will be saturated by noise. The final stages of noise reduction are not performed until low-pass filtering of the synchronous detector output.

The noise in the IF reference channel is also dominated by the TRG W9600-9 mixer contribution. However, since the unmodulated signal in this channel is more than 30 dB above the noise, the noise can be neglected.

3. Noise Spectral Characteristics

This section examines the spectral characteristics of the noise in the receiver, focusing on the audio frequency section in order to show how signal-to-noise ratio at the system output relates to the system configuration and parameters. Two questions must be considered. The first concerns the output of the audio frequency summer (refer to Figure 2.5). This output contains, as a result of squaring the detected 800 Hz modulating signal, two terms of interest. As shown by Equation (3.40), one term is at DC and the other at 1600 Hz, twice the modulation frequency, and both are proportional to the 94 GHz power returned from the target. Which term should be used? The detailed analysis, below, of the effect of the squarer on signal and noise shows that the 1600 Hz term is the more desirable term to use. The second question to be examined is whether full wave rectification or synchronous detection to convert the 1600 Hz signal to DC produces a better signal-to-noise ratio at the system output. Examination of the signal and noise spectra in the receiver are necessary to answer these questions.

The one-sided signal-plus-noise spectrum, $2S_{s+n}$, at the output of the MCL ZAPD-1 zero degree power divider, point {9} (refer to Figure 2.4), is shown in Figure 3.2. Figure 3.3 is a close-up version of



Figure 3.2. Signal-plus-noise spectrum at MCL ZAPD-1 power divider output, point {9}.

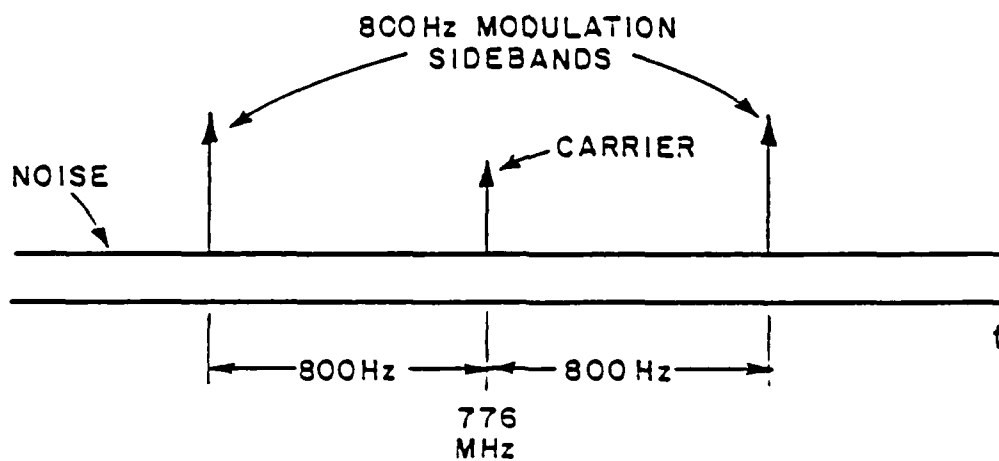


Figure 3.3. Close-up of modulated 776 MHz signal in Figure 3.2, showing carrier and sidebands.

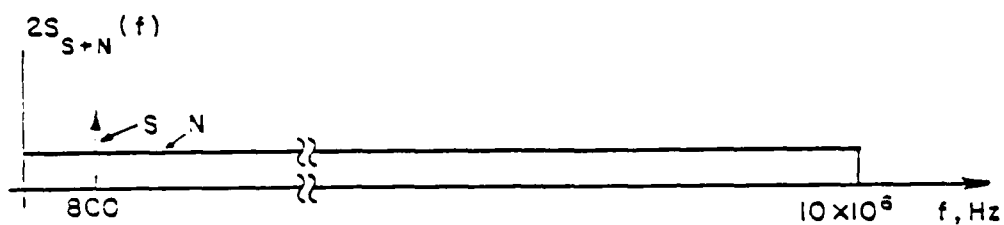


Figure 3.4. Signal-plus-noise spectrum at ZEM-2 double balanced mixer outputs, points {10}, {20}.

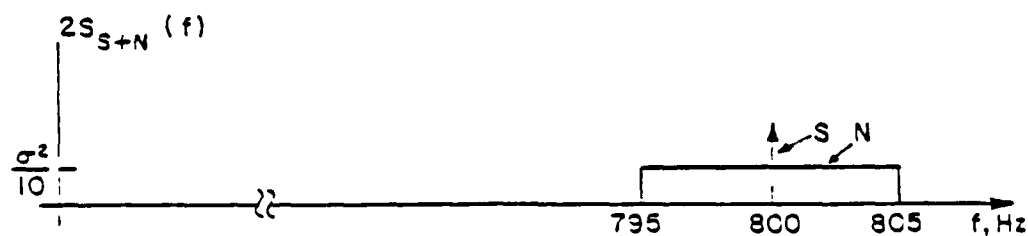


Figure 3.5. Signal-plus-noise spectrum at squarer input, points {12}, {22}.

Figure 3.2, showing the 776 MHz carrier and the modulation sidebands. The MCL ZEM-2 double balanced mixers have two inputs, denoted "RF" and "L.O.," and one output denoted "IF." These are not the RF, L.O., and IF signals mentioned previously; hence the "RF," "L.O.," and "IF" signals associated with the ZEM-2 double balanced mixers will be left in quotation marks. The mixers operate such that the output is equal to the "RF" (modulated 776.058 MHz IF signal) input multiplied by a square wave at the "L.O." (unmodulated 776.058 MHz IF reference) frequency [18]. Since the "L.O." square wave can be decomposed into a fundamental plus harmonics, but only the difference frequency of the fundamental and the "RF" signal falls within the passband of the audio frequency section which follows, this has the effect of shifting the "RF" (modulated 776.058 MHz IF) signal to baseband (i.e., recovering the modulation), as if the "RF" signal were simply multiplied by a sinusoidal signal at the "L.O." frequency. Figure 3.4 shows the signal-plus-noise spectrum at the MCL ZEM-2 double balanced mixer outputs {10}. The output at point {20} could also be considered, but since the processing in the I and Q channels is identical, the same result is obtained. Figure 3.5 shows the signal-plus-noise spectrum at the input to the squarer, point {12} (refer to Figure 2.5), where $\sigma^2/10$ is the noise power per unit bandwidth (watts/Hz). The bandwidth has been reduced greatly by the digital filter.

The analysis of the squarer's effect on signal and noise follows Schwartz [19] and Blachman [20]. At the input to the squarer, the signal voltage present is

$$u(t) = s(t) + n(t), \quad (3.61)$$

where

$$s(t) = A \cos(\omega_m t + \theta) \quad (3.62)$$

and $n(t)$ is narrow-band noise. The shape of the power spectral density of $n(t)$ is determined by the digital filters and is sketched in Figure 3.5. The output voltage of the squarer at {13} is

$$v(t) = [s(t) + n(t)]^2 = s^2(t) + 2s(t)n(t) + n^2(t). \quad (3.63)$$

The $s^2(t)$ term is the only term which contributes to output signal; the $2s(t)n(t)$ and $n^2(t)$ terms both contribute to output noise only. Therefore, the output signal spectrum is the spectrum of the $s^2(t)$ term, $2S_{sxs}(f)$, given in Equation (3.64),

$$2S_{sxs}(f) = 1/8 A^4 \delta(f - 2f_m) + 1/4 A^4 \delta(f), \quad (3.64)$$

where $\delta(f)$ is the impulse function and f_m is the modulating frequency. This spectrum is shown in Figure 3.6. The $2s(t)n(t)$ term contributes noise whose spectrum at the squarer output is denoted by $2S_{sxn}(f)$,

$$2S_{sxn}(f) = 2A^2 S_n(f - f_m) + A^2 \sigma^2 \delta(f), \quad (3.65)$$

where σ^2 is the average noise power at the squarer input and $S_n(f)$ is the noise power spectrum at the squarer input, shown in Figure 3.5. The spectrum represented by Equation (3.65) is shown in Figure 3.7. The spectral contribution of the $n^2(t)$ term is $2S_{n xn}(f)$, given in Equation (3.66),



Figure 3.6. SxS spectrum at squarer output.



Figure 3.7. SxN spectrum at squarer output.

$$2S_{n \times n}(f) = 4 S_n(f) * S_n(f) + \sigma^4 \delta(f), \quad (3.66)$$

where * indicates convolution. The spectrum represented by Equation (3.66) is shown in Figure 3.8. The sum of Equations (3.64), (3.65), and (3.66) equals the spectrum of $v(t)$, $2S_v(f)$, given in Equation (3.67).

$$\begin{aligned} 2S_v(f) = & 1/8 A^4 \delta(f-2f_m) + 4 S_n(f) * S_n(f) \\ & + 2A^2 S_n(f-f_m) + (1/4 A^4 + A^2 \sigma^2 + \sigma^4) \delta(f) \end{aligned} \quad (3.67)$$

It is shown in Figure 3.9.

The output spectrum shown in Figure 3.9 is valid at the summer output {24}. It will now be shown why it is desirable to use the signal located at 1600 Hz rather than the signal located at DC to determine the $(A_7)^2$ term in Equation (3.40), and thus the amplitude of the returned RF signal. Observe that in Equation (3.67), there are three DC terms: $1/4A^4$, $A^2\sigma^2$, and σ^4 . Of these three, only the first term is unambiguously related to the signal. Both $A^2\sigma^2$ and σ^4 terms are noise terms, in the sense that their presence in the output injects an uncertainty, depending on σ , into the input/output relationship of the system. From Figure 3.9 it is clear that the signal-to-noise ratio at this point (the summer output, {24}) can be improved by low-pass filtering to remove the noise around DC. However, since there is an impulse function noise term located at DC, i.e., a noise term with the same functional dependence as the DC signal term, it is impossible to remove this noise by filtering. In fact, the DC noise terms account for one half of the total noise in the DC to 10 Hz band independently of the



Figure 3.8. $N \times N$ spectrum at squarer output.



Figure 3.9. Signal-plus-noise spectrum at squarer output, points {13}, {23}.

signal level, so the best signal to noise improvement possible by filtering is only 3 dB. It is clear that the problem is the noise terms at DC, which can not be separated from the signal. Thus it is desirable to find an alternate method of determining the signal level.

This alternate method is to observe the signal at 1600 Hz rather than DC. Equation (3.67) shows that the only term at 1600 Hz is the A^4 term, which is a signal term. There is noise around 1600 Hz, from 1590 Hz to 1610 Hz, as can be seen in Figure 3.9, but there is no $\delta(f-1600 \text{ Hz})$ noise term; so in this case reducing the bandwidth can substantially reduce the noise and therefore improve the signal-to-noise ratio. All that remains is to convert the 1600 Hz signal to DC in such a way that the noise bandwidth can be reduced by low-pass filtering. (In principle, one could filter at 1600 Hz and then rectify, but in practice it is difficult or impossible to obtain the required narrow bandwidth.)

Two methods of converting the 1600 Hz sinusoidal signal to DC were considered. The first is simply to full wave rectify the sinusoid and low-pass filter the resulting signal to yield a DC value. However, this method suffers under low signal-to-noise ratio conditions. For example, take the case where there is noise present, but no signal. The full wave rectifier will then rectify the previously zero-mean noise, resulting in an average DC noise term at the low-pass filter output. This solution is unsatisfactory, since the reason for using the 1600 Hz term is to eliminate DC noise terms. Thus it is necessary to use another method of converting the sinusoid to a DC value.

The method used is synchronous (coherent) detection. The synchronous detector inverts the 1600 Hz sinusoid every half cycle, thus performing essentially the same function on the sinusoid as the full wave rectifier (see Figure 3.10). The synchronizing square wave is derived from the modulation source and its phase must match that of the sinusoid. (Phase adjustment is provided.) The difference between the full wave rectifier and the synchronous detector is in their effect on noise. While full wave rectified noise has a DC component, noise processed by the synchronous detector does not, as will be discussed heuristically and shown rigorously. The reason is that the noise in the synchronous detector is only inverted every half period, which does not change its zero-mean characteristic. Thus it is possible to low-pass filter the output of the synchronous detector and remove as much of the noise as is desired. An additional advantage of the synchronous detector is that it provides the removal of the quadrature component of the noise at 1600 Hz after low-pass filtering. The output spectrum of the synchronous detector near DC is shown in Figure 3.11, and is derived as follows. Let the synchronous detector input $v_1(t)$, shown in Figure 3.10, be

$$v_1(t) = A \cos(\omega t + \theta), \quad (3.68)$$

where

$$\omega = 2\pi \times 1600 \text{ Hz} \quad (3.69)$$

in this case. The square wave, $v_s(t)$, is

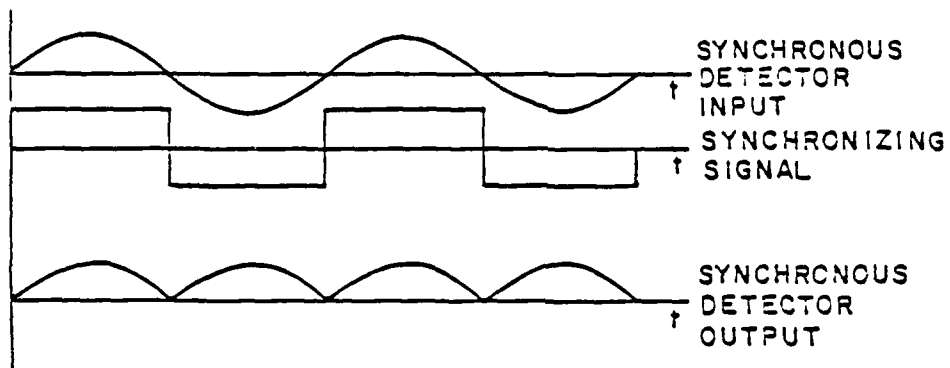


Figure 3.10. Synchronous detector operation.



Figure 3.11. Signal-plus-noise spectrum at synchronous detector output, point {25}.

$$v_s(t) = \sum_{n=1}^{\infty} (-1)^{n-1} \frac{\cos[(2n-1)\omega t]}{2n-1} \quad (3.70)$$

The detector output is the product of these terms,

$$\begin{aligned} v_1(t)v_s(t) &= A \cos(\omega t + \theta) \cos \omega t - [A/3] \cos(\omega t + \theta) \cos 3\omega t \\ &+ [A/5] \cos(\omega t + \theta) \cos 5\omega t - \dots, \end{aligned} \quad (3.71)$$

where only the first term produces a DC term. Expanding the first term of Equation 3.71 yields

$$V_{out} = [A/2][\cos(\theta) + \cos(2\omega t + \theta)]. \quad (3.72)$$

After low-pass filtering, V_{out} is

$$V_{out} = [A/2] \cos(\theta), \quad (3.73)$$

where adjustment is provided to set θ to zero. In the same way that the synchronous detector shifts the frequency of the 1600 Hz signal, the noise is shifted from its position around 1600 Hz to DC. Note that there is no impulse noise term at DC in Figure 3.11, indicating that using the 1600 Hz term and synchronous detection performs the task it was asked to do, yielding a DC signal with no impulsive DC noise term. The noise in the 0-10 Hz band is reduced by low-pass filtering in selectable circuits having time constants of 1 and 10 seconds, respectively, i.e., equivalent bandwidths of 1 Hz and 1/10 Hz.

D. SUMMARY

This chapter has shown that the quadrature receiver design produces a DC output which is independent of the phase of the received 94 GHz signal. The target should be firmly anchored to assure that the phase will not vary due to range changes. In considering signal amplitudes, it was shown that the components which are likely to be driven into non-linear behavior are the first Avantek UTC10-115M integrated amplifier in the IF signal path and the MCL ZEM-2 double balanced mixers. Devices in the audio frequency range have been set experimentally so that each will remain in its linear range as long as the IF components are not overdriven.

Noise power was considered to show the necessity for bandwidth reduction in the IF signal channel. With this filtering accomplished, noise power is too low to saturate any component in the system. The noise spectrum was considered in order to show why two design decisions were made. The first was that of the two terms produced by the audio frequency squarer, at DC and 1600 Hz, the 1600 term must be used to achieve optimum signal-to-noise characteristics, and the second that the 1600 Hz term should be converted to DC by means of a synchronous detector rather than by full-wave rectification to achieve the best signal-to-noise performance.

CHAPTER IV

TEST RESULTS

A. INTRODUCTION

This chapter gives the results of using the transmissometer with signals obtained both through the internal calibration channel and over short test ranges (130, 240, and 500 meters) with 3.75, 6, and 16 inch corner reflectors as targets. The size of each reflector is characterized by the dimension ℓ as shown in Figures 4.3 and 4.4. The results of using the calibration channel include equations for determining atmospheric attenuation from the outputs of the transmissometer system and estimates of the dynamic range and sensitivity of the system. The results obtained over the test range are extrapolated to predict the maximum range, R_{\max} , for which the transmissometer will perform over its full dynamic range. The problem of clutter is discussed and recommendations are made regarding the clutter problems.

Fairly extensive field tests, including meteorological instrumentation, had been planned. However, the failure of two IMPATT oscillators in late July and August and resulting delays forced us to limit field testing. The testing that was done is sufficient to characterize system performance.

B. CALIBRATION CHANNEL TEST RESULTS

1. Overview

System calibration was performed so that the system performance could be characterized accurately. From the data, curves and equations were generated which characterize the attenuation of the modulated 94 GHz signal vs. V_{out} . These equations can be used to determine the attenuation of the 94 GHz signal given the system output V_{out} and auxiliary information, including the gain mode of the audio frequency circuitry.

2. Procedure

The calibration curves were obtained in the following manner. First, the TRG W822-24C transmitting antenna feed horn was replaced by a waveguide load to prevent any power from being radiated from the transmitting antenna, and the receiving antenna was shorted to assure that no signal was received by it. Then a second 50 dB adjustable waveguide attenuator (Hughes 45726H-1000) was put in place of the TRG W559-6 directional coupler in the calibration channel (refer to Figure 2.6). Setting this attenuator at 50 dB attenuation reduced the modulated 94 GHz signal level, P_2 (see Figure 2.3) present at the TRG W9600-9 mixer to -80 dBm with the TRG 510W/387 variable attenuator set to zero dB. Recall from Table 3.2 that with A_{if} set to zero dB, -80 dBm is the maximum allowable input to the system. Thus, with this calibration scheme, modulated 94 GHz signal returns over the 42.5 dB

range from -80 to -122.5 dBm were simulated by adjusting the TRG 510W/387 variable waveguide attenuator from 0 dB to 42.5 dB in 2.5 dB steps. After each adjustment, V_{out} was allowed to settle and was recorded. Data points were taken with $\tau=1$ sec. when in the "low gain" region and $\tau=10$ sec. when in the "high gain" mode for improved sensitivity. This process was repeated for five phase settings of the Hughes 45766H-1200 variable phase shifter to determine whether or not V_{out} is independent of the phase of the 94 GHz signal in practice, as the theory indicates it should be.

Figure 4.1 shows a curve generated by this method. The multiple traces on the curve represent different phase settings of the Hughes 45766H-1200 variable phase shifter. The two distinct levels occur due to the automatic gain switching in the audio frequency circuitry, which adds 20 dB gain when the output signal, V_{out} drops below 0.050 volts.

It can be seen from Figure 4.1 that, as the attenuation increases and signal power decreases, reducing the output signal-to-noise ratio, the certainty of the attenuation value read from the curve decreases. For instance, with V_{out} at 0.1 volts DC and the gain monitor in the "high gain" mode, it is difficult to tell from the curve whether the attenuation is 39 or 40 dB or in between, indicating approximately 1 dB of uncertainty. To achieve greater accuracy, the modulated 94 GHz signal was increased by 30 dB, thus increasing P_2 by 30 dB, and 30 dB of attenuation was introduced in the IF signal channel ($A_{if}=30$ dB) with the Telonic step attenuator, so that the overall signal level remained the same at the end of the IF channel. Since the primary noise source is the TRG W9600-9 mixer, before the Telonic attenuator in the signal path

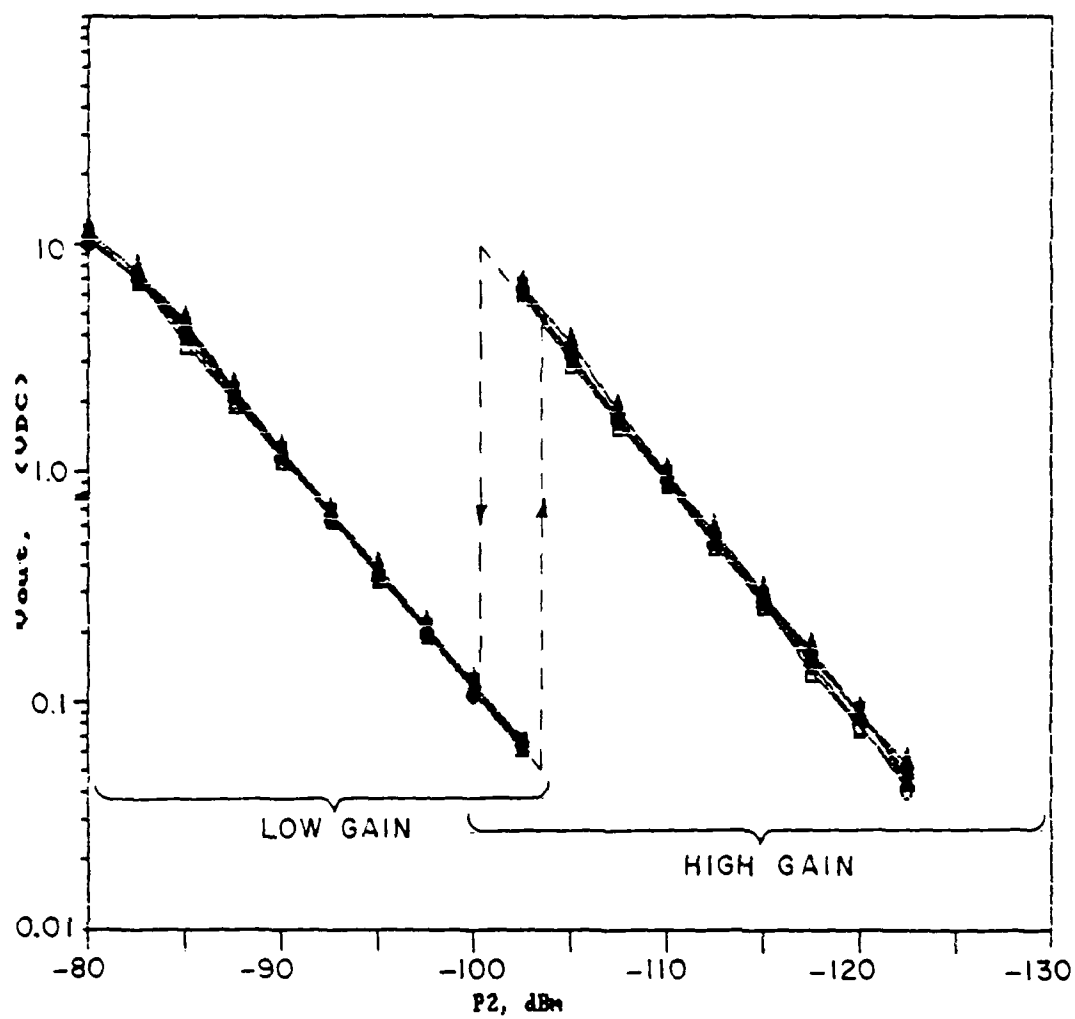


Figure 4.1. V_{out} vs. received 94 GHz signal power, P_2 .

(Figure 2.4), the increase in signal by 30 dB increases the signal-to-noise ratio by 30 dB, allowing very accurate data to be recorded. Figure 4.2 is an example of such data, simulating modulated 94 GHz signal returns of $P_2 = -50$ to -100 dBm. The data in Figure 4.1 was recorded using the same method as that in Figure 4.1, except that the TRG 510W/387 attenuator was varied over a 50 dB range in 2.5 dB steps for each phase setting rather than 42.5 dB. Note the better agreement of the curves in Figure 4.2 relative to those in Figure 4.1. Also note that there is a slight non-linearity which occurs when V_{out} is in the range from 2 to 7 VDC. This non-linearity amounts to approximately 1 dB, and is a result of a non-linearity in the MF-10 digital bandpass filters (see Figure 2.5) used in the audio frequency circuitry.

3. Attenuation Equations

Equations for determining the one-way atmospheric attenuation A (in dB) along the path have been produced to fit the data shown in Figure 4.2. The derivation of these equations is given in Appendix C. The parameters needed to determine the value of A are listed in Table 4.1. Equation (4.1) gives the attenuation under all conditions determined by the gain modes of $V_{out-cal}$ and $V_{out-test}$:

$$\begin{aligned}
 A = & 5 \log_{10}(V_{out-cal}/V_{out-test}) + 5(C_{test} - C_{cal}) \\
 & + (1/2) (A_{if-cal} - A_{if-test}) - 20 \log_{10}(R_{test}/R_{cal}) \\
 & + 5 \log_{10}(\sigma_{test}/\sigma_{cal}) \quad (dB). \quad (4.1)
 \end{aligned}$$

TABLE 4.1
ATTENUATION EQUATION PARAMETERS

<u>Symbol</u>	<u>Explanation</u>	<u>Units</u>
R_{cal}	Distance from transmissometer to calibration target	meters
R_{test}	Distance from transmissometer to target used in testing	meters
σ_{cal}	Radar cross section of calibration target	m^2
σ_{test}	Radar cross section of target used in testing	m^2
$V_{out-cal}$	Value of V_{out} when transmissometer aligned with calibration target	VDC
$V_{out-test}$	Value of V_{out} under test conditions	VDC
A_{if-cal}	Setting of Telonic 8120S step attenuator when $V_{out-cal}$ measured	dB
$A_{if-test}$	Setting of Telonic 8120S step attenuator when $V_{out-test}$ measured	dB
C_{cal}	A constant dependent on gain mode when $V_{out-cal}$ measured: 8.0 in high gain mode and 6.1 in low gain mode	dB
C_{test}	A constant dependent on gain mode when $V_{out-test}$ measured: 8.0 in high gain mode and 6.1 in low gain mode	dB

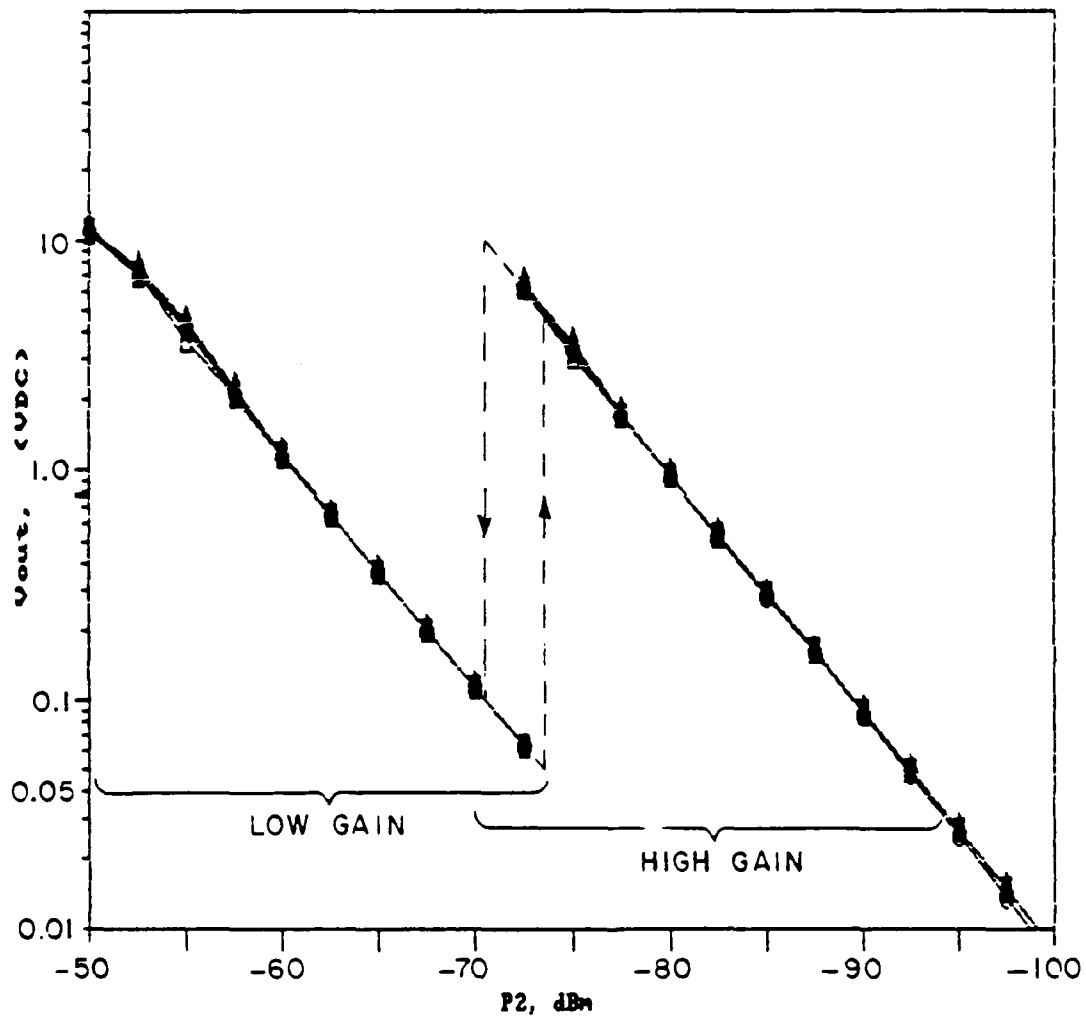


Figure 4.2. V_{out} vs. received 94 GHz signal power, P_2 .

4. Sensitivity and Dynamic Range

Refer to Figure 4.1. It can be seen that with the input P_2 to the TRG W9600-9 mixer equal to -120 dBm or less, the lines begin to diverge. These data were taken with the filter setting of $\tau=10$ sec. in the "high gain" region, for improved sensitivity. Time did not allow tests to identify unambiguously the reason for this divergence or, indeed, its repeatability. Regardless of the source, $P_2=-120$ dBm can be taken to be a signal input for which an assuredly accurate V_{out} is obtained and is thus a measure of the minimum system sensitivity. This is probably a very conservative estimate because the -120 dBm sensitivity figure is not determined by the system noise floor.

Another observation from Figure 4.1 is that the transmissometer system has a dynamic range of 40 dB with approximately $\pm 1/2$ dB of accuracy.

C. OUTDOOR TEST RESULTS

These outdoor results were obtained using ranges from 130 to 500 meters and 3.75, 6, and 16 inch corner reflectors. The results are tabulated in Table 4.2, where R_{max} , the maximum assured range for which the transmissometer will operate over its full 40 dB dynamic range, has been calculated from the data, as explained below. This is also likely to be a conservative estimate, since it is based on a receiver sensitivity of -120 dBm. However, it must also be considered that this estimate does not take into account the effect of clutter, which can reduce R_{max} . Clutter is discussed in section D of this chapter.

TABLE 4.2
OUTDOOR TEST RESULTS

Range m	Reflector (VDC)	V _{out}	Gain mode (dB)	A _{if} ^a	Extrapolated R _{max} for each specific reflector (meters)
I.					
130	3.75 inch ^b	0.2	low	50	820 ^e
130	6 inch ^b	1.0	high	70	1300 ^e
130	6 inch ^{b,d}	1.0	high	70	1300 ^e
240	16 inch ^c	1.0	high	70	2400 ^e
II.					
500	3.75 inch ^b	0.3	high	50	1200
500	6 inch ^b	2.0	high	50	1900

- a. A_{if} equals the numerical setting of the Telonic 8120S step attenuator.
- b. See Figure 4.4 for corner reflector detail.
- c. See Figure 4.3 for corner reflector detail.
- d. Surface of reflector polished to test effect of minor corrosion and dirt on radar cross section.
- e. Since these values were calculated from measurements in the near field, these extrapolated R_{max} values underestimate the achievable range of the system. The values predicted from the 500 meter range (section II of this table) should be more realistic.

The data in the first five columns of Table 4.2 were used to determine the maximum range, R_{\max} , in the following way. Use the radar equation [7]

$$P_r = \frac{P_t G_t G_r \lambda^2 \sigma_t t_r}{(4\pi)^2 R^4} 10^{-(2\alpha R/10)} \quad (4.2)$$

where P_t is transmitter power at the IMPATT output, G_t is the gain of the transmitting antenna, G_r is the gain of the receiving antenna, λ is the wavelength, σ is the radar cross-section of the target, t_t is the transmittance between the transmitter's IMPATT power source and transmitting antenna, t_r is the transmittance between the receiving antenna and TRG W9600-9 mixer/preamplifier input, α is the average one-way specific attenuation along the path in dB/km, and R is the distance from transmitter to target. The important aspect of this equation is the $1/R^4$ term. Assume $\alpha=0$ (clear air conditions) for these calculations. Also assume that the returns from clutter are negligible. (Clutter will be discussed further in section D of this chapter.) All other terms will be considered constant while R is varied to determine the transmissometer's range capability from the data recorded in Table 4.2.

With all terms constant in Equation (4.2) except R and P_r , the equation can be written as

$$P_r = k/(R^4) \quad (4.3)$$

or

$$k = P_r R^4 . \quad (4.4)$$

THEORETICAL RADAR CROSS SECTION
 σ FOR WAVELENGTH λ IS

$$\sigma = \frac{4\pi l^2}{\lambda^2}$$

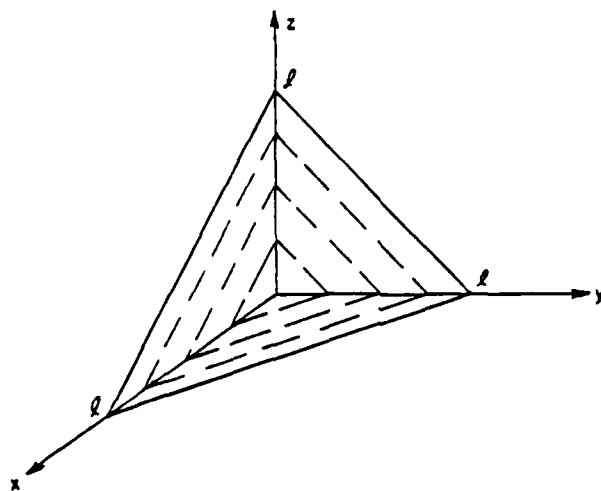


Figure 4.3. Triangular trihedral corner reflector.

THEORETICAL RADAR CROSS SECTION
 σ FOR WAVELENGTH λ IS

$$\sigma \approx \frac{15.6 l^2}{\lambda^2}$$

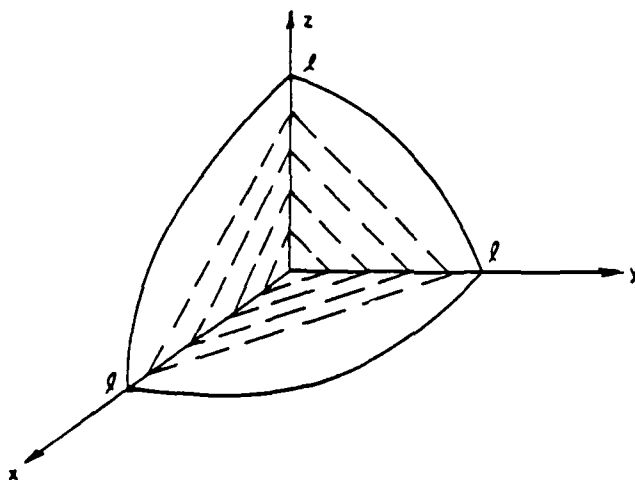


Figure 4.4. Circular trihedral corner reflector.

With $R=R_1$, Equation (4.4) becomes

$$k = P_{r1} R_1^4 \quad (4.5)$$

and with $R = R_{max}$, Equation (4.4) becomes

$$k = P_{rmax} R_{max}^4. \quad (4.6)$$

Combining Equations (4.5) and (4.6) yields

$$k = P_{r1} R_1^4 = P_{rmax} R_{max}^4 \quad (4.7)$$

which can be written as

$$R_{max}^4 = P_{r1} R_1^4 / P_{rmax}, \quad (4.8)$$

or

$$R_{max} = R_1 (P_{r1} / P_{rmax})^{(1/4)}, \quad (\text{meters}) \quad (4.9)$$

where R_1 is the range in meters at which data was taken, P_{rmax} is 10^{-11} watts (-80 dBm), a value chosen to give maximum range and still allow the system to work over a 40 dB dynamic range, and P_{r1} can be calculated from Equation (4.10) or (4.11) if V_{out} , A_{if} , and the gain mode are known. Equations (4.10) and (4.11) are derived directly from Equations (C.1) and (C.2) in Appendix C, with only the additive constants changed to allow the setting of the Telonic 81206 attenuator to be arbitrary instead of fixed at 30 dB.

$$P_{r1} = \frac{\log_{10} V_{out} - 11.0}{0.1} + A_{if} \text{ (dB) (high gain)} \quad (4.10)$$

$$P_{r1} = \frac{\log_{10} V_{out} - 9.1}{0.1} + A_{if} \text{ (dB) (low gain)} \quad (4.11)$$

Since P_{r1} is in dBm, it is simpler to rewrite Equation (4.9) to use values of power in dBm, which is done in Equation (4.12),

$$R_{max} = R_1 \{10^{[(P_{r1} + 80)/10]}\}^{(1/4)} \text{ (meters)}. \quad (4.12)$$

In Equation (4.12), R_1 is in meters, P_{r1} is in dBm, $P_{rmax} = -80$ dBm has been substituted, and R_{max} is given in meters.

The results of calculating R_{max} for the 3.75, 6, and 16 inch corner reflectors are summarized in Table 4.2. Section I contains test results with the reflector in the near field of the antenna, which caused significant gain reduction; the R_{max} values calculated from this data are useful for intercomparison but greatly underestimate the actual achievable range since the full antenna gain was not realized during the measurements. Note the identical 1300 meter values of R_{max} obtained when testing the 6 inch reflector while unpolished and then polished. This result indicates that surface roughness introduced by slight corrosion, dirt, and old masking tape adhesive is insignificant. Section II contains test results taken using a range approximately equal to one half of the far-field distance, insuring gain reduction by no more than 1 dB. Note that for the 3.75 and 6 inch reflectors tested both in the near-field and (nearly) far-field regions, R_{max} calculated using the far-field data is approximately 1.5 times as large as that calculated using the near-field data, indicating an increase in effective gain of 6 dB as the far-field is approached.

An estimate of σ for each of the reflectors used in testing is useful. The calculations of the σ values estimated from the measurements for each reflector follow. Using the radar equation, Equation (4.2), it is possible to estimate σ , the radar cross section of the reflector, for the 3.75, 6 and 16 inch corner reflectors tested. Solving Equation (4.2) for σ yields

$$\sigma = \frac{P_r (4\pi)^3 R^4}{P_t G_t G_r \lambda^2 t_t t_r} \quad (\text{m}^2), \quad (4.13)$$

where P_r (watts) is determined for each case by using Equations (4.10) and (4.11).

R is the range used in meters,

P_t is 0.2 watts,

$G_t = 53 \text{ dB} = 10^{5.3}$ (numeric),

$G_r = 47 \text{ dB} = 10^{4.7}$ (numeric),

$\lambda = 3.19 \times 10^{-3}$ meters,

$t_t = 0.15$,

and $t_r = 0.6$.

Substituting all known quantities into Equation (4.13) yields

$$\sigma = (1.1) P_r R^4. \quad (4.14)$$

Using the data from section I of Table 4.2 and Equations (4.10) and (4.11) to calculate P_r and substituting in Equation (4.14) gives values of σ for the 3.75, 6, and 16 inch corner reflectors of

$$\sigma_{3.75, I} = 5 \text{ m}^2, \quad (4.15)$$

$$\sigma_{6,I} = 31 \text{ m}^2, \quad (4.16)$$

and

$$\sigma_{16,I} = 365 \text{ m}^2. \quad (4.17)$$

Using the data in section II of Table 4.2 gives

$$\sigma_{3.75,II} = 22 \text{ m}^2, \quad (4.18)$$

$$\sigma_{6,II} = 137 \text{ m}^2. \quad (4.19)$$

The theoretical values of σ , denoted by σ_{th} , for triangular trihedral reflectors (see Figures 4.3), such as the 16 inch reflector used may be determined from Equation (4.20), where " l " (meters) is seen in Figure 4.3 and λ (meters) is the wavelength. The theoretical values for circular trihedral reflectors (see Figure 4.4), such as the 3.75 and 6 inch reflectors used may be determined from Equation (4.21), where " l " (meters) is seen in Figure (4.3) and λ (meters) is the wavelength [21].

$$\sigma_{th-tri} = \frac{4\pi l^4}{\lambda^2} (\text{m}^2) \quad (4.20)$$

$$\sigma_{th-cir} = \frac{15.6 l^4}{\lambda^2} (\text{m}^2) \quad (4.21)$$

$$\sigma_{th3.75} = 125 \text{ m}^2 \quad (4.22)$$

$$\sigma_{th6} = 825 \text{ m}^2 \quad (4.23)$$

$$\sigma_{th16} = 33,700 \text{ m}^2 \quad (4.24)$$

TABLE 4.3
COMPARISON OF RADAR CROSS SECTION CALCULATIONS

Corner Reflector	σ_{th} (m ²)	Section I		Section II	
		σ_I (m ²)	$\sigma_{I,\sigma th}$ (dB)	σ_{II} (m ²)	σ_{II}/σ_{th} (dB)
3.75 inch	125	5	-14.0	22	-7.6
6 inch	825	31	-14.3	137	-7.8
16 inch	33,700	365	-19.7	---	---

Comparison of the theoretical and experimental values of σ is made in Table 4.3. Consider the ratio of σ_I to σ_{th} expressed in dB in column 4 of Table 4.3. The -14.0 and -14.3 dB values for the 3.75 and 6 inch reflectors are consistent with one another. The -19.7 dB value for the 16 inch reflector shows that it is not made for use at 94 GHz. The outer edges of this reflector are misaligned by 2 millimeters, 1 millimeter and 0.5 millimeter, respectively, which causes some of the reflected signal to return out-of-phase and cancel the in-phase return, thus reducing the effective radar cross section of the target. The sixth column in Table 4.3 gives the ratio of σ_{II} to σ_{th} derived from the data taken at approximately one half of the far-field distance. This shows a significant improvement in the measured values of both the 3.75 and 6 inch reflector; both are approximately 7.7 dB below their respective theoretical values, an increase of approximately 6 dB with respect to the near-field test. The fact that both 3.75 and 6 inch

reflectors are 7.7 dB below their respective theoretical values raises the possibility that a 7.7 dB loss might occur elsewhere in the system. Therefore it is recommended that a test be made with a target of known radar cross section at 94 GHz. This test will determine whether the radar cross sections of the 3.75 and 6 inch corner reflectors are actually 7.7 dB below their respective theoretical values or whether some of this loss may be introduced at some other point in the transmissometer. Some possible sources of loss are: 1 dB from using a range of only one-half the far-field distance; physical antenna misalignment; improper focusing of antennas; circular to rectangular waveguide transitions attached to antennas; other possible losses in transmitter or receiver front end.

D. CLUTTER

In the discussion of maximum range in the preceding section, signal returns from clutter were neglected. The conclusion that the system's guaranteed maximum range is at least 1.9 kilometers with the 6 inch target as discussed in the previous section is valid in the absence of returns from clutter, because the power returned from the target at a 1.9 kilometer range would be great enough to operate the system over its full dynamic range. However, the assumption that so little signal reflected by clutter reaches the receiver will be unrealistic for many situations. In fact, outdoor tests indicate that signals reflected by clutter can be on the same order of magnitude as the return from a target at range R_{\max} over flat, grass covered terrain, which should produce relatively low clutter returns.

Clutter returns from the 500 meter test range were calculated from the following data: $V_{out} = 0.03$ VDC, $A_{if} = 50$ dB, high gain mode. Equation (4.10) yields the clutter return $P_r = -75$ dBm. Recall that R_{max} was calculated by assuming $P_{rmax} = -80$ dBm to insure the full use of the system dynamic range of 40 dB. Thus, with a target at R_{max} , the clutter dominates the signal with a signal-to-clutter ratio of -5 dB, and no valid data would be obtained at this range for this ground. This limitation may not apply if the instrument is used on a tower, as has been proposed for some applications.

Several steps can be taken to reduce clutter returns. First, microwave absorber has been installed around the transmitting and receiving antennas to reduce any direct leakage between the two antennas. Second, the range used must be as free of clutter as possible, especially at short distances from the transmissometer, since the power returns from clutter go as $1/(R^4)$ as seen in the radar equation (Equation (4.2)). Other possibilities are to use a range shorter than 1.9 kilometers, thus increasing the returned power from the target and in turn allowing greater IF attenuation (A_{if}), thus decreasing the clutter returns relative to the signal returns from the target. For instance, a signal-to-clutter ratio of 18 dB is achieved with the 500 meter test range and 6 inch reflector. A 10 dB signal-to-clutter ratio is obtained using the same range and the 3.75 inch reflector. Also a target of greater radar cross section could be used, which would increase the signal return from the target and would affect the signal-to-clutter ratio in the same way as would decreasing the range. The use of precision targets made for 94 GHz operation is recommended.

The most desirable solution, however, is to use the system with a modulated target. Such a target allows the unmodulated returns from clutter to be ignored as long as they do not saturate any component, thus allowing the full dynamic range of the system to be used even in the presence of clutter returns. Appendix A discusses an implementation of a modulated target.

E. SUMMARY

This chapter has shown the use of the calibration channel to determine equations for the atmospheric attenuation as a function of V_{out} and other available parameters. System dynamic range capabilities were determined as well as system sensitivity. Dynamic range is 40 dB with $\pm 1/2$ dB uncertainty, and the minimum detectable input to the system at [2] is $P_2 = -120$ dBm.

Data from a 500 meter test range, using 3.75 and 6 inch corner reflectors, were used to determine the system's maximum target range. This was determined to be approximately 1.9 kilometers for the 6 inch reflector and 1.2 kilometers for the 3.75 inch reflector in the absence of clutter, but it should be noted that the values of σ calculated from the data for the 6 and 3.75 inch reflectors were both approximately 7.7 dB below theoretical values. Thus, the use of high-precision reflectors intended for use at 94 GHz could improve the maximum range and would determine whether or not some of the apparent 7.7 dB reduction in radar cross section is actually due to loss at some other point in the system.

The detrimental effects of clutter were discussed along with possible methods for reducing clutter effects. Use of a modulated target with the system would greatly reduce the effect of clutter. Further investigation into the use of the transmissometer system with a modulated target is therefore highly recommended. A first attempt at such a target is documented in Appendix A, and improvements are suggested there.

CHAPTER V

OPERATING INSTRUCTIONS

A. INTRODUCTION

This chapter provides a detailed set of operating instructions so that the operator need not be intimately familiar with the theory of operation of the transmissometer in order to use the system.

B. INITIAL SET-UP

Power, ground lines, and signal to the Hughes 45216H-1000 modulator are supplied to the transmissometer through the gray multi-conductor cable (chosen on the basis of availability) connected at the bottom of the transmissometer (refer to Plate 5.1). Table 5.1 shows how these connections should be made by color coding them to the required source. Each conductor, with the exception of the +24 VDC line and the ground line for the +24 VDC supply, consists of a twisted pair of wires, so that colors of both wires in the pair are given. For example, a twisted pair whose colors are given as Orange/Red and Orange/Black has one wire which is orange with a red strip and another orange with a black stripe. A ground line from each power supply is also connected to the transmissometer, where a common ground is established by connecting all grounds to the chassis of the transmissometer in order to prevent ground loop currents. Table 5.1 also gives current requirements for power supplies.

PLATE 5.1
TRANSMISSOMETER BOTTOM PANEL



TABLE 5.1
CABLE CONNECTIONS

Wire Color(s)	Source	Current Requirement
Red & Red/White	+15 VDC	5.0 A
White & White/Red	-15 VDC	1.0 A
White/Black	+24 VDC	100 mA
Green & Green/White	+28 VDC	3.0 A
Blue & Blue/White	+40 VDC	500 mA
Red/Black & Black/Red	Hughes Mod/Lev Supply, white wire	
Orange & Orange/Red	Hughes Mod/Lev Supply, black wire	
White/Red/Black & Red/White/Black	Hughes Mod/Lev Supply, yellow wire	
Orange/Green & Orange/Black	Hughes Mod/Lev Supply, red wire	
Green/Black & Green/ Black/White	Gnd from +28 VDC supply Gnd from Hughes Mod/ Lev Supply	
Black/White/Red	Gnd from +24 VDC supply	
Blue/Black & Blue/Red	Gnd from +40 VDC supply	
Black & Black/White	Gnd from ± 15 VDC source	

For proper operation of the transmissometer, the audio frequency signal processing circuitry needs a reference signal derived from the modulation source. When the source of modulation in this system is the Hughes Ferrite Modulator/Leveler Supply, the reference must be derived from it. This is accomplished by connecting the "Ext Mod Input" on the Hughes Ferrite Modulator/Leveler Supply to the system clock input marked "CLK" on the bottom of the transmissometer (refer to Plate 5.1). In case any other modulation source is used, for example in the case of using a modulated target, the "CLK" input requires a reference signal with an amplitude between 20 mV and 10 V peak-to-peak. If the internal modulation is used, set the center knob on the face of the Hughes Ferrite Modulator/Leveler Supply to "INT SQ WAVE MOD" and turn the "LEVEL SET" potentiometer fully counterclockwise. Now the Hughes Ferrite Modulator/Leveler Supply is prepared to modulate the 94 GHz signal. If the center knob is not in the "INT SQ WAVE MOD" position of the "LEVEL SET" potentiometer is not fully counterclockwise, the 94 GHz signal will not be modulated. Turn the Hughes Ferrite Modulator/Leveler Supply on.

Once the power supplies are connected, before turning the system on, point the transmissometer into free space to avoid unwanted signal returns during the set-up procedure. Also, make sure that both transmitting and receiving antennas and whatever target is used remain free of moisture to avoid unwanted attenuation [11].

C. OPERATION

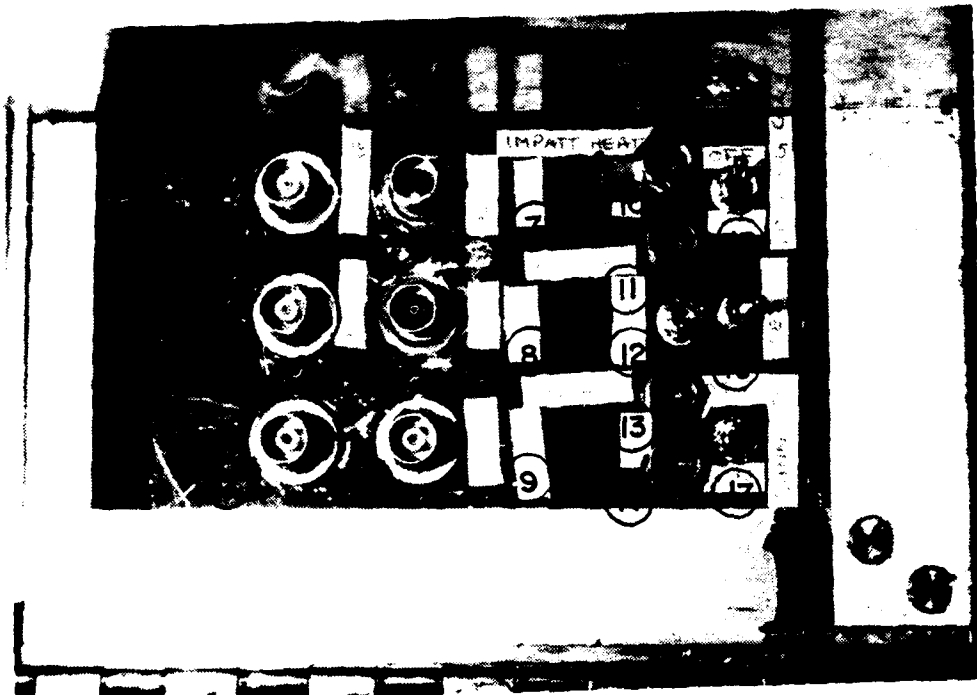
1. Power on

First, turn on the ± 15 VDC, and +28 VDC supplies. Now power is supplied to the TRG W9600-15 balanced mixer and W9600-9 balanced mixer/preamplifier, Avantek UTC10-115M, UTC10-109 and ESL* 776 MHz, 33 dB gain IF amplifiers, the Techtrol HX0-178 97.007224 MHz crystal and its oven, and to the audio frequency circuitry. The Hughes 47196H-1120B IMPATT oscillator is switched separately, at the transmissometer itself, as are the Hughes 47746H-1001 Gunn oscillators. With the IMPATT power switch off, turn on the +40 VDC power supply and set it to zero volts. (The IMPATT power switch is located on the side panel near the bottom of the transmissometer, see Plate 5.2.) With the +40 VDC supply set at zero volts, switch the IMPATT power on. Now slowly bring the supply voltage up to +40 VDC. The IMPATT device begins to draw current at about +20 VDC, and reaches its full current of 325 mA at about +35 VDC. An internal current regulator keeps the current constant as the voltage is increased above +35 VDC. The IMPATT oscillator is now on. The Gunn devices are not turned on with the rest of the equipment because these devices draw substantially more current when first turned on than during normal operation, so that if both Gunn devices were turned on simultaneously, the power supplies would reach their current limit and shut off. Thus it is necessary to turn the Gunn devices on one at a time. Turn the switch marked "LOCKING GUNN" (see Plate 5.2) to the "ON"

* ElectroScience Laboratory, The Ohio State University.

PLATE 5.2

TRANSMISSOMETER SIDE PANEL



1. Locking Gunn 97 MHz IF Monitor
2. L.O. Gunn 97 MHz IF Monitor
3. V_{sync}
4. V_{lock}
5. V_{lo}
6. Flat Plate Detector Output
7. IMPATT Heater Switch
8. Filter Selection Switch ($\tau=1$ sec or 10 sec)
9. IMPATT power switch
10. $\tau=10$ sec Filter zeroing potentiometer
11. $\tau=1$ sec filter zeroing potentiometer
12. Phase 180° Switch
13. Synchronous detector symmetry adjustment
14. Synchronous detector phase adjustment
15. Locking Gunn Power
16. Clock Select
17. L.O. Gunn Power

position. Now turn the switch marked "LO GUNN" (again, refer to Plate 5.1) to the "ON position. Now all power is on. Allow the system fifteen minutes to warm up before proceeding to the next step.

2. Checking Gunn Oscillator Operation

After the warm-up period, check that the Gunn oscillators are properly phase-locked (that is, operating at the correct frequency) by reading Gunn monitor voltages V_{lock} and V_{I0} , which are accessible via BNC connectors inside the small side door at the bottom of the enclosure (see Plate 5.2). Attach a DC voltmeter to V_{lock} . This should read 3.75 VDC (± 0.10 VDC). If the voltage is outside this range or not constant, turn to section E.1 of this chapter.

If V_{lock} is now correct, attach the voltmeter to V_{I0} . This voltage should be 4.71 VDC (± 0.10 VDC). If V_{I0} is outside this range or not constant, turn to section E.2 of this chapter.

3. Operation with Calibration Channel

This section is intended primarily as a tutorial for the operator who has never used this transmissometer. By using the calibration channel, which acts as a well-controlled signal path from the transmitter to receiver, results similar to those obtained with a calibrated target are seen. After observing the results obtained with the calibration channel, the operator will know what sort of results to expect when using the transmissometer in field use with a calibrated target.

The first step in using the calibration channel is to see to it that the transmissometer is pointed into free space, in order to avoid unwanted signal returns from the calibrated target or clutter. Next, turn the waveguide switch, located on the right side of the transmissometer from "OFF" to "ON" position, see Plate 5.3 for switch position. Observe the output of the synchronous detector, V_{sync} , on an oscilloscope. This signal is available via a BNC connector on the side panel near the bottom of the transmissometer (see Plate 5.2). This signal should appear to be a full-wave rectified 1600 Hz sine wave as shown in Figure 5.1. If V_{sync} is clipped as in Figure 5.4, refer to Section E.3. of this chapter. Should the waveform look more like Figure 5.2 or 5.3, then it is necessary to adjust either the phase or symmetry of the 800 Hz synchronizing signal used in the synchronous detector, or possibly both. Adjustment potentiometers for phase and symmetry are located on the side panel near the bottom of the transmissometer (refer to Plate 5.2). Adjust these potentiometers until a waveform similar to that of Figure 5.1 is obtained. If the phase potentiometer cannot be adjusted far enough to accomplish this, or if a sinusoidal waveform appears, switch the setting of the "PHASE 180°" switch (on the same panel) and readjust the phase potentiometer so that the synchronous detector output appears as Figure 5.1. This phase and symmetry adjustment procedure is used also when operating the system with a calibrated target.

With the synchronous detector output displayed on the oscilloscope, it is now possible to adjust the frequency of the modulation. This

PLATE 5.3
POSITION OF WAVEGUIDE SWITCH

WAVEGUIDE SWITCH



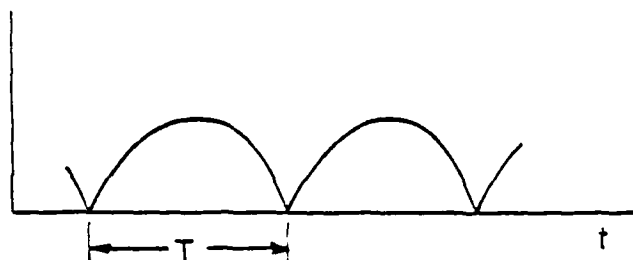


Figure 5.1. Proper synchronous detector output.

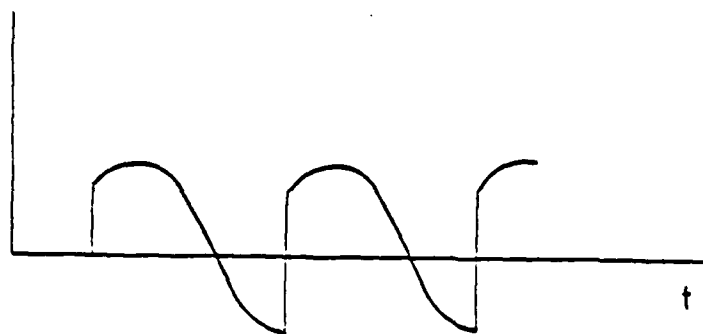


Figure 5.2. Synchronous detector output, phase misadjusted.

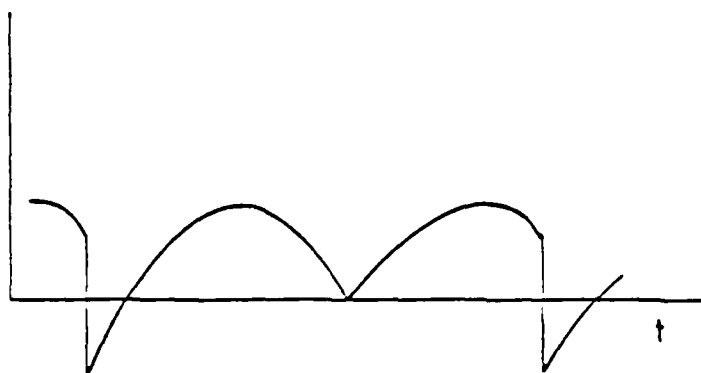


Figure 5.3. Synchronous detector output, symmetry misadjusted.

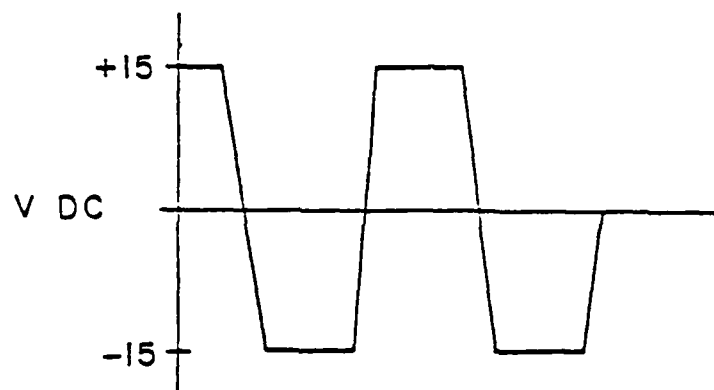


Figure 5.4. V_{sync} clipped.

frequency can be adjusted by the "MOD FREQ ADJ" potentiometer on the Hughes Ferrite Modulator/Leveler Supply. Adjust the frequency so that the time corresponding to that marked "T" in Figure 5.1 is 0.3125 msec; this corresponds to 800 Hz modulation since the detector detects a signal at twice the modulation of frequency. A frequency of precisely 800 Hz is not required for proper operation; the audio frequency clock will operate with a modulating frequency from 700 to 1050 Hz.

Now observe the signal V_{out} , which is available through a BNC connector at the bottom of the transmissometer, on a DC voltmeter. (Refer to Plate 5.1 for location of the proper BNC connector). With the Telonic attenuator (see Plate 5.4) set to 0 dB, the "FILTER" switch (see Plate 5.2) set to " $\tau=1$ sec", V_{out} should be approximately +1 VDC and the "GAIN MON" output should indicate "low gain" mode (i.e. ± 15 VDC, rather than 0 VDC, which indicates "high gain" mode). When using the transmissometer system with a calibrated target, V_{out} will vary in proportion to the signal received by the system.

Now set the Telonic 8120S 0 to 100 dB IF step attenuator (see Plate 5.4) to 100 dB. This effectively eliminates any signal beyond the attenuator, allowing for the system to be zeroed. With the DC voltmeter still reading V_{out} , set the "FILTER" switch on the side panel of the transmissometer (see Plate 5.2 for switch location) to 1 sec. Allow the filter time for V_{out} to settle to a constant value before performing any adjustments. Now slowly adjust the $\tau=1$ sec. filter zeroing potentiometer, marked "11" and positioned just above the "FILTER" switch, so that V_{out} reads zero volts. Now set the "FILTER" switch to

PLATE 5.4

POSITION OF TELONIC ATTENUATOR KNOB



TELONIC 81205
0-100dB STEP
ATTENUATOR
(VARIES A_{IF})

" $\tau=10$ sec.", and again allow the filter to settle. Adjust the $\tau=10$ sec. filter zeroing potentiometer, marked "10" so that V_{out} reads zero. Now the audio frequency filters are zeroed. Both this process of zeroing the audio frequency filters and adjusting phase and symmetry should be performed on a regular basis (hourly, or as needed). The transmissometer is now ready for use with a calibrated target.

4. Operation with Calibrated Target

It is assumed in this section that the steps in Sections B.1 and B.2 of this chapter (power on and check for proper operation of Gunn oscillators) have been accomplished. If this is not the case, do so now. To operate the transmissometer with a calibrated target, turn the waveguide switch (see Plate 5.3) to the "TARGET" position. Now line up the transmissometer and calibrated target by eye as well as possible; a low-power telescope affixed to the antenna mount can be very helpful for this purpose.

Locate the target by slowly rotating the transmissometer with the vertical and horizontal position controls, scanning the target area. At the same time observe the synchronous detector output. The magnitude of the synchronous detector output increases dramatically when the transmissometer and calibrated target are aligned. The beamwidths of the receiving and transmitting antennas are 0.7° and 0.4° , respectively, resulting in a very sharp peak in output when they are aligned with the target. If the synchronous detector output is clipped, this indicates that the system is saturated. This will cause no damage to the system.

Refer to Section E.3. of this chapter to correct this situation. Adjust the alignment so that the synchronous detector output is a maximum, thus indicating the maximum return from the calibrated target. Should the synchronous detector output need phase or symmetry adjustment, perform this adjustment as it is described in Section C.3 of this chapter. To assure that the power level in the IF signal channel is not too high, observe the value of V_{out} and the gain mode and adjust the Telonic attenuator from the 0 dB setting to the 10 dB setting. If the gain mode remains the same when the attenuator is switched, V_{out} should decrease by approximately a factor of ten (for example, from 4.67 VDC to 0.479 VDC). If the gain mode changes from "low gain" to "high gain", then the value of V_{out} should increase by approximately a factor of ten (for example, from 0.104 VDC to 0.963 VDC). If this is not the case, adjust the Telonic attenuator to a value such that a 10 dB decrease in the attenuator's value will cause a change in V_{out} by a factor of ten. If the setting of the Telonic attenuator is 40 dB or higher, the Avantek amplifier before the Telonic attenuator may be saturated. Therefore, if this is the case, the input power should be reduced by increasing the range, R, or using a target with a lower radar cross section, as indicated in Figure 3.1.

With the transmissometer and calibrated target now aligned for maximum return, V_{out} should remain stable under clear-air conditions. The transmissometer is now prepared to measure atmospheric attenuation at 94.0 GHz. Refer to Section D of this chapter, Data Acquisition, for recording procedures for these data.

D. DATA ACQUISITION

1. V_{out}

The output of the system is V_{out} . Whether V_{out} is connected to a strip chart recorder, a computer analog input, or some other means of recording, there are two things that the operator needs to be aware of. The first is that there are actually two versions of V_{out} available. The difference between the two is that one is passed through a low-pass filter with a time constant $\tau=1$ second while the other uses $\tau=10$ seconds to further narrow the bandwidth and thus further reduce the noise. The choice of which signal is connected to the V_{out} connector at the bottom of the transmissometer is made via a switch marked "FILTER" on the side panel of the transmissometer. The $\tau=10$ sec. setting should be used when V_{out} is in the "high gain" mode to improve the output signal-to-noise ratio. See Plate 5.2 for the location of the switch.

2. Gain Level

The second note regarding V_{out} is that there are two gain levels used, as seen in Figure 4.2. The left section of the curve in Figure 4.2 is known as the "low-gain" region and the right section is known as the "high-gain" region. This nomenclature indicates an additional 20 dB of gain which is introduced by the audio-frequency circuitry under low audio-frequency signal conditions. The gain is introduced because if V_{out} were expected to cover the entire 40 dB dynamic range without switching gain, it would have to go from 10.0 VDC to 0.001 VDC; at 0.001

VDC, V_{out} would be indistinguishable from op-amp DC offsets. Therefore, when V_{out} drops below 0.050 VDC in the "low gain" region, the gain of the first amplifier in the audio frequency section (see Figure 2.5) is increased by 20 dB (see Figure 3.11). This brings V_{out} up to 5.0 VDC, well out of the range of op-amp offsets. When in the "high-gain" region, the amplifier reduces its gain to 0 dB when V_{out} reaches 10.0 VDC. This gives the gain-switching circuitry a 5.0 VDC range between switching points so that it will not oscillate between gain regions, due to small signal changes.

The "Gain Mon" output, located on the bottom panel of the transmissometer (see Plate 5.1) is used to indicate which gain region V_{out} is in. A "Gain Mon" output of approximately 0 VDC indicates "high gain" mode, whereas a +15 VDC output indicates "low gain" mode. Thus both V_{out} and "Gain Mon" must be monitored to properly interpret V_{out} using Equation (4.1) and thus determine the attenuation caused by the atmospheric condition at that time.

E. TROUBLESHOOTING

1. Locking Gunn Oscillator

Most of the problems likely to be encountered with the Gunn oscillators can be solved very quickly. Should V_{lock} not be steady near the correct value of 3.75 VDC, simply turn the "LOCKING GUNN" switch off and on again. By doing this a few times, the locking Gunn will usually lock at the correct point, unless the unit has not had sufficient time

to warm up. If this procedure does not cause the unit to phase-lock properly, check the +15, -15 and +28 VDC supplies to see that the proper voltages are being supplied to the Gunn. If the supply voltages are too low (the ± 15 supplies at ± 12 VDC, for instance) the unit will not phase-lock at all. If the supply voltages are correct and turning the unit off and on does not help, refer to Appendix B, which contains the procedure for tuning the phase-locked Gunn oscillators. This is not an easy procedure to perform, so it is recommended that all other checks be exhausted first.

2. L.O. Gunn Oscillator

If the locking Gunn is properly locked, but the LO Gunn is not, the following procedure should be followed. Turn the "LOCKING GUNN" (see Plate 5.2) switch off and on again. Observe V_{10} . If it is constant near 4.7 VDC, then the unit is properly phase-locked. If the voltage is not constant, try turning the switch off and on a few more times. Should V_{10} happen to be about 4.44 VDC, then the LO Gunn is phase-locked, but at the wrong frequency. Switching the locking Gunn off and on a few more times should cause V_{10} to become stable at about 4.7 VDC. If V_{10} remains unstable, and the unit has had sufficient time to warm up, refer to Appendix B, which gives the procedure for tuning the Gunn oscillators.

3. Improper V_{sync}

If V_{sync} appears clipped as in Figure 5.4, rather than as it should be in Figure 5.1, then the signal input to the audio-frequency circuitry has increased too rapidly for the gain switching circuitry to follow, because this circuitry is dependent on V_{out} from the $\tau=1$ sec. filter. This problem arises in two situations. First, it may occur when the calibration channel is first turned on. The $\tau=1$ sec. filter is not fast enough to respond to the abrupt signal change, resulting in the audio-frequency circuitry becoming saturated. The second situation is when the target is first sighted in. When the target is first "found", the signal increase may also saturate the audio-frequency circuitry.

To solve this problem, adjust the Telonic attenuator (see Plate 5.4) so that the V_{sync} waveform appears to be more like Figures 5.1, 5.2 or 5.3, rather than 5.4. If the calibration channel is in use, the attenuator may now be returned to the 0 dB position, by increasing the attenuator one step at a time. Allow a few seconds for the filter to settle between attenuator changes. If a target is in use, continue in Chapter V, Section 8.4, which discusses how to set the attenuator.

CHAPTER VI

CONCLUSIONS AND RECOMMENDATIONS

In its present form, the transmissometer can be used with a target, such as a corner reflector, to determine atmospheric attenuation. However, for long target ranges the system's dynamic range may be severely limited by clutter along the path. The range at which this will occur depends on the target radar cross section and the clutter on the path, especially that at short distances. For this reason it is recommended that a further study be performed to develop a modulated target. A preliminary, not wholly satisfactory design is discussed in Appendix A. Such a target would largely eliminate problems caused by clutter. Use of the instrument on a sufficiently high tower should also reduce the clutter problem.

If the system is used with a corner reflector as a target, it is highly recommended that a high-precision corner reflector of known radar cross section at 94 GHz be used. The radar cross section of the two better corner reflectors used in testing appeared to be approximately 7.7 dB below their theoretical values. Using the system with a target whose radar cross section at 94 GHz is known would be likely to provide two benefits: it might extend the target range, and it would provide additional confirmation of the system calibration; i.e., results of using such a target would determine whether or not the apparent 7.7 dB degradation in radar cross section suffered by the two corner reflectors

tested is actually due, in part, to some undiscovered losses in the transmissometer system. Some possible sources of the loss are: 1 dB from using a range of only one half the far-field distance; physical antenna misalignment; improper focusing of antennas; losses in the circular to rectangular waveguide transitions attached to antennas; other possible losses in transmitter and/or receiver front end.

With regard to the system stability, examined in Chapter III, Section B, only the audio-frequency circuitry was found to be somewhat temperature sensitive. For this reason, consideration might be given to redesigning the audio-frequency circuitry to be more temperature independent. Alternately, a thermostatically controlled heater could be installed to eliminate temperature-sensitivity problems. A 1 dB non-linearity is introduced by the digital filters used in this circuitry. If this is considered unacceptable, the use of another type of bandpass filter is suggested.

Finally, in the case where the transmissometer will be used only to take atmospheric data with a modulated target, the Hughes 45216H-1000 Full-band modulator could be removed from the transmitter and placed in the calibration channel, so that it could still be used to modulate the 94 GHz signal for calibration purposes. The advantage is that it would remove the 2.5 dB insertion loss of the modulator from the signal path, thus nearly doubling the transmitted power. However, this would involve redesigning the physical configuration of the calibration channel, which has no room for the modulator at present, and it should be recalled that range varies as the fourth root of power, so that the range would be increased only by a factor of 1.2.

APPENDIX A

MODULATED TARGET

A. ADVANTAGES

As we have already seen, the transmissometer transmitter has the capability of modulating the transmitted signal. So why not just use this modulation rather than going to the trouble of using a target to reflect and modulate the signal? Because, when internal modulation is used, clutter returns, as well as crosstalk between the antennas, and low-level leakage between the transmitter and receiver, are indistinguishable from the signal return from the target. Depending on the target radar cross section the the desired range, this may limit the system performance.

Let us consider an example. The signal is modulated before transmission, and is reflected by a calibrated target (i.e., a corner reflector) and returns to the receiver. In addition to the return from the calibrated reflector, there is return from clutter, crosstalk between the antennas, and low-level leakage between the transmitter and receiver. The unwanted return from clutter, crosstalk and leakage and the return from the calibrated target are all modulated, and there is no way to separate them. If the unwanted return is significant compared to the return from the target, which is likely for long target ranges, the unwanted return will cause significant errors in the resulting data.

On the other hand, when a continuous-wave signal is transmitted and modulated by the target, then the unwanted signal, which is unmodulated, can be differentiated from the return from the modulated target by detecting the modulation. Thus, as long as the unmodulated 94 GHz return does not saturate the RF mixer or any IF amplifiers, it is disregarded by the coherent final detection process of the system, and only the modulated return from the target is detected. Therefore it is desirable to use a modulated target.

A particularly severe form of clutter arises if it is desired to use the transmissometer in an enclosed space, i.e., the beam is transmitted through a "window". Without target modulation, the reflection from the window must be kept well below the signal from the target, a very severe requirement. With target modulation, the window reflection must only be sufficiently low to prevent system saturation.

Another advantage of using the modulated-target technique is that it allows for the possibility of using several targets at various ranges, operating at different modulating frequencies, with only the addition of more audio-frequency signal processing electronics. An important application would be in assessing the non-uniformity of the attenuation over a path. Another possible application of two targets would be in a system where it is desirable to have the results absolutely independent of the transmitter power. This could be accomplished by having two reflectors at different distances; then the ratio of signal power returned from the two reflectors would be a measure of the attenuation over the distance separating the two

reflectors. At present, the output power of the transmitter appears very stable and easy to monitor, and the instrument is equipped for operation with only a single modulated reflector.

B. MODULATED TARGET IMPLEMENTATION

The modulated target (see Figure A.1) consists of a six inch parabolic reflector with a rotating sub-reflector. The sub-reflector (see Figure A.2) consists of a teflon lens, a polarization-sensitive reflector, and absorber, all of which is enclosed in an aluminum cylinder open at one end. The lens focuses the signal on the reflector (see Figure A.3 for reflector detail). The signal power reflected should be proportional to $\cos A$, where A is the angle between the reflective strips of the reflector and the linear polarization of the signal (see Figure A.4).

The sub-reflector assembly is spun by a synchronous motor at 24,000 rpm or 400 rps. This results in the reflected signal being modulated at 800 Hz, because the angular relationship between the reflector and the polarization of the signal is repeated twice per revolution.

Initial results using the modulated target in outdoor tests with the transmissometer were encouraging but not wholly satisfactory. The 94 GHz signal reflected by the target does contain the desired 800 Hz modulation component. However, for some reason the phase of the 800 Hz signal as observed at points {10}, {11}, {20}, and {21} of the receiver now depends on the phase of the 94 GHz signal while only its amplitude should depend on the RF phase for proper quadrature receiver operation.

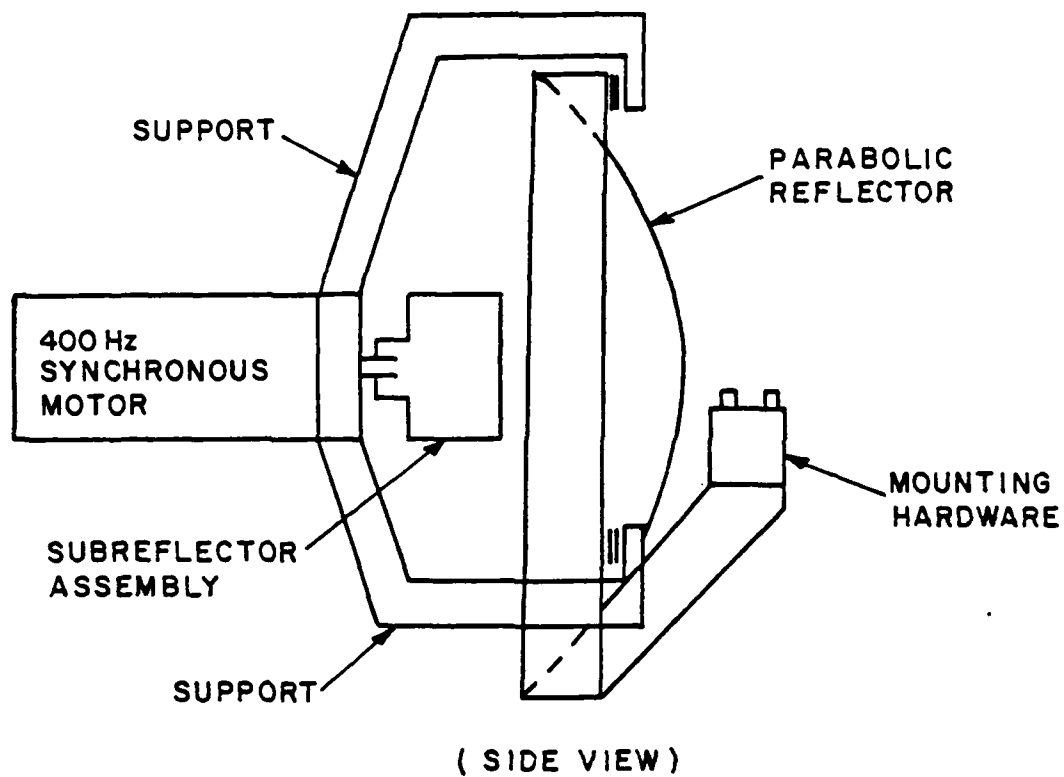


Figure A.1. Modulated target.

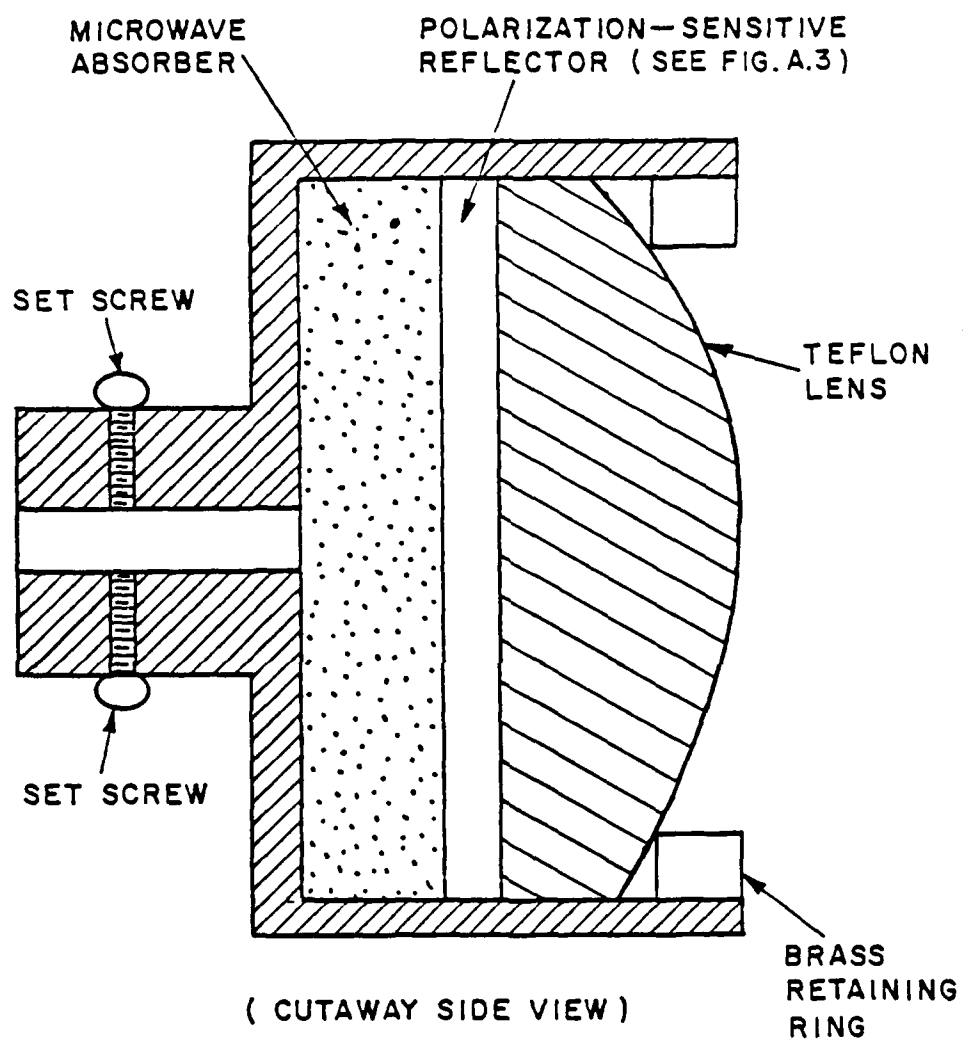


Figure A.2. Subreflector.

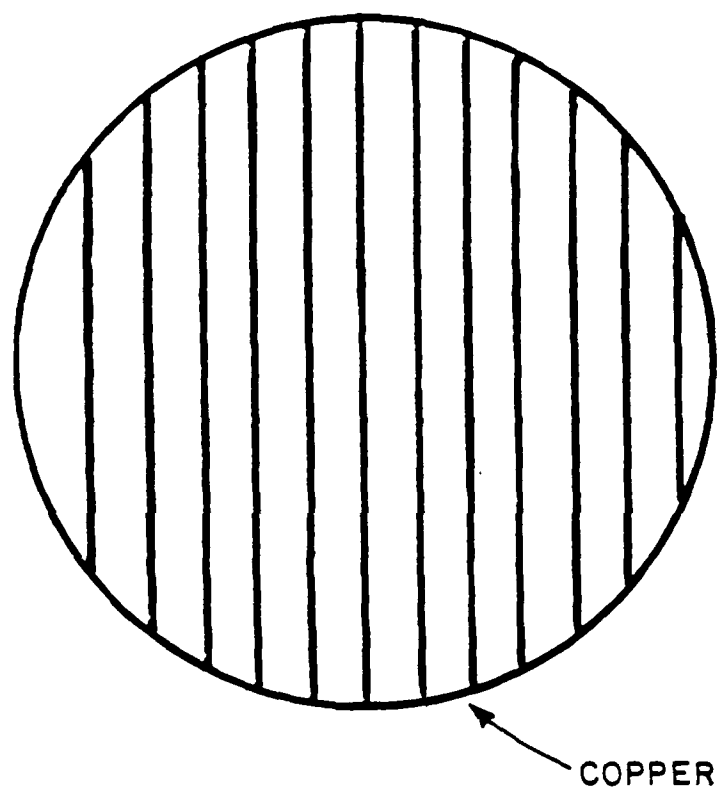


Figure A.3. Polarization-sensitive reflector.

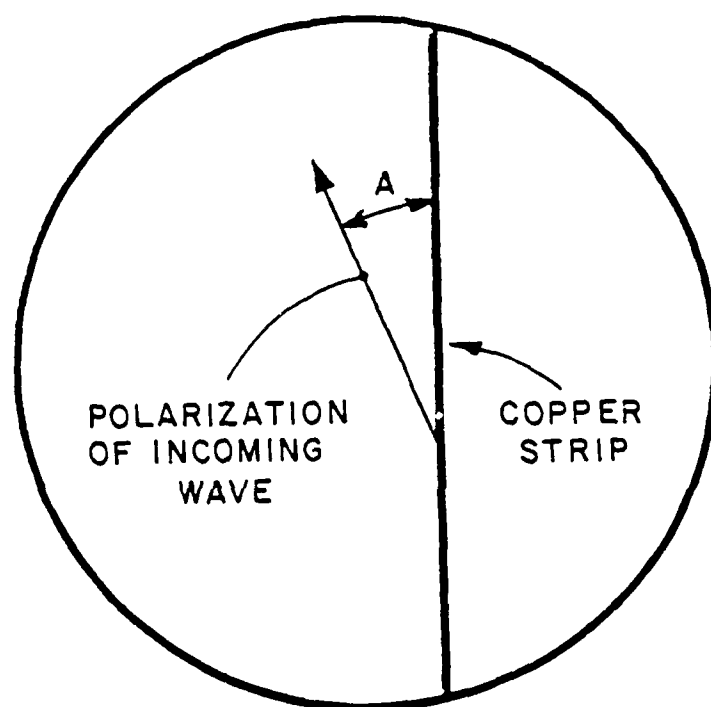


Figure A.4. Angle "A".

This makes it impossible for the summer to process the 800 Hz signal properly. Until this problem is solved, this implementation of the modulated target cannot be used. One possible clue which requires further investigation is the effect of time-harmonic RF phase shifts on the audio frequency processor, discussed in Chapter III, Section B.4.

If the RF phase modulation is indeed the problem, the difficulty with the rotating target may well have been alignment. It is well known that the amplitude of the return from a "cat's eye" reflector is relatively independent of the direction of arrival over a range about the symmetry axis; it is not clear that this is necessarily true of the phase. Thus it would be that the target alignment is more critical than was appreciated at the time of the test.

RF phase modulation could also be produced by vibration of the target. If this is the case, the target and its mount might be redesigned for more mechanical stability. Another approach would be to use electrical, instead of mechanical, modulation. An example would be a receiving antenna with a load that can be modulated by means of a diode at the audio rate.

In the expectation that these problems can be solved, provision has been made for a modulated target to be used with the system. The only changes in operation that need to be made are with respect to the transmissometer system clock input. First, the "CLK" input of the transmissometer must be connected to a signal derived from the modulation source. Second, the "CLOCK SELECT" switch, marked "16" on the transmissometer side panel, must be set for the frequency of the

reference input. In the case of this modulated target, the reference input is derived by frequency doubling from the 400 Hz signal used to run the 400 Hz synchronous motor, and the "400 Hz" setting of the "CLOCK SELECT" switch must be selected. If an 800 Hz reference source is used, select "800 Hz."

APPENDIX B

INFREQUENTLY REQUIRED TUNING

A. PHASE-LOCKED GUNN OSCILLATORS

Remove the cover from the back of the transmissometer enclosure. Refer to Plates 2.4 and 2.5 to find the phase-locked Gunn oscillator which needs to be tuned. (The Gunn may be left on.) Locate the Gunn oscillator inside the transmissometer enclosure and refer to Figure B.1. The box in Figure B.1 has a piece of aluminum tape covering one face. Remove the tape and save it. Now four holes are exposed. With a small non-conducting screwdriver, turn the Gain Adjust potentiometer fully clockwise. Now turn the Sweep Adjust potentiometer fully clockwise also. Hook up the Gunn Monitor to a DC voltmeter. (This voltage is available via a BNC connector on the transmissometer side panel, marked V_{lock} or V_{10} , see Plate 5.2.) Connect the L.O. or Locking Gunn 97 Mhz IF Monitor, available on the same panel, to a spectrum analyzer.

Adjust the Gunn Adjust potentiometer so that the Gunn Monitor voltage is set to its proper value (either $V_{lock} = 3.75$ VDC or $V_{10} = 4.71$ VDC). This should also cause the IF signal to line up with the 97 MHz crystal signal on the spectrum analyzer.

Now set the Sweep Adjust potentiometer so that the IF signal on the spectrum analyzer sweeps back and forth from 0 to 200 MHz. Set the Gain Adjust potentiometer so that a good lock is obtained. The definition of a "good lock" is shown in Figure B.2. Replace the tape and back cover of the transmissometer enclosure.

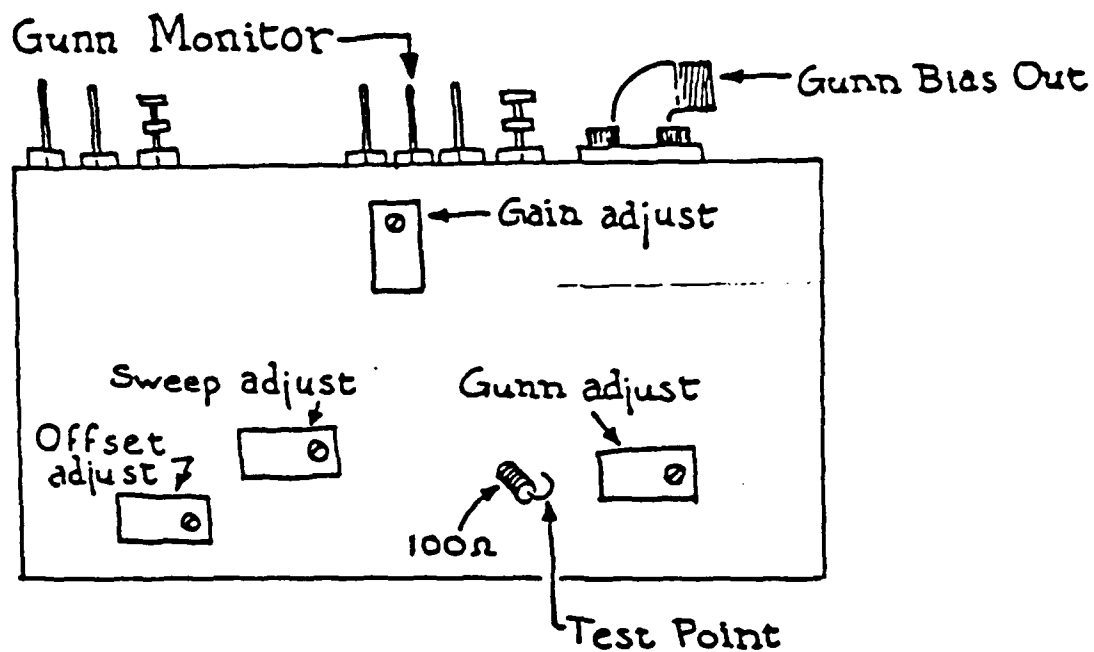


Figure B.1. Gunn adjustment potentiometer positions.

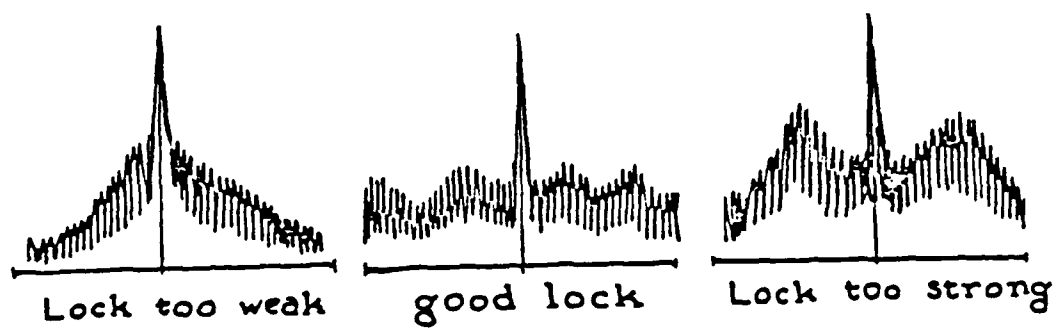


Figure B.2. 97 MHz phase-locked Gunn oscillator IF signal.

B. SQUARER ADJUSTMENT

The drift of the squarers with time will cause some of the peaks of V_{sync} to be significantly larger than others. When this occurs, the squarers need to be readjusted.

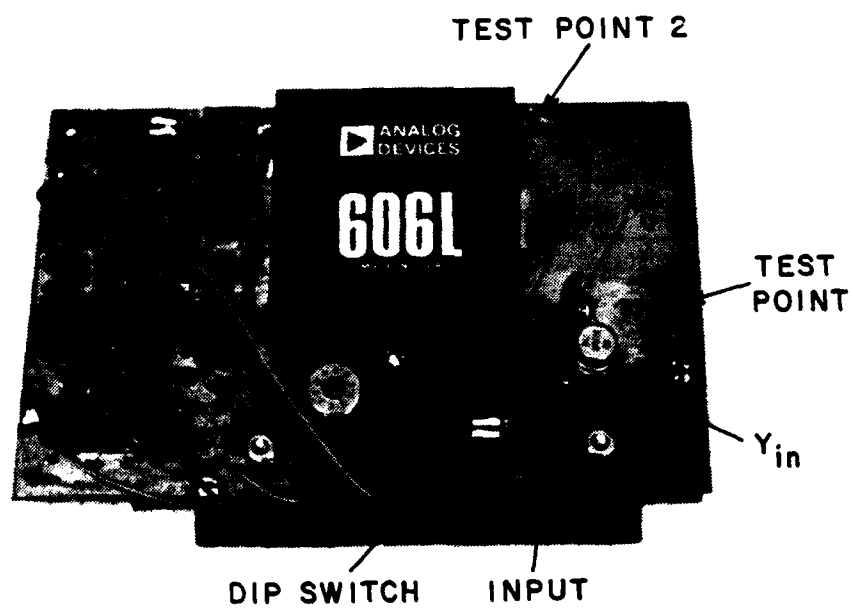
Remove the back panel of the transmissometer. Locate the audio frequency circuitry shown in Plate 2.5. Turn the power switch located just above the circuit boards (marked ± 15 V) off. (This turns off power to the circuit boards only). Remove board B (nearest the power switch). Insert an appropriate extender card into the slot and plug board B into it so that the items marked in Plate B.1 are accessible. Toggle both switches of the dip switch. Turn the power on.

With the pin marked "INPUT" in Plate B.1 grounded, adjust Z_0 so that the voltage at the "TEST POINT" equals zero VDC. Now with "INPUT" set to 10.0 VDC, adjust Y_{in} for "TEST POINT" equal to 10.0 VDC. Apply -10.0 VDC to "INPUT" and adjust X_0 to reduce the output error to 1/2 its original value. Readjust Y_{in} to take out the remaining error. Check the "TEST POINT" value with "INPUT" grounded. If nonzero, repeat this paragraph until no error remains. Toggle the dip switch settings back to their original positions, 1 open, 2 closed.

Turn power off, replace the board and repeat the process on board A. Turn power on when finished.

PLATE B.1

CIRCUIT BOARD A (OR B)



C. GAIN SWITCHING POINTS

Remove the transmissometer back cover. Refer to Plate 2.5 to find the audio frequency circuitry. Turn off the power switch located just above the circuit boards. Replace Board 3 with a card extender and plug Board 3 into it. Turn the power switch back on. Refer to Figure B.3. Monitor pin 2 on the 741 integrated circuit with a DC voltmeter. Adjust potentiometer 1 so that the voltmeter reads +0.50 VDC. Now monitor pin 5 of the 1458 integrated circuit and adjust potentiometer 2 so that the voltmeter reads +10.0 VDC. Turn off power, replace the board and turn power on.

D. I, Q CHANNEL GAINS

Over a long period of time, the settings for I and Q channel gains may need to be equalized. This is performed by removing the back cover from the transmissometer. Turn the waveguide switch (refer to Plate 5.3) so that the calibration signal is "on". As in Chapter V, Section B.3., adjust the transmissometer so that returns from a target or clutter are minimal. Insert a phaser-shifter such as a General Radio constant-impedance trombone line 874-LTL into the IF signal channel at point {7} (see Figure 2.4). Hook up an oscilloscope (and/or and AC voltmeter) to Test Point 2 (see Plate B.1) on boards A and B. (Two 800 Hz sine waves should be observed).

Adjust the phase-shifter such that the signal from board B is a maximum. Record the value of the signal from Board B. Now adjust the

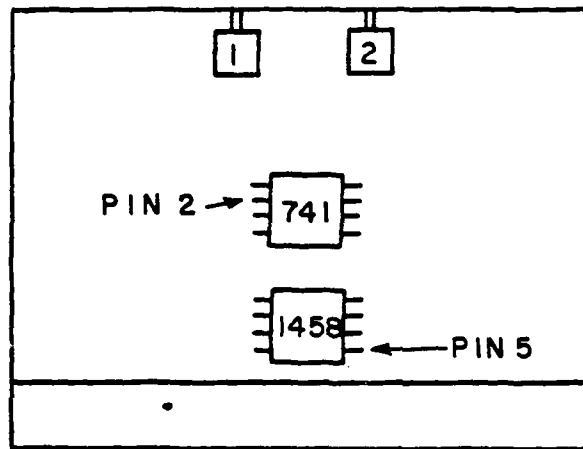


Figure B.3. Audio frequency circuit board #3.

phase-shifter such that the signal from A is a maximum and record its value. Determine which gain needs to be adjusted and adjust the gain so that the maximum values recorded for A and B are equal. Gains are adjusted by the potentiometers to the far right (Q gain adjust) and far left (I gain adjust) of board 4.

APPENDIX C

ATTENUATION EQUATION DERIVATION

Equations used to determine the atmospheric attenuation, A , along the path have been produced using the data shown in Figure 4.2. The derivation of these equations follows. The equations of the lines in Figure 4.2 in both "high gain" and "low gain" modes are determined first. The constants are chosen so that the lines approximate the data in Figure 4.2 within $\pm 1/2$ dB. The equation for the "high gain" line is given by Equation (C.1) and the equation for the "low gain" line is given by Equation (C.2),

$$\log_{10} V_{\text{out}} = 8.0 + 0.1 P_2 \quad (\text{high gain}) \quad (\text{C.1})$$

$$\log_{10} V_{\text{out}} = 6.1 + 0.1 P_2 \quad (\text{low gain}) \quad (\text{C.2})$$

Equations (C.1) and (C.2) are now used, in part, to calculate A , given the following parameters: σ_{cal} (m^2); R_{cal} ; $V_{\text{out-cal}}$ (V); $A_{\text{if-cal}}$ (dB); σ_{test} (m^2); R_{test} (m); $V_{\text{out-test}}$ (V); $A_{\text{if-test}}$ (dB); and the gain mode, where σ_{cal} is the radar cross section of a target used for calibration purposes, which is placed at a range R_{cal} , so that with the Telonic attenuator set to $A_{\text{if-cal}}$, the signal return produces a voltage $V_{\text{out-cal}}$ after processing. Similarly, σ_{test} , R_{test} , $V_{\text{out-test}}$, and $A_{\text{if-test}}$ represent the same quantities under test conditions. R_{cal} must be sufficiently small so that the atmospheric attenuation under clear

air conditions can be neglected when taking calibration measurements, but large enough to be in the far field. A distance on the order of 500 meters is suggested. The attenuation, A, is determined in the following way. Using Equation (4.2), the radar equation,

$$P_2 = \frac{t_r t_t P_t G_t G_r \lambda^2 \sigma t^2}{(4\pi)^2 R^4} \quad , \quad (C.3)$$

where t^2 is substituted for $10^{-(2aR)}$ in Equation (4.2) (see Equation (2.2)). Substituting values under both test and calibration conditions and dividing yields

$$\frac{P_{2\text{-test}}}{P_{2\text{-cal}}} = \frac{t^2 (R_{\text{cal}})^4 \sigma_{\text{test}}}{(R_{\text{test}})^4 \sigma_{\text{cal}}} \quad . \quad (C.4)$$

Solving Equation (C.4) for t^2 gives

$$t^2 = \frac{P_{2\text{-test}}}{P_{2\text{-cal}}} \frac{R_{\text{test}}^4}{R_{\text{cal}}^4} \frac{\sigma_{\text{cal}}}{\sigma_{\text{test}}} \quad . \quad (C.5)$$

From Equation (2.2),

$$A = -10 \log_{10} t = -5 \log_{10} t^2 \quad (C.6)$$

or

$$A = -5 \left[\log_{10} \frac{P_{2\text{-test}}}{P_{2\text{-cal}}} + \log_{10} \frac{(R_{\text{test}})^4}{(R_{\text{cal}})^4} + \log_{10} \frac{\sigma_{\text{cal}}}{\sigma_{\text{test}}} \right] \quad (C.7)$$

or

$$A = \frac{1}{2} [P_{2\text{-cal}} - P_{2\text{-test}}] - 20 \log_{10} \left[\frac{R_{\text{test}}}{R_{\text{cal}}} \right] + 5 \log_{10} \left[\frac{\sigma_{\text{test}}}{\sigma_{\text{cal}}} \right], \quad (\text{C.8})$$

where both P_2 values are in dBm. Now all that remains is to relate each P_2 to a value of V_{out} , which is accomplished by using Equations (C.1) and (C.2). Because the equations were derived from data taken with A_{if} set to 30 dB,

$$\log_{10} V_{\text{out}} = C + 0.1[P_2 - (A_{\text{if}} - 30)], \quad (\text{C.9})$$

where P_2 is in dBm and C is 6.1 in low gain mode and 8.0 in high gain mode. Solving for P_2 in dBm yields

$$P_2 = 10(\log_{10} V_{\text{out}} - C) + A_{\text{if}} - 30. \quad (\text{C.10})$$

Substituting this value of P_2 into Equation (C.8), with C_{cal} and C_{test} having values of 6.1 in low gain mode and 8.0 in high gain mode, yields

$$\begin{aligned} A = & (1/2) [10(\log_{10} V_{\text{out-cal}} - C_{\text{cal}}) + A_{\text{if-cal}} - 30 \\ & - \{10(\log_{10} V_{\text{out-test}} - C_{\text{test}}) + A_{\text{if-test}} - 30\}] \\ & - 20 \log_{10} [R_{\text{test}}/R_{\text{cal}}] + 5 \log_{10} [\sigma_{\text{test}}/\sigma_{\text{cal}}] \end{aligned} \quad (\text{C.11})$$

or

$$\begin{aligned} A = & 5 \log_{10}(V_{\text{out-cal}}/V_{\text{out-test}}) + 5(C_{\text{test}} - C_{\text{cal}}) \\ & + (1/2) (A_{\text{if-cal}} - A_{\text{if-test}}) - 20 \log_{10}(R_{\text{test}}/R_{\text{cal}}) \\ & + 5 \log_{10}(\sigma_{\text{test}}/\sigma_{\text{cal}}) \quad (\text{dB}). \end{aligned} \quad (\text{4.1})$$

Equation (4.1) gives A (in dB) in terms of the parameters mentioned above and C_{test} and C_{cal} , which are dependent on the gain mode of the system. Thus Equation (4.1) yields the attenuation A .

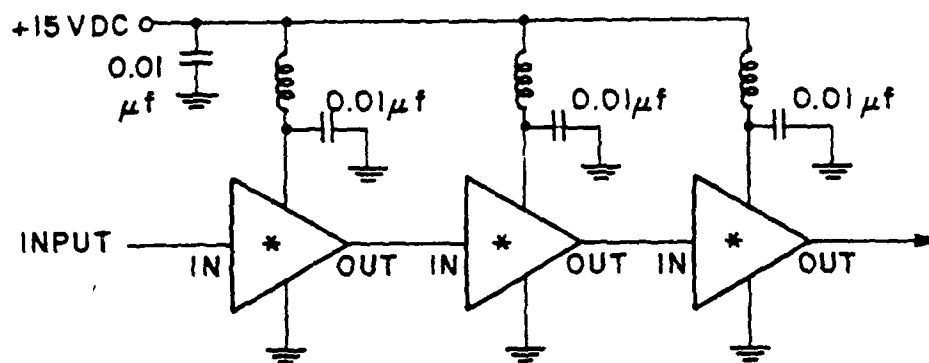
APPENDIX D
CIRCUIT DIAGRAMS

1. ESL 776 MHz, 33 DB AMPLIFIER

Figure D.1 shows the circuit diagram of the ESL 776 MHz, 33 dB amplifier.

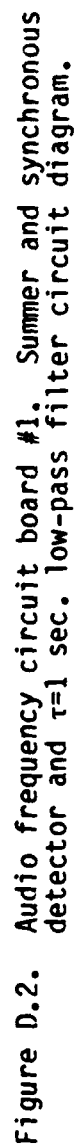
2. AUDIO-FREQUENCY CIRCUITRY

The circuit diagram of the six audio-frequency boards are shown in Figures D.2 to D.6.



* AVANTEK GPD-402
INTEGRATED AMPLIFIER

Figure D.1. ESL 776 MHz, 33 dB gain amplifier circuit diagram.



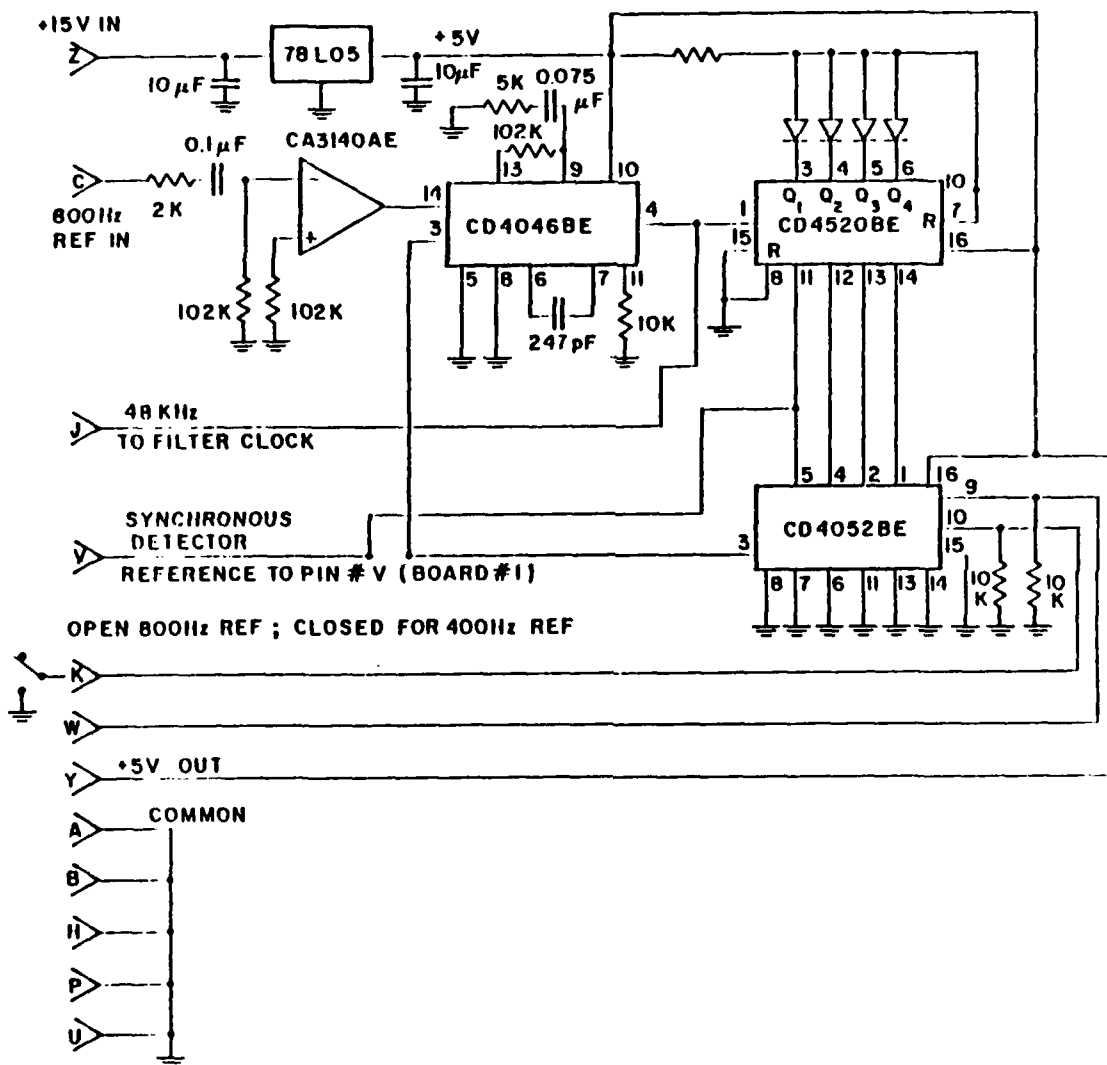


Figure D.3. Audio frequency circuit board #2. 48 kHz clock generator circuit diagram.

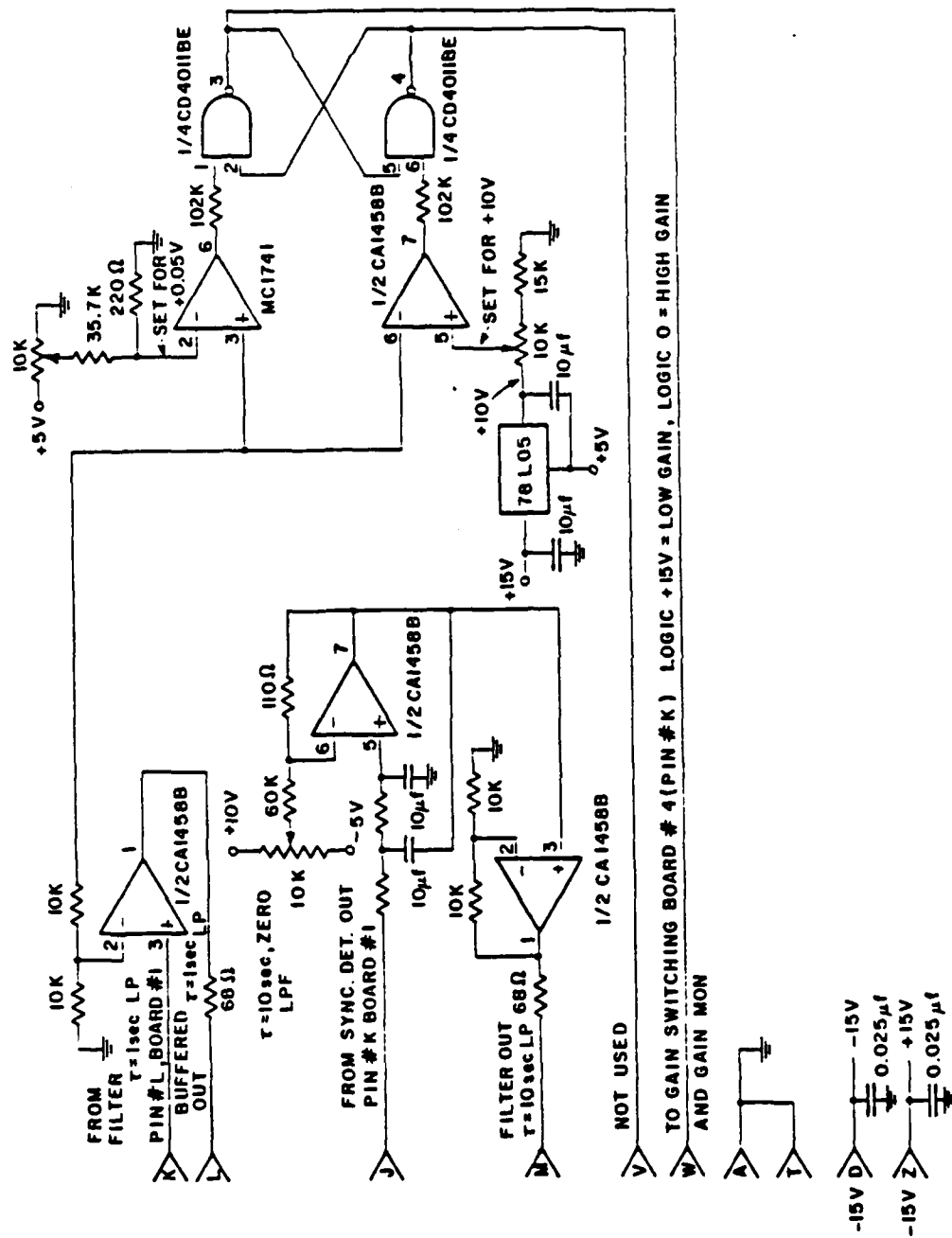


Figure D.4. Audio frequency circuit board #3. Gain switching logic and $\tau=10$ sec. low-pass filter circuit diagram.

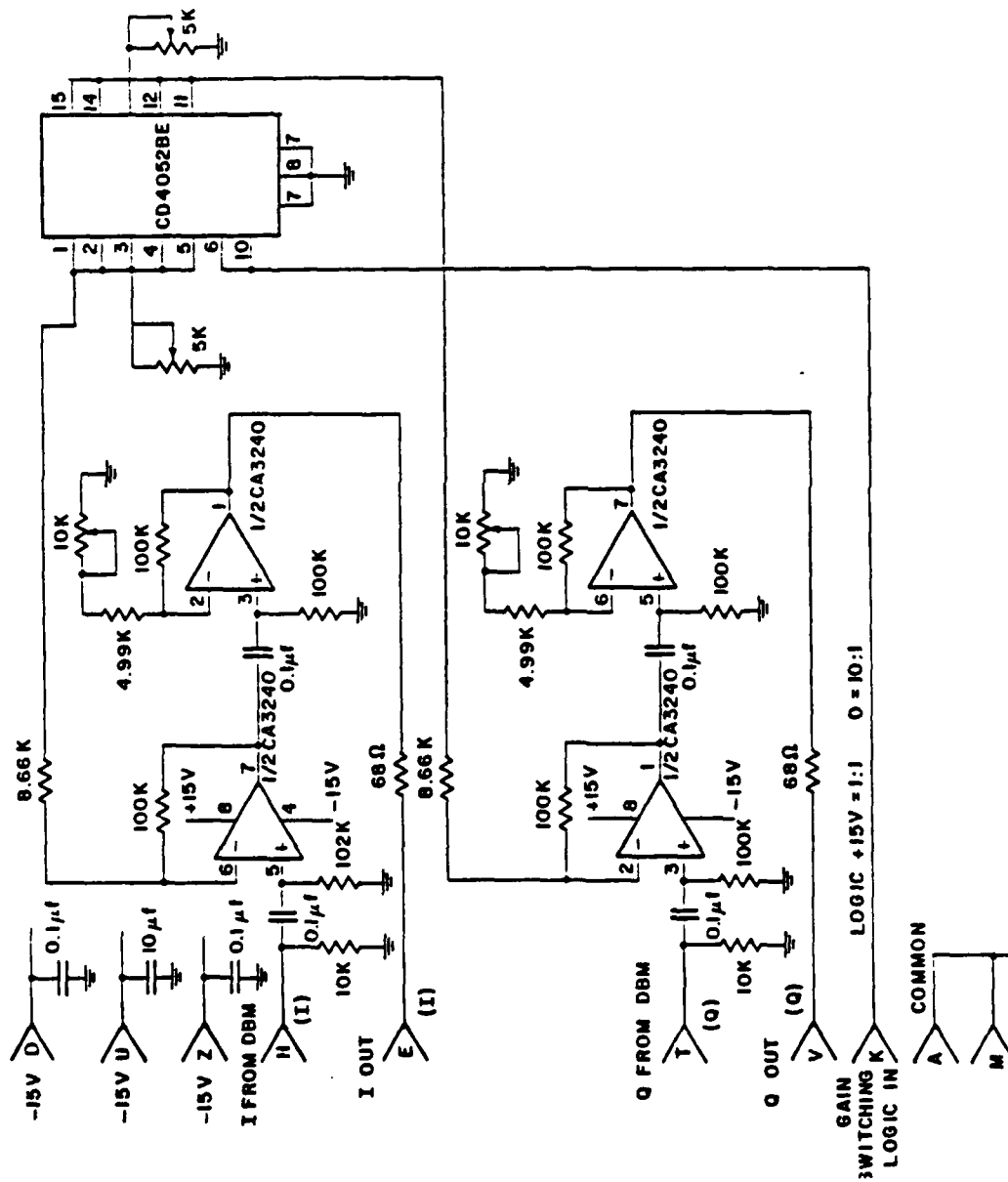


Figure D.5. Audio frequency circuit board #4. Audio frequency preamplifier (gain=1 or 10) circuit diagram.

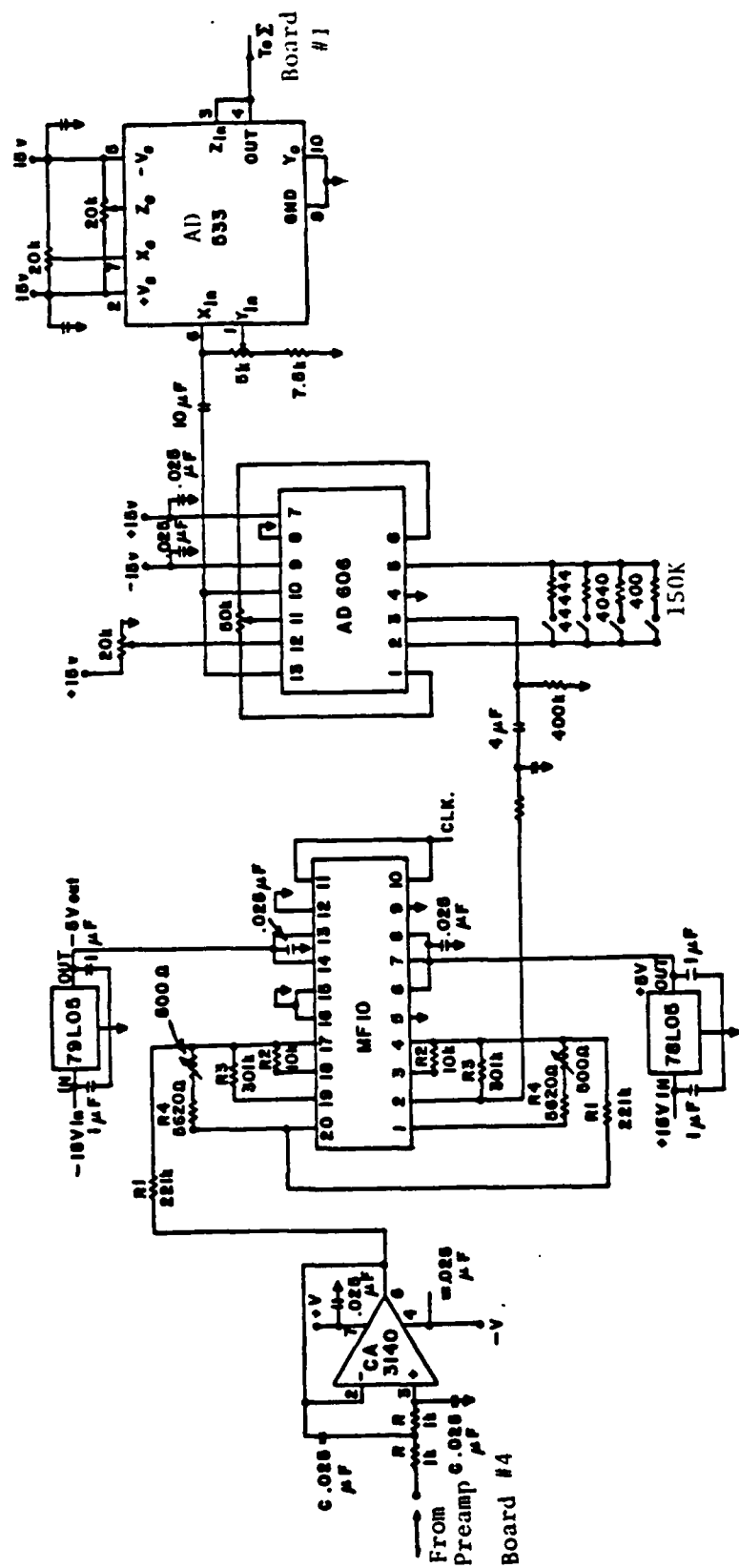


Figure D.6. Audio frequency circuit board A,B. Anti-aliasing low-pass filter, digital bandpass filter, amplifier, and squarer circuit diagram.

REFERENCES

- [1] Buyukdura, O. M. and Levis, C. A., "A Comparison of Several Systems for Transmission Measurements at 94 GHz", Report AFWAL-TR-81-1281, Air Force Systems Command, Avionics Laboratory, Air Force Wright Aeronautical Laboratory, Wright-Patterson Air Force Base, Ohio. Also published as Report 713671-1, The Ohio State University ElectroScience Laboratory, August 1981.
- [2] Levis, C. A., Damon, E. K. and Buyukdura, O. M., "A Meteorologically Instrumented Range for Millimeter-Wave Sensors", published as Report 712604-1, The Ohio State University ElectroScience Laboratory, September 1981.
- [3] "Attenuation by Atmospheric Gases", Report 719-1, Recommendations and Reports of the CCIR, Vol. 5, 1982.
- [4] Liebe, H. J., "Updated Model for Millimeter Wave Propagation in Moist Air", Radio Science, Vol. 20, pp. 1069-1089, September-October 1985.
- [5] Pierluissi, J. H., Tomiyama, K., Fowler, W. D., Gomez, R. B., "Resonant Transmittance Model for Millimeter Wave Propagation", IEEE Transactions on Antennas and Propagation, Vol AP-30, pp. 741-746, July 1982.
- [6] Falcone, V. J., Jr., Abreu, L. W., "Millimeter Wave Propagation Modeling", Proceedings of the Society of Photo Optical and Instrumentation Engineers, Vol. 259, pp. 58-66, October 1-2, 1980.
- [7] Persinger, R. R., Stutzman, W. L., Castle, R. E., Jr., Bostian, C. W., "Millimeter Wave Attenuation Prediction Using a Piecewise Uniform Rain Rate Model", IEEE Transactions on Antennas and Propagation, Vol. AP-28, pp. 149-153, March 1980.
- [8] Oguchi, T., "Electromagnetic Wave Propagation and Scattering in Rain and Other Hydrometeors", Proceedings of the IEEE, Vol. 71, pp. 1029-1078, September 1983.
- [9] Wallace, H. B., "Millimeter Wave Propagation Measurements at the Ballistic Research Laboratory", Optical Engineering, Vol. 22, pp. 24-31, January-February 1983.

- [10] Kobayashi, H. K., "Atmospheric Effects on Millimeter Radio Waves", Reprot ASL-TR-0049, U.S. Army Electronics Research and Development Command, Atmospheric Sciences Laboratory, White Sands Missile Range, NM (NTIS No. AD-A081414).
- [11] Keizer, W. P. M. N., Sneider, J., and Dehaan, C. P., "Propagation Measuremetns at 94 GHz and Comparison of Experimental Rain Attenuation with Theoretical Results Derived From Actually Measured Raindrop Size Distributions", Proceedings of the International Conference of Antennas and Propagation, London, England, IEE Conference Publication No. 1609, Part 2, pp. 82-86, November 28-30, 1978.
- [12] Kobayashi, H. K., "Effect of Hail, Snow and Melting Hydrometeors on Millimeter Radio Waves," Report ASL-TR-0092, U.S. Army Electronics Research and Development Command, Atmospheric Sciences Laboratory, White Sands Missile Range, NM (NTIS No. AD-A107 429/3).
- [13] McMillan, R. W., Bohlander, R. A., Ochs, G. R., Hill, R. J., Clifford, S. F., "Millimeter Wave Atmospheric Turbulence Measurements: Preliminary Results and Instrumentation for Future Experiments", Optical Engineering, Vol. 22, pp. 32-39, January-February 1983.
- [14] Meinel, H., Plattner, A., "Millimetre-Wave Propagation Along Railway Lines", IEE Proceedings Part F, Vol. 130, pp. 688-694, December 1983.
- [15] Kaneko, K. and Kato, H., "Millimeter-Wave IMPATT Negative-Resistance Amplifiers", Review of the Electrical Communication Laboratories (Japan), Vol. 26, pp. 1057-1069, July-August 1978.
- [16] Haykin, S., Communication Systems, John Wiley & Sons, pp. 544-547, 1978.
- [17] Roden, M. S., Digital and Data Communication Systems, Prentice-Hall, pp. 251-264, 1982.
- [18] Tucker, D. G., Circuits with Periodically-Varying Parameters, D. Van Nostrand & Co., pp. 86-90, 1964.
- [19] Schwartz, M., Communication Systems and Techniques, McGraw-Hill, Inc., pp. 108-114, 1966.
- [20] Blachman, N. M., Noise and Its Effect on Communication, McGraw-Hill, Inc., pp. 89-92, 1966.
- [21] Ruck, G. T., Barrick, D. E., Stuart, W. D., Krichbaum, C. K., Radar Cross Section Handbook, Vol. 2, Plenum Press, 1970, p. 591.



MISSION *of* **Rome Air Development Center**

RADC plans and executes research, development, test and selected acquisition programs in support of Command, Control, Communications and Intelligence (C³I) activities. Technical and engineering support within areas of competence is provided to ESD Program Offices (POs) and other ESD elements to perform effective acquisition of C³I systems. The areas of technical competence include communications, command and control, battle management information processing, surveillance sensors, intelligence data collection and handling, solid state sciences, electromagnetics, and propagation, and electronic reliability/maintainability and compatibility.